A Combination Hyaluronic Acid-Collagen Fiber Scaffold for Tympanic Membrane Repair

by

Mireya Yareth Cervantes González

Submitted in partial fulfilment of the requirements
for the degree of Master of Applied Science

At

Dalhousie University

Halifax, Nova Scotia

August 2022

Table Of Contents

List of Tables

List of Figures

Abstract

Tympanic membrane perforation (TMP) is one of the most common conditions in otology. If left untreated, TMP can result in recurrent ear infections, chronic TMP, and loss of hearing. Treatments designed to repair TMP usually involve reconstruction of the tympanic membrane with autologous tissue grafts. These autologous grafts have several limitations, e.g., the invasive procedures used to harvest the tissue and difference in tissue mechanics between the graft and native tympanic membrane tissue. To address these issues, a novel biomaterial comprised of hyaluronic acid (HA) and surface-anchored type I collagen (ColI) fibers was developed and characterized. Here, a dual crosslinking reaction was optimized for production of stable HA films with appropriate mechanical and biochemical properties. The crosslinked HA films were fabricated by spin processing followed by solution casting. HA film degradation and swelling were observed under physiological conditions. The thickness and chemical composition of the films were determined. Col1 fibers were attached to the crosslinked HA film, and the tensile properties of the combination material were examined. Finally, *in vitro* evaluation of cell attachment and migration was performed with fibroblasts and keratinocytes. Crosslinked HA films were stable for longer than 21 days when immersed in phosphate-buffered saline (PBS) at 37 ºC. The mechanical properties of the films approximated those of the native human tympanic membrane. Dermal fibroblast attached and proliferated on the HA-ColI fiber scaffolds with no apparent cytotoxicity. Moreover, it was observed that the fibers in the scaffold promoted migration of human keratinocytes. These data confirm the key functions of the material for TMP repair and suggest that further development and testing are warranted to move towards commercialization of the materials for the intended use.

List of Abbreviations & Symbols Used

2D	Two-dimenional
3D	Three-dimensional
A	Cross-sectional area
ANOVA	Analysis of variance
ATR	Attenuated total reflectance
BDDE	1,4-butanediol diglycidyl ether
C-AM	Calcein-acetoxymethyl
CD44	Cluster of differentiation 44
ColI	Type I Collagen
COM	Chronic otitis media
COOH-	Carboxylic acid group
Da	Dalton
DDR1	Discoidin domain receptor 1
DDR2	Discoidin domain receptor 2
D_{dry}	Dry diameter
DMEM	Dulbecco's modified eagle's medium
D-PBS	1x Dulbecco's phosphate buffered saline
DTP	3,3'-dithiobis (propionic hydrazide)
D_{wet}	Wet diameter
E	Elastic modulus
ε	Strain
ECM	Extracellular matrix
F	Force
F-actin	Actin filaments
FBS	Fetal bovine serum
FTIR	Fourier transform infrared spectroscopy
G6b-B	Receptor G6b
GAG	Glycosaminoglycan
GPVI	Glycoprotein VI receptor
HARE	HA receptor for endocytosis
HBSS	Hanks balanced salt solution
HMWHA	High molecular weight hyaluronic acid
Hyaluronic acid	HA
ITA	Itaconic acid
L_0	Initial length
ΔL	Change in length
LAIR-1	Leukocyte associated immunoglobulin-like receptor-1

LMWHA	Low molecular weight hyaluronic acid
LRC	Leukocyte receptor complex
LYVE-1	Lymphatic vessel endothelial receptor
M	Molarity
MCT	Mercury-Cadmium-Telluride
MPa	Megapascals
NaOH	Sodium hydroxide
N-TERT	Keratinocyte cell line
OCT	Optical coherence tomography
ODA	Octadecylamine
OH-	Hydroxyl group
OSA	Octenyl succinic anhydride
OSCAR	Osteoclast associated receptor
paraformaldehyde	PFA
PBS	Phosphate-buffered saline
PEG	Polyethylene glycol
PEGDE	Polyethylene glycol diglycidyl ether
PEO	Polyethylene oxide
PI	Propidium iodide
RHAMM	Receptor for HA mediated motility
rpm	Revolutions per minute
RT	Room temperature
σ	Stress
t	Time
TA	Tannic acid
TCP	Tissue culture plastic
t_{film}	Thickness of film
TLR-2	Toll-like receptors 2
TLR-4	Toll-like receptors 4
Tympanic membrane	TM
Tympanic membrane perforation	TMP
uPARAP/Endo180	Urokinase plasminogen activator receptor-associated protein
UV-C	Ultraviolet light with wavelengths between 100-280 nm
w/v	Weight/volume
w/w	Weight/weight
W_{dry}	Dry weight
w_{film}	Width of film

W_o	Initial weight
WSI	Immortalized dermal fibroblast cell line
W_t	Weight at time t
W_{wet}	Wet weight

Chapter 1. Introduction

1.1 Clinical Relevance of Tympanic Membrane Rupture

Tympanic membrane perforation (TMP) is a common complication that occurs in otology, with over 200,000 cases per year in the United States of America [1]. TMP has numerous origins. For example, it can arise from chronic otitis media (COM), barotrauma (i.e., sudden change in pressure), head trauma, or insertion of foreign objects into the ear [2]. Most commonly, perforations are caused by physical trauma or otitis media. However, TMP can also be a cause of COM. Suppurative COM affects over 31 million people worldwide each year, leading to a significant health care burden [3]. The most common long-term complications in patients with COM are persistent TMP and conductive hearing loss. During an ear infection, fluids accumulate behind the TM, forming a buildup of pus in the middle ear. The pressure from this buildup of pus is often sufficient to cause TMP [4]. Even though most acute perforations heal within one month without surgery, in 20% of patients [5], [6], healing may fail, which may result in chronic TMP if this persists for more than 3 months [7]. COM is a common complication for children from 6 to 12 months of age, which has profound effects on speech and language, social, behavioral, and cognitive development. This can impact early education, social interactions and performance in school [8]. Thus, to treat TMP, surgical procedures are required, which typically involve the use of grafts to patch the perforation. Detailed information about the procedures and materials that are used is given in section 1.3.

1.2 Tympanic Membrane Characteristics

An overview of the tympanic membrane anatomy, characteristics and function is required to understand and contemplate what is needed for designing a graft for TMP. The

tympanic membrane (TM), also known as the eardrum, is a thin delicate translucent tissue that divides the middle ear from the outer ear canal. The main functions of the TM are to serve as a barrier to protect the middle and inner ear from the external environment and in hearing conduction [9]. The TM is comprised of three layers of tissue: the outer cutaneous layer, the fibrous middle layer (i.e., lamina propria), and a layer of mucous membrane on its innermost surface. The TM is held in place by a thick ring of cartilage, a tough but flexible tissue [10]. Figure 1 provides an overview of the TM and its components. The thickness of the TM varies greatly across the membrane, but the mean value across the pars tensa ranges between 79 and 97 μm [11]. The thinnest part of the membrane is found in the central region between the umbo and annular ring (50-70 μm), and the thickness increases sharply over a small distance to approximately 100-120 μm when moving from the central region either towards the peripheral rim of the pars tensa or towards the manubrium. The thickness value found for the pars flaccida ranges from 30-230 μm [11]. Moreover, the diameter of the TM ranges from 8 to 10 mm and has a mass of around 14 mg [12]. The TM vibrates when sound waves enter the ear, and the vibration continues through the ossicles. The ossicles amplify the sound and send the sound waves to the inner ear and into the cochlea. Once the sound waves reach the inner ear, they are converted into electrical impulses. The auditory nerve sends these impulses to the brain. Then, the brain translates these electrical impulses as sound [13], [14]. Thus, the transmission of sound depends on the integrity of the TM, and a damaged TM may lead to permanent hearing loss.

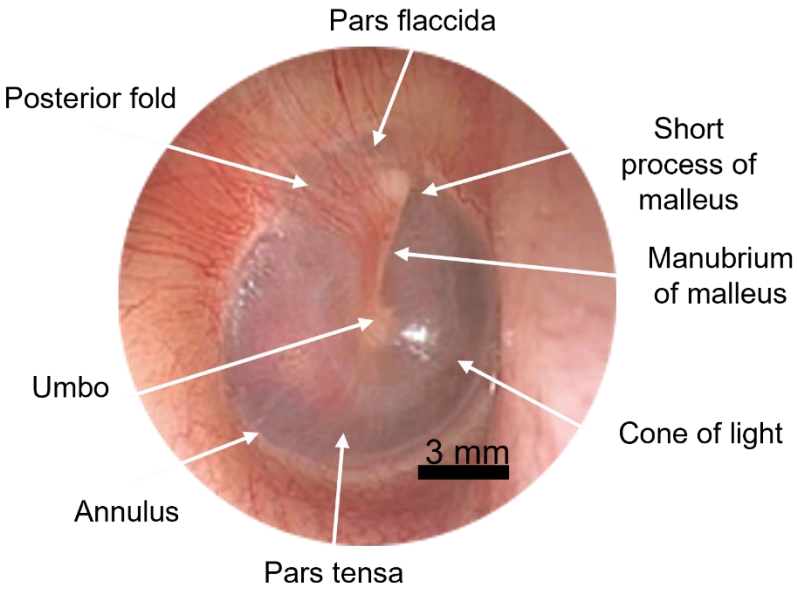

Figure 1: Photograph of a human tympanic membrane, provided by Dr. Robert Adamson's lab. Here, the parts of the membrane are labeled.

1.3 Current Strategies for Tympanic Membrane Repair

Various treatment methods have been attempted due to the severity of the possible deleterious effects of TMP, such as contamination by exposure to pathogens introduced via the external auditory canal causing COM and hearing loss. The two most frequently performed surgical procedures for treating TM rupture are myringoplasty and tympanoplasty [15], both of which aim to re-establish an intact TM, prevent recurrent infections, and ultimately restore hearing [16]. Myringoplasty is the simplest repair, where the hole is covered with a small piece of graft, fat, or Gelfoam® to temporarily seal the defect and encourage the body's normal healing processes. It can be performed in approximately 30 minutes and works better in small center perforations (i.e., one to two quadrants of the TM) [17]. Conversely, tympanoplasty is more invasive as it includes creating an incision mostly in the ear canal (tympanomeatal incision). There are several variations in how tympanoplasty is performed, such as lateral graft tympanoplasty (Figure

2) and butterfly tympanoplasty. In general, the technique consists of patching the hole with a graft of the patient's own tissue, either perichondrium or a connective tissue called fascia. The surgeon will place the new tissue behind or on top of the rupture, and remove the outer edges of the wound to make an acute injury and promote healing [18]. Both approaches (myringoplasty and tympanoplasty) utilize graft materials that should slowly dissolve over 2 to 3 months while the TM heals.

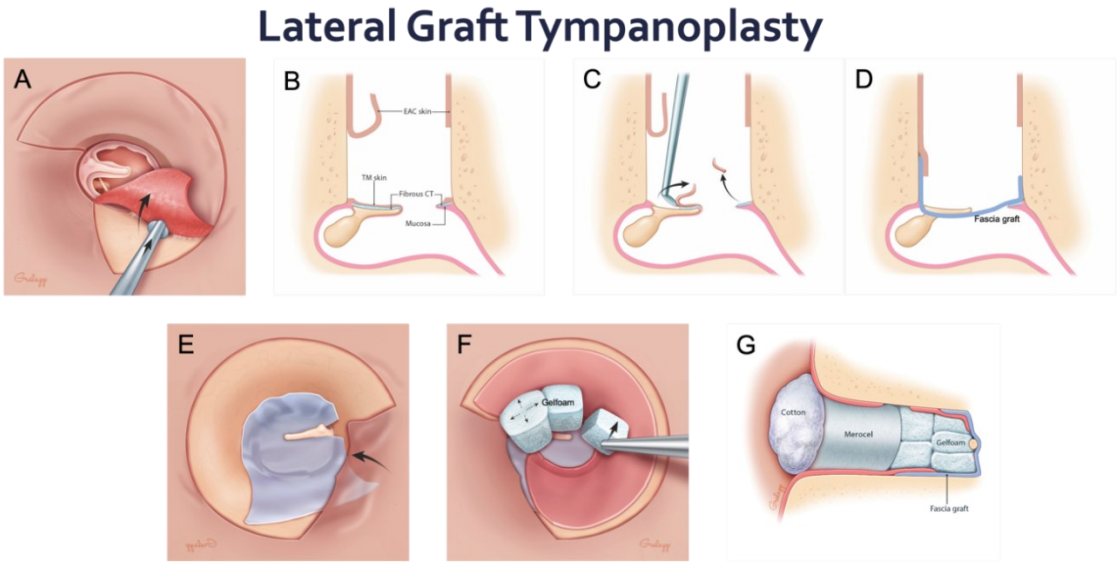

Figure 2: Overview of the lateral graft tympanoplasty procedure. A) In this technique, a superior incision describes a vascular strip flap to be elevated laterally. B) Schematic illustration of the initial stages of the lateral technique. EAC. – external auditory canal; TM, Tympanic membrane; CT, Connective tissue. C) Removing the squamous layer from the TM remnant. D) Placement of the fascia graft. E) After placing the graft, a replacement is done of the superior flap overlapping the fascia graft. F) Packing with Gelfoam® is performed. This step is important to reduce the likelihood of anterior blunting or lateralization. G) Finally, further packing materials are added, such as merocele and cotton. Reprinted with permission from Otologic Surgery Atlas, obtained from [19]. Illustrations Copyright © chrisgralapp.com.

Grafts employed for TM repair include a diverse assortment of natural and semi-synthetic materials. The most commonly used natural materials are autologous grafts such as temporalis fascia, tragal cartilage, perichondrium, periosteum, vein, fat, or skin [20]. Among these, the gold standard is temporalis fascia, as it is close to the operation field and

relatively easy to harvest. The graft failure of temporalis fascia is mainly attributed to poor stability characteristics linked to the presence of connective fibrous tissue with irregular elastic fibers within the fascia [21]. The limitations of this type of graft are the invasive medical procedures to harvest the tissue, possible donor site morbidity, lack of transparency, and the differing tissue mechanics and material properties of the graft when compared with intact TM [22]. The transparency of the material for healing the TMP is important because it permits a clinician to inspect the middle ear [8]. The differences in material properties may interfere with the conductive pathway of hearing resulting in longer healing time and greater likelihood that surgical revision will be required. These limitations have increased the demand for partially synthetic materials, (i.e., materials that come from natural sources but are combined with biodegradable synthetic polymers or that are chemically modified), or fully synthetic materials (such as poly glycerol sebacate) to replace the use of autologous grafts [20].

The theoretical benefits of partially synthetic products, such as AlloDerm®, which is a freeze-dried acellular dermal matrix with preserved basement membrane processed from human allograft donors [23], include the elimination of morbidity related to graft harvesting, faster healing, less risk of infection, less pain for the patient with no visible scarring, and a faster procedure leading to early discharge [10]. However, the use of these grafts makes the procedure more expensive, and no proven advantages compared to autologous grafts have so far been demonstrated [10]. To overcome the aforementioned limitations, various engineered biomaterials have been developed over the years utilizing components present in the wound healing process. In particular, hyaluronic acid has gained popularity following the discovery of its prominent roles in wound healing [24], [25].

1.4 Hyaluronic Acid and Its Properties

Hyaluronic acid (HA), also known as hyaluronan or hyaluronate, is a naturally occurring glycosaminoglycan (GAG) found in the extracellular matrix (ECM) of numerous tissue types including skin, synovial fluid between joints, and vitreous body of the eyes. The unique features distinguishing HA from other GAGs are its simple structure and high molecular weight, as well as the fact that it does not contain sulfated sugars. HA is normally not covalently linked to a core protein and is synthesized by hyaluronan synthetases on the inner surface of the cell membrane, causing HA to be directly translocated into the extracellular space [25]. Structurally, HA is a linear anionic heteropolysaccharide composed of a repeating disaccharide unit of D-glucuronic acid and N-acetyl-D-glucosamine bound together through alternating β-(1,3) and β-(1,4) glycosidic linkages (Figure 3) [26]. The disaccharide moiety can be repeated up to 25,000 times, producing very long polymers with molecular weights reaching more than 10^6 Da [27]. The structure and composition of HA makes it highly hydrophilic and able to bind several times its weight in free water molecules. The functions of HA in the human body include tissue turgidity due to its water-binding capacity, lubrication, and an important role in wound healing. During wound healing, HA enhances the differentiation and proliferation of endothelial cells and facilitates cell migration, angiogenesis, and regulation of inflammation [28]. These biofunctionalities come from the interaction of HA with cellular receptors: CD44, RHAMM, TLR-2 and TLR-4, HARE and LYVE-1 [29]. High molecular weight HA (HMWHA) is the native form of the molecule. Nevertheless, in certain conditions (e.g., the wound healing process), it can be decomposed into smaller fragments referred to as low molecular weight HA (LMWHA) [30]. The molecular weight of HA is

an important feature of this molecule, since HA molecular weight is known to elicit differential cell responses [31]. In general, HMWHA helps to maintain the structural integrity of the cell microenvironment and acts as a physical barrier to cell movement and expansion, while LMWHA can activate inflammatory responses [32] and promote cell proliferation and migration [33], as will be discussed in the next paragraphs.

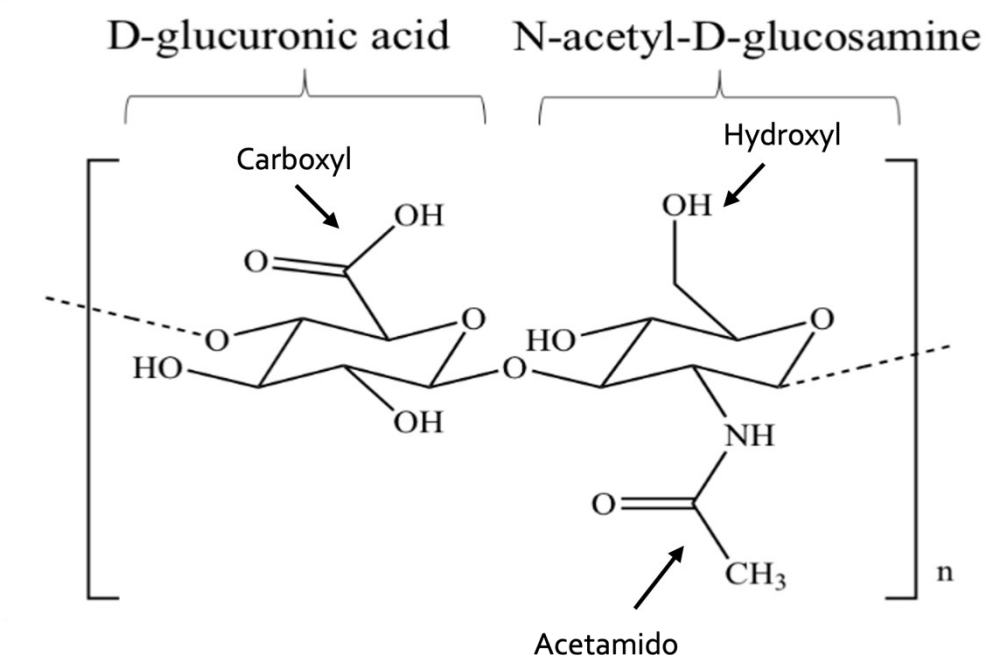

Figure 3: Chemical structure of the HA disaccharide unit. Reprinted with permission from Frontiers in Veterinary Science, obtained from [34]. Copyright © 2019: https://creativecommons.org/licenses/by/4.0/.

CD44 receptors are the most well characterized cell surface receptors for HA and have several roles in cell signaling related to cell migration, proliferation, development, tumorigenesis, and inflammation [35]. When the receptor interacts with HMWHA, homeostasis is maintained in cells and tissues. On the other hand, when a wound is present, HA degradation products (i.e., LMWHA) interact with CD44 giving rise to many essential processes such as cell migration of fibroblasts and keratinocytes into the wound, and the

internalization of LMWHA [36]. The mechanisms by which LMWHA sustains inflammation and the other mentioned responses is still poorly understood, but it has been proposed that the low molecular weight fragments may alter receptor clustering, and therefore, the signaling of cell surface receptors activated by native HMWHA, such as CD44 and RHAMM [37]–[39]. The way CD44 binds to HA is by a link domain present in the amino-terminal globular region of the receptor, and it consists of 90 amino acids [40]. Receptor for HA-mediated motility (RHAMM), as its name indicates, results in increased cell motility when activated by HA binding [41]. The binding between RHAMM and HA does not occur by a link domain like in CD44-HA, instead, they are linked by the BX7B motif (B represents either arginine or lysine and X7 contains no acidic residues) [42]. Toll-like receptors 2 and 4 (TLR-2 and TLR-4), which are largely expressed on the cell surface of immune cells, function as pattern recognition receptors in innate immune responses against various pathogens [43] and can be activated by LMWHA [44]. HA receptor for endocytosis (HARE) mediates systemic clearance of HA from circulation [45]. Lastly, the lymphatic vessel endothelial receptor (LYVE-1) works to absorb the HA from tissue to the lymph, regulating tissue hydration and tissue biomechanical properties [46].

The main limitations for using HA for wound healing in its natural state are its low strength, high deformability, and rapid degradation and clearance *in vivo*. Despite these drawbacks, HA is widely used in biomedical applications due to its viscoelastic properties, cytocompatibility, biodegradability, biofunctionality, as well as the presence of many sites for modification with reactive groups [47]. HA possesses multiple alcohol and carboxylic acid groups along with a single amide functional group (Figure 3) that allows for numerous chemical modifications that can be categorized in two different ways: conjugation and

crosslinking. In conjugation, a compound is covalently coupled to the HA chain by a single bond, whereas in crosslinking, different HA chains are linked together by two or more bonds [48]. These alterations can help to overcome the limitations of the polysaccharide by improving, modulating, or controlling the therapeutic action of HA, which is useful when developing new products [49].

1.5 Hyaluronic Acid in Tympanic Membrane Wound Healing

HA is involved in all stages of wound healing as was briefly stated in the previous section. The four sequential but overlapping stages of the wound healing process are shown in Figure 4. They consist of i) hemostasis, i.e., stoppage of bleeding by the activation of the blood clotting system; ii) the inflammatory stage, consisting of inflammation and edema formation, and when necessary destruction of bacteria and removal of debris to prepare the wound bed for the growth of new tissue; iii) the proliferative stage, where the granulation tissue is formed; and iv) the remodeling stage, which involves either resolution or scar formation [50]. The proliferative phase features three distinct sub-stages: filling the wound, contraction of the wound margins and covering the wound (i.e., re-epithelialization). In the final sub-stage of the proliferation stage, the epithelial cells rise from the wound bed or margin and begin to migrate across the wound.

In the hemostasis stage, HA accumulates and binds to fibrinogen to form a temporary matrix that supports the growth of fibroblasts and endothelial cells [51]. Later, in the inflammatory stage, HA stimulates the production of pro-inflammatory cytokines and facilitates primary adhesion of cytokine-activated lymphocytes to the endothelium. Moreover, HA modulates inflammation, acting as a free radical scavenger and antioxidant [52]. During the proliferative stage, HA stimulates the migration and proliferation of

endothelial cells and the production of collagen (types 1 and 8) [53], thereby promoting angiogenesis [54]. As an integral part of the basal epithelial layer, HA promotes re-epithelialization by directly enhancing the migration of keratinocytes via a CD44-mediated mechanism [55]. Furthermore, the persistently high level of HA during wound healing is also responsible for highly organized collagen deposition and scarless wound healing.

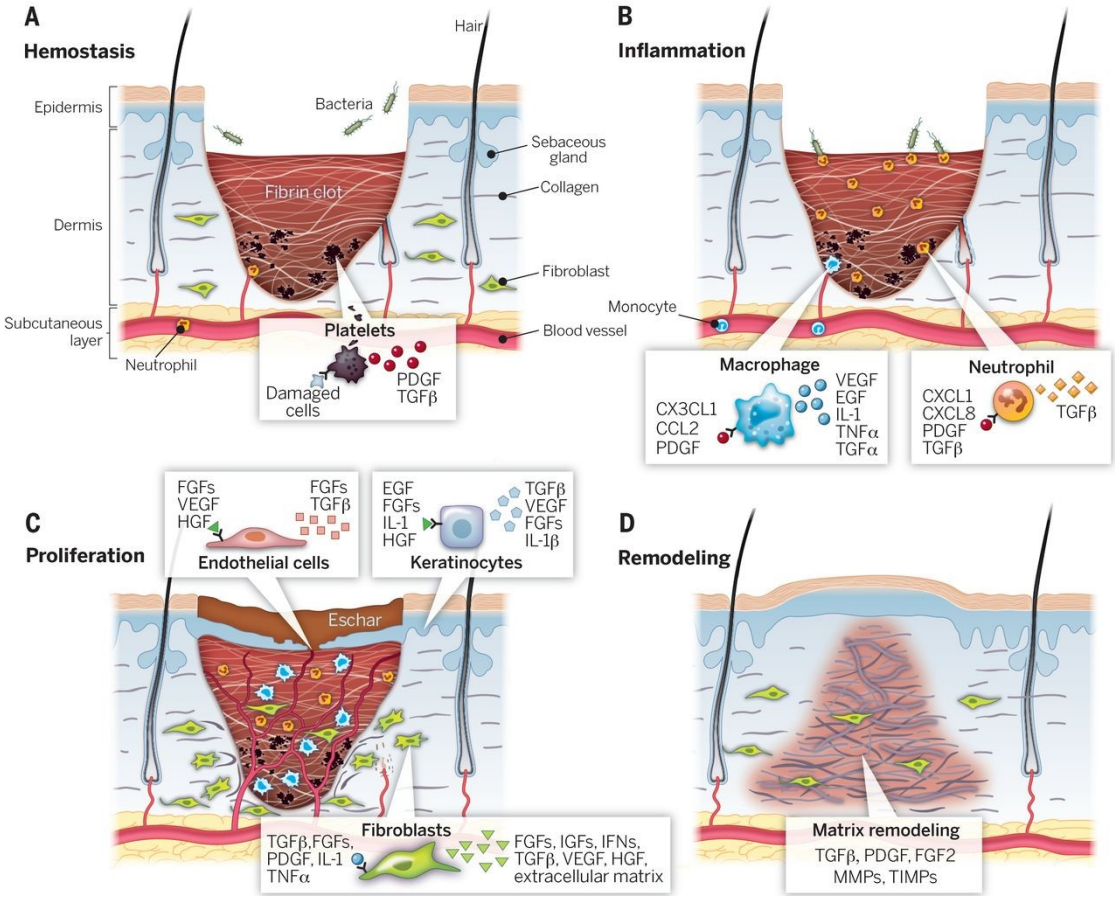

Figure 4: Schematic overview of the wound healing process. Reprinted with permission from American Association for the Advancement of Science, obtained from [56]. Copyright © 2014; permission conveyed through Copyright Clearance Center, Inc.

TM wound healing is unique in comparison to other sites of the body, such as the skin. After an injury, the response of the body is to start the healing process, which means it will undergo the four sequential but overlapping phases of hemostasis, inflammation,

proliferation, and migration. In TM healing, the first two stages remain the same, but proliferation and migration occur in the reverse order as shown in Figure 5 [57].

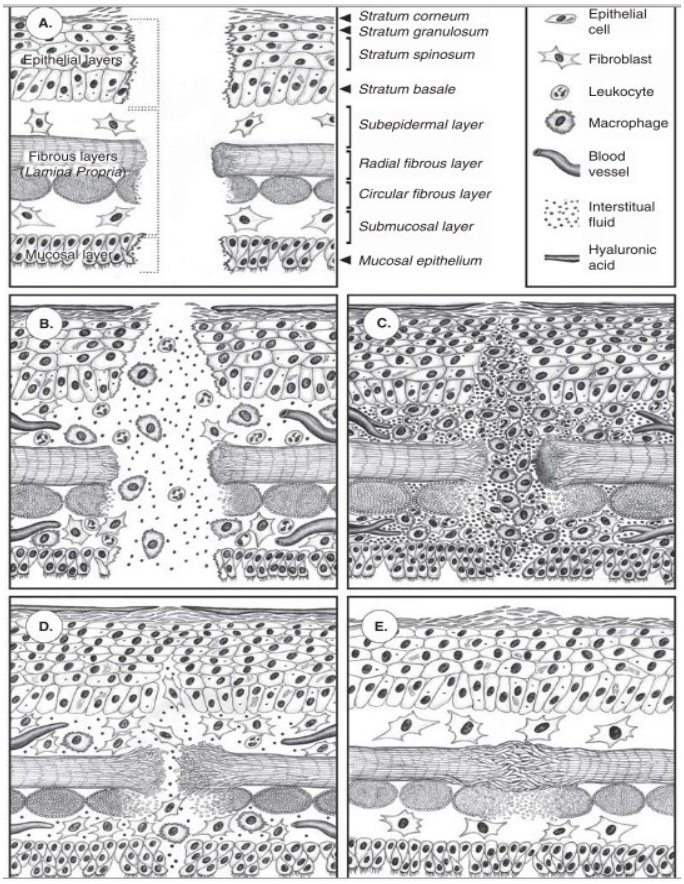

Figure 5: Schematic overview of the TM wound healing process. (A) Three distinct layers of tissue of the TM: outer epithelial, middle fibrous, and inner mucosal layer. (B) Retraction of the perforation margin is supplemented by build-up of exudate and inflammatory cells. (C) The keratin-HA layer functions as a scaffold for migrating epithelial cells, and HA also attracts inflammatory cells to the wound site. (D) The outer epithelial layer is the first to close followed by the mucosal layer. (E) HA creates a better-quality neo-membrane with a well-organised fibrous layer. Reprinted with permission from Taylor & Francis, obtained from [8]. Copyright © 2012; permission conveyed through RightsLink by Copyright Clearance Center, Inc.

During the TM healing process, it is important to avoid dehydration of the wound edges such that the cells that survive the initial injury remain viable to participate in the wound healing process [58]. The prevention of dehydration allows the thickening of the perforation border, which takes around 1-2 days with the use of topical HA instead of 3

days without the use of HA [59]. Through the migratory stage of normal tissue healing, granulation tissue usually develops and serves as a scaffold for re-epithelialization. In comparison, in TM perforation, the squamous epithelium bridges across the perforation first, conducted by a keratin spur. The keratin layer functions as a platform and is thought to be the first to close the wound prior to the epithelial layer and fibrous layer [60], [61]. HA encourages the formation of this keratin layer and forms a film of hyaluronate-keratin, allowing the migration of cells from the squamous epithelium [62]. In comparison to non-injured TM, where migration is from the annulus to the umbo/handle of the malleus, HA stimulates a centripetal migration of epithelial cells [63]. While the keratinocyte layer progression is the most important element in TMP closure, the lamina propria also plays an important role in preserving the functional properties of the TM. The lamina propria is a layer that is made of noncellular connective tissue elements, such as collagen and fibronectin [9]. Sometimes, failure of this layer causes a neo-membrane (i.e., the membrane after healing) consisting of an epithelial and mucosal layer with few disorganized fibrils in between [63]. This results in a flaccid TM which has poor mechanical properties that can further lead to reduced sound conduction and be prone to additional damage. It has been demonstrated that HA can regulate the orientation of the fibroblasts and collagen fibers, leading to minimal scarring [64]. Collagen plays an important role in sound transmission as well [65]. Therefore, improving the middle layer healing improves the functional mechanical properties of the TM, such as vibration. Another important difference between cutaneous and TM wound healing is that in the former, mitotic activity is highest at the wound edge, while in the latter, there is an insufficiency of proliferative cells in the basal layer at the TM wound borders and the proliferation occurs at a site distal from the injury

[65]. The TM regeneration centers have been identified to be in the handle of the malleus (also known as manubrium of malleus) and the annulus [66]. However, immunohistochemistry studies demonstrated high concentrations of HA at both the aforementioned regeneration centres, as well as at the margins of the TMP [66]. The wound edge of the TMP is suspended in air, therefore no underlying tissue matrix is available to support the regenerating epithelium and migrating vessels. Hence, exogeneous HA is expected to provide extra support as it is part of the ECM and plays a significant role in the TM wound healing process.

1.6 Collagen Type I Fibers

Type I collagen (ColI) is the most abundant protein in all vertebrates, making up 90% of collagen in the human body [67]. It assembles into fibers that form the structural and mechanical matrix of connective tissue, skin, and bone. The main function of ColI is to give the tissue resistance to force [68]. This type of collagen also plays an essential role in skin wound healing, since it replaces collagen III during the remodeling phase, forming a provisional framework for cell ingrowth. It has been demonstrated that the expression of ColI significantly increases on the third day after a TM injury and levels remain high up to the end of the observed period [69].

ColI presents specific motifs that promote interaction with diverse families of receptors, including integrins, mannose family receptor uPARAP/Endo180, discoidin domain receptors DDR1 and 2, OSCAR, GPVI, LAIR-1 and G6b-B of the leukocyte receptor complex (LRC) [70], as shown in Figure 6. This provides a biological template that favours cell attachment and promotes chemotactic responses [71]. The presence of those motifs allow collagen to promote cell adhesion better than other materials such as

HA [72]. ColI has shown excellent biocompatibility, biodegradability, bioactivity, and cytocompatibility. Due to the above-mentioned characteristics, it is one of the components that is integrated into many wound healing materials. Most of the studies integrate ColI as a solution to coat the wound dressings [73], [74], [75]–[79].

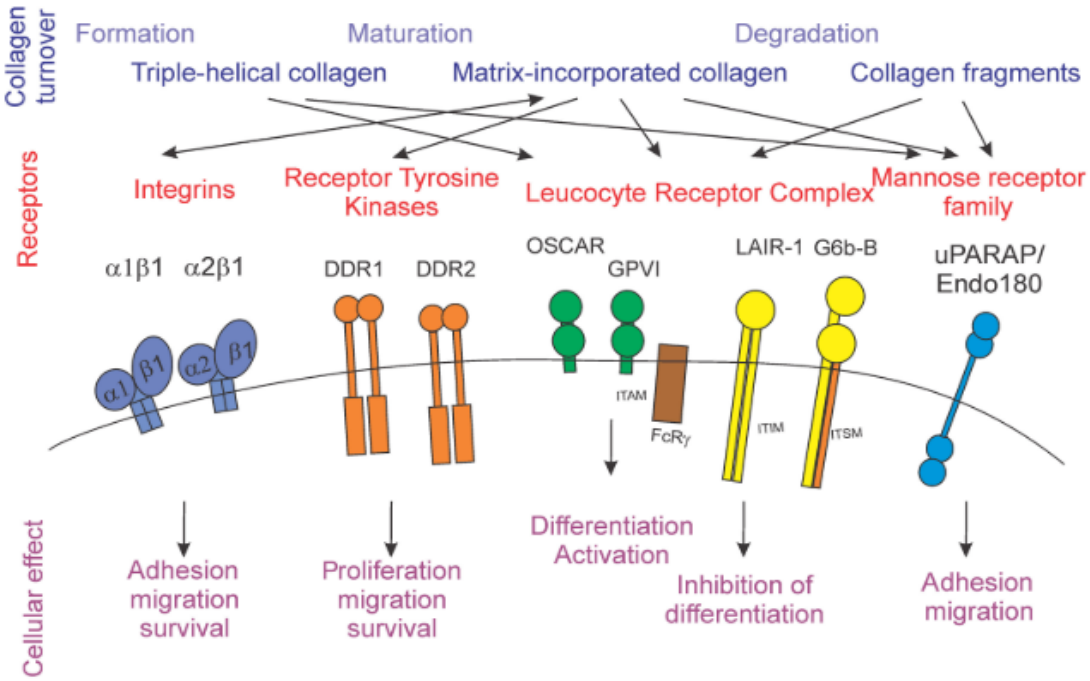

Figure 6: Schematic representation of the stages of collagen turnover showing different forms of collagen (blue), different collagen receptor families (red) and individual receptors, and the cellular outcomes for collagen receptor-mediated signals (purple). Reprinted with permission from Frontiers in Physics, obtained from [70]. Copyright © 2017: https://creativecommons.org/licenses/by/4.0/.

1.7 HA- ColI Scaffold for TMP

Chronic TMP is one of the most common diseases in otology and it has the potential to become a severe problem if left untreated, resulting in recurrent otitis media and loss of hearing. There are treatments available to address this condition, but the materials that are currently employed need to be improved to provide a safer, faster, and a less expensive procedure. HA is a ubiquitous polysaccharide found in the ECM in all stages of wound healing, making it a great candidate for the treatment of TMP. Some of the most important

advantages of this polymer are: i) its versatility, i.e., it can be chemically modified to achieve desired mechanical properties; ii) the ability to absorb water, which is important in TMP because it helps to prevent dehydration of the perforation margin; iii) it is a non-immunogenic molecule; iv) it can moderate inflammation by functioning as a free-radical scavenger and antioxidant; v) it provides a porous structure, which is important because this helps with diffusion of oxygen and nutrients; and vi) it can help to produce a better quality neo-membrane. In otology, HA is widely used as a packing material or as a topical gel [80], [81]. For this project, HA will be used as a scaffold for helping to promote cell migration of keratinocytes. LMWHA is used because, as mentioned in Section 1.4, it tends to promote inflammation, cell proliferation and migration, which are all required for wound healing. To obtain LMWH, HMWHA is hydrolyzed in acid and then crosslinked to slow the degradation time. In addition, some of its properties are modified, such as the capacity for water absorption, malleability, and mechanics. In addition, ColI fibers are produced using an automated method for contact drawing [82] and attached to the HA film surface. This method was selected instead of more common ones, such as electro spinning or wet spinning, since contact drawing is inexpensive and possesses other advantages that will be further explained in Chapter 5. The use of these ColI fibers provides additional adhesion sites for cells to increase attachment to the material and help to promote cell migration across the TMP. Additionally, the ColI fibers may encourage the creation of a more stable neo-membrane, since, as mentioned before, occasionally the fibril layer of the TM fails to regenerate, leaving the repaired membrane with poor mechanical properties that affect its function. Importantly, the use of collagen in the form of fibers was selected, as fibers are the natural form factor into which ColI molecules assemble; this provides topographical

cues to the cells. This is a novel approach that, to the best of my knowledge, has not been used before in TM wound healing or in wound healing in general.

As mentioned above, the overall goal of this project is to develop a scaffold comprising an HA crosslinked film with attached ColI fibers for TMP repair. The first objective was to crosslink the HA to reduce the swelling of HA and slow its degradation time to produce a material that can be used in TMP treatment. To this end, I determined the optimal HA chemical crosslinking reaction and the best fabrication method to produce an HA film. I interacted with an otolaryngologist and observed a tympanoplasty surgery to gain a better understanding of the requirements for the material. With those requirements in mind, I then characterized the crosslinked HA film to assess the degradation and swelling profiles as a function of the chemical crosslinking process.

The second objective was to use ColI fibers to provide topographical and biochemical cues to promote cell attachment, as well as enhance migration of cells from the wound margin. To accomplish this, I functionalized the HA film with ColI fibers, which required an optimization of the procedure to attach ColI fibers to the HA film. Furthermore, tensile properties were examined to ensure adequate properties for surgical handling. Afterwards, I performed *in vitro* experiments to assess cytotoxicity, proliferation, attachment, and migration of N/TERT keratinocytes on the HA-ColI scaffold.

1.8 HA-ColI Scaffold Design Requirements

A novel crosslinked HA-ColI scaffold needs to fulfill specific requirements, e.g., surgical handling and biocompatibility. Design criteria were developed in cooperation with otolaryngologist Dr. Paul Hong and after a state-of-the-art literature review on materials

used for TMP repair. Table 1 shows the design criteria, design inputs and rationale for the HA film.

Table 1: Design criteria of HA film for TMP repair.

Design criteria	Design input	Rationale
Biocompatible	The material and by-products of degradation are non-cytotoxic and non-immunogenic.	If the material is toxic, the cells will die.
Components	The selected polymers to create the material should help to promote wound healing.	When the materials are derived from biopolymers involved in wound healing, complete healing is more likely.
Crosslinking	A crosslinking reaction with few steps and reagents is preferred. Additionally, the crosslinker should not possess high toxicity to cells.	A crosslinking reaction with the aforementioned characteristics will be faster and cheaper than having several steps with numerous reagents.
Thickness	A thickness of around 30 µm is desired.	The thickness of human TM is in the range of 30 to 120 µm [11].
Manipulation	The materials should have adequate tensile properties, so they do not break during handling.	When the material is used in tympanoplasty, it will be handled with forceps to bend and place it in the perforation area. The material must also be able to withstand slight tension when removed from the packaging and while adjusting placement.
Transparency	It is preferred that the film to repair the TM is transparent.	Transparency mimics a normal TM and allows a clinician to observe the middle ear [8].
Colour	The HA film should have a colour that makes it easy to visualize.	HA on its own is completely transparent which makes it difficult to see in the ear. The transparency is still important as stated before but adding an extra colour that does not resemble typical body fluids, can make it easier to see the film and manipulate it.

Chapter 2. Chemical Modifications of HA

As shown in the previous chapter, HA has great potential to be used as a scaffold material for TMP repair. However, it cannot be applied in its natural state because it will get degraded within a few minutes and because of its gel-like consistency. For this reason, HA needs to be chemically crosslinked to obtain a stable material that can stay in place while healing of the TM takes place. Moreover, the crosslinking can help to achieve desired mechanical and swelling properties, i.e., the stress and strain the material can handle as well as how much water it is able to absorb.

Here, a double crosslinking was selected to obtain a HA material with desired properties (stable for at least 14 days and not much swelling, as will be discussed in chapter 4). The first analyzed alternative was polyethylene glycol diglycidyl ether (PEGDE) as the first crosslinker and tannic acid (TA) as the second one. This combination proved to no show the necessary outcome, i.e., the films were not stable under immersion in PBS and they swell a lot. Thus, a second approach was conducted with PEGDE and itaconic acid (ITA).

2.1 Chemical Crosslinking with PEGDE and TA

There are several different chemical modifications possible for HA [83] but for the application proposed here, the modification described by Lee et al. [84] was initially selected (Figure 7). This chemical modification involves covalent and physical crosslinking using two different crosslinkers, PEGDE and TA. In the first crosslinking reaction, the hydroxyl groups of HA and the epoxide groups of PEGDE react to form ether groups upon an increase in pH [85]. This reaction is carried out in solution. The second crosslinking reaction is carried out on the solid crosslinked material using TA to form

hydrogen bonds that stabilize the HA and PEGDE network. This second crosslinking reaction relies on diffusion of the crosslinker and allows the materials to be cut to shape and/or contoured before crosslinking. TA is a natural occurring polyphenol found in plants and fruits, which exhibits antibacterial, antioxidant, and anti-inflammatory properties, offering additional potential advantages as a crosslinker [86].

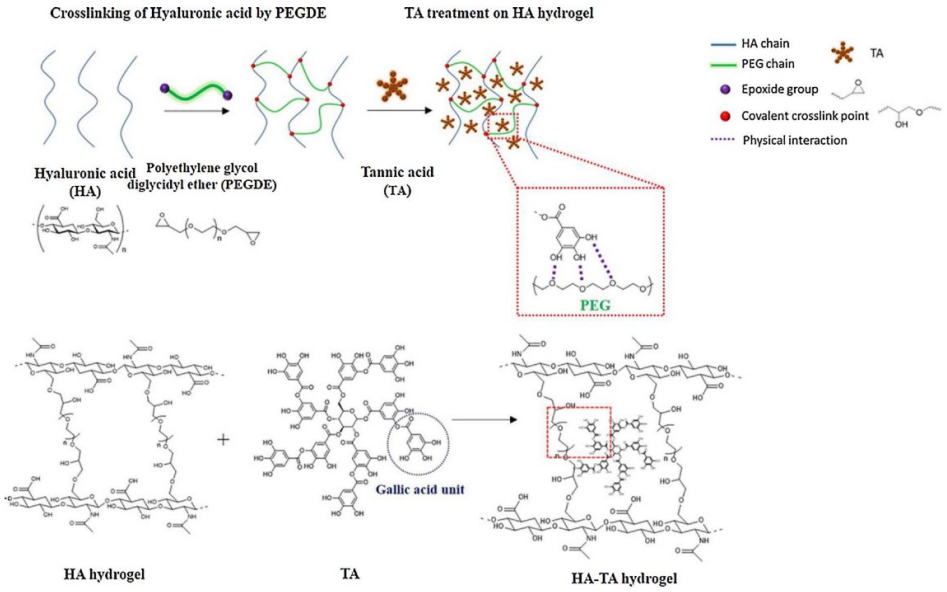

Figure 7: Schematic illustration of HA-PEGDE-TA synthesis with the interactions between PEG and TA. Reprinted with permission from Elsevier, obtained from [84]. Copyright © 2018; permission conveyed through RightsLink by Copyright Clearance Center, Inc.

The dual crosslinking reaction using PEGDE and TA was selected because it is relatively simple and requires fewer steps and reagents, making it also less costly. Furthermore, the study by Lee et al. [84] suggested an improvement in cell attachment and proliferation without any cytotoxicity making it an ideal candidate for wound healing applications. The crosslinkers used here are also less toxic than other commonly used crosslinkers, e.g., glutaraldehyde and 1,4-butanediol diglycidyl ether (BDDE) [87]. Furthermore, the resulting material is transparent and somewhat adhesive, offering potential advantages for monitoring the middle ear and in surgical placement, respectively.

I adapted and optimized this established crosslinking protocol by Lee et al. [84] for generating a thin material for TMP repair, the design criteria for which are shown in Table 1. The optimization targeted increasing the degree of crosslinking and reducing the difficulty of getting the reagents properly mixed in the reaction.

2.1.1 Materials and Methods

The protocol of Lee et al. [84] deploying PEGDE (average M_n 2,000) and TA as crosslinkers consisted of using an HA concentration of 2% w/w, with a crosslinking ratio between HA and PEGDE of 2:1. Distilled water was used as the solvent for all the solutions that were prepared here and the temperature for all the steps was set to 20ºC (room temperature). For the second crosslinking reaction with TA, five different TA concentrations were examined: 0, 0.05, 0.1, 0.15 and 0.2% (w/v).

First, HMWHA was dissolved overnight in 0.3M NaOH. The purpose of this step was to activate the hydroxyl group of HA to form ether bonds with PEGDE [88]. For preparing a 15 mL reaction, 300 mg of HA (~$1.5 - 1.8 \cdot 10^6$ Da, Sigma-Aldrich) was dissolved in 15 ml of a mix of distilled water and NaOH (to obtain a solution of 0.3M NaOH). The solution was left to mix overnight. Next, 748 mg of PEGDE was added to the HA solution while the solution was mixed vigorously at 600 rpm. The solution was mixed at 600 rpm for another 30 min, and after that, it was mixed at 60 rpm for 24 h. Next, the HA-PEGDE hydrogels were cast in a cell culture plate for one day at RT to be washed with NaCl for removal of any remnant reactants. Then, five different solutions (40 mL each) were prepared using distilled water and TA (0% w/v, 0.05% w/v, 0.1% w/v, 0.15% w/v and 0.2% w/v TA). The HA-PEGDE hydrogels were then divided in 5 different containers

to immerse them in each 40 mL TA solution for two days. Finally, the double crosslinked hydrogels (HA-PEGDE-TA) were washed with phosphate buffered saline (PBS).

2.1.2 Results

Following the protocol of Lee et al. [84], there were issues with using an HA solution of 20% w/w. It was not possible to mix the solution with the other reactants and the resulting hydrogels were heterogeneously crosslinked, as suggested by the heterogenous colouration of the materials (white opaque and brownish transparent regions), as shown in Figure 8A for a hydrogel crosslinked with 0.1% w/v TA. Therefore, I decided to lower the concentration of HA. The concentrations I tried were 15, 10, 5, and 2% w/w HA. The resulting hydrogels showed that without modifying other factors (e.g., ratio of HA to crosslinker, pH, temperature, etc.), the lowest concentration of HA that was able to form hydrogels was 15% w/w. A lower concentration resulted in the complete dissolution of the material when it was immersed in water or PBS. At this point, using 15% HA showed the same results as the previously reported protocol. Nevertheless, the resulting hydrogels were not optimal for application in TMP repair, i.e., the hydrogels increased in weight by 40-fold due to water uptake which resulted in swelling, and they were too fragile, as they broke just by trying to hold them with tweezers.

Four different TA concentrations were used: 0.05%, 0.1%, 0.15% and 0.2% w/v. Lee et al. showed that having a higher concentration of TA increased the crosslinking density, as shown by a reduction in swelling. However, as shown in Figure 8, in my adaptation of the crosslinking protocol, the main difference that the concentration of TA made was a change in colour (going from a yellowish colour to a brown colour) with increasing TA concentration. The degree of swelling also decreased, but not to an extent

that would allow the material to be used for repairing a TMP. I also observed that with a higher concentration of TA, the material became more brittle.

The next modification to the protocol to deal with the stability, swelling, and brittleness issues was to increase the ratio of PEGDE to HA and change the way PEGDE was added to the HA solution. In my initial attempts, PEGDE was added in powder form, which resulted in non-uniform crosslinking of the HA and may explain why the material dissolved when placed in water. To overcome this issue, I dissolved PEGDE in water and then added it to the HA with vigorous stirring (more than 400 rpm). Furthermore, by having molar ratios of 2:1 and 1:1 of HA:PEGDE, the concentration of HA solution could be decreased to 2% w/w and still form stable hydrogels that did not break when handling with tweezers or dissolve in water (Figure 8B and C). Importantly, I also decided to increase the degree of crosslinking of the HA to reduce the swelling of the material. However, the material still swelled more than desired.

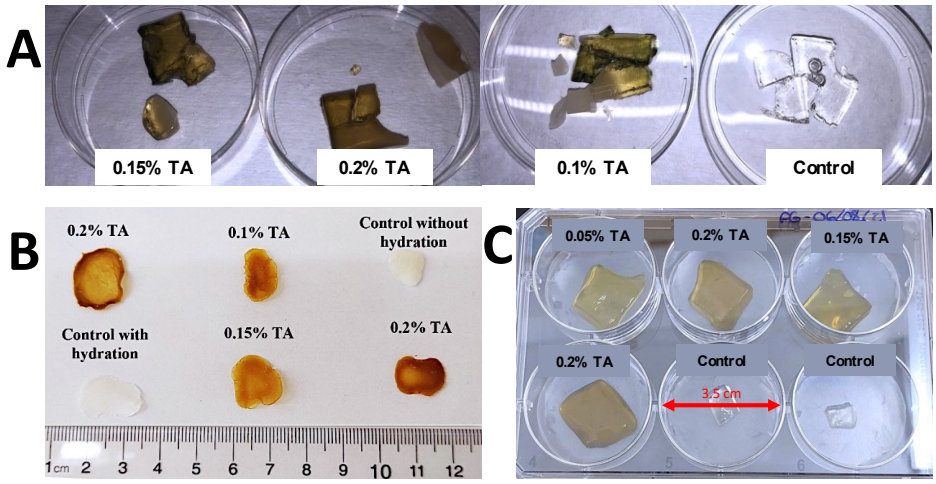

Figure 8: HA crosslinking with PEGDE and TA. A) I followed the protocol of Lee et al. without making any modifications to it. Samples were formed from 20% w/w HA with a HA:PEGDE ratio of 9:1. B) and C) have 2% w/w of HA and a molar ratio of HA:PEGDE of 2:1. B) Dried samples with different concentrations of TA. C) Hydrated samples with different concentrations of TA. The red line indicates the diameter of each well. The controls in this figure are HA hydrogels crosslinked only with PEGDE.

I evaluated the crosslinking reaction based on qualitative visual and mechanical criteria, i.e., if the material was homogeneous, held its shape, changed in size after immersion in water, and could be handled with tweezers. After this qualitative evaluation, a deeper and quantitative characterization was done, as presented in Chapter 4.

2.1.3 Crosslinking only with PEGDE

Since the visual and quantitative data obtained by crosslinking HA with PEGDE and TA did not fulfill the design criteria stated in Table 1, I began exploring different chemistries that could be used for the fabrication of a crosslinked HA film. As without the use of TA the hydrogels were not brittle, nor did they degrade after immersion in water or PBS, I performed crosslinking just using PEGDE with a 2% w/w HA solution and with a molar ratio of 2:1 HA to PEGDE. The results of this experiment showed that the material was stable under water immersion. However, the hydrogel was soft (almost like a slime) and difficult to manipulate (Figure 9).

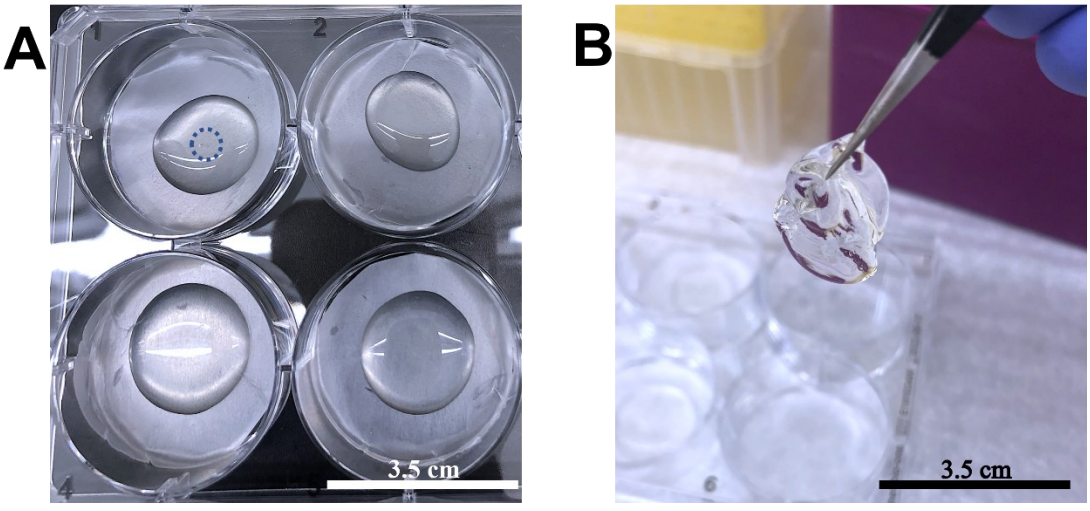

Figure 9: 2% w/w HA crosslinked with PEGDE. A) Hydrogel after 3 days of hydration. The blue dashed circle in the first well represents the initial size of the HA-PEGDE hydrogel. B) Handling of the hydrogel with tweezers.

2.2 Chemical Crosslinking with PEGDE and ITA

In the search for how to improve the crosslinking reaction, a decision was needed whether the chemistry and selected crosslinkers should be changed completely or if just a part of the reaction scheme should be changed. As was shown, using PEGDE alone for crosslinking was not sufficient, but keeping it was crucial as will be discussed in Section 2.3.3. Therefore, I looked for other possible secondary crosslinkers that could help to reduce the swelling of the hydrogels. The features I was looking for in this second compound were that it was nontoxic, biodegradable, inexpensive, and, if possible, that it had some bioactivity related to wound healing, meaning a compound that could regulate inflammation or infection. This investigation led me to the study conducted by Calles et al. [89] where they crosslinked HA with PEGDE and itaconic acid (ITA). I selected this approach because they were already implementing some of the optimizations I made to the protocol for HA-PEGDE-TA, such as having an HA concentration of 2% w/w and a molar ratio of HA/PEGDE similar to what was working best for me (2:1 HA to PEGDE). The only issue with the approach of Calles et al. was the lack of explanation of what the role of ITA was in the crosslinking, and what properties this organic acid had. However, in other literature, it was reported that this compound is biodegradable and non-toxic, and due to its carboxylic groups (Figure 10), it can participate in esterification reactions with compounds that have hydroxyl groups [90], such as HA.

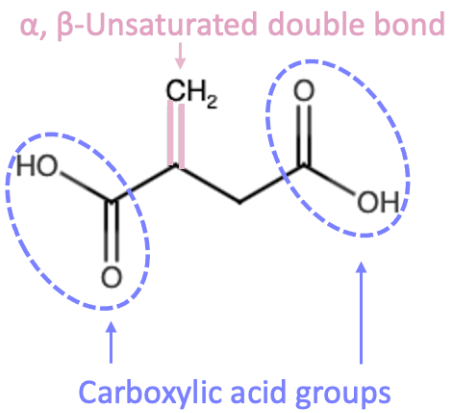

Figure 10: Chemical structure of itaconic acid. Created using Chem-Space.

The chemical modification first presented by Calles et al. is as follows. Briefly, the hydroxyl groups of HA react with the carboxylic groups of ITA to form ester bonds. The addition of ITA lowers the pH, which later affects the crosslinking of PEGDE with HA-ITA and promotes formation of ester and ether bonds between PEGDE with HA [88]. Both crosslinks are carried out in solution. Since all the reagents are dissolved together in water, a homogeneous crosslinked material is formed.

2.2.1 Materials and Methods

To start, HMWHA must be dissolved under acidic conditions. Although the purpose of this step is not mentioned by Calles et al., the dissolution in acidic conditions greatly decreases the viscosity of the HA, making it easier to work with and ensuring a soluble end-product, in addition to helping to activate the hydroxyl groups of HA. The activation occurs due to the deprotonation of this group, imparting a negative charge, and thus, promoting ester bond formation [83]. Initial hydrogel synthesis attempts without preceding dissolution in acid solvent all resulted in heterogeneous end products. As I sought to form extremely thin hydrogels using this reaction, from this point on, the hydrogels will be referred to as films. In the optimized protocol, the HA-PEGDE-ITA film

was synthetized from HA-PEGDE-ITA solutions using distilled water as a solvent and all the steps were carried out at room temperature (20ºC). HA was used at a concentration of 2% w/w and the amounts of reagents were adjusted to obtain 1:2:1 molar ratios of HA:PEGDE:ITA. The materials were prepared in 15 mL batches.

The amounts of each reagent used in the crosslinking reaction were as follows: 97.33 mg of ITA (Sigma-Aldrich) dissolved in distilled water (12 ml of the 15 ml total reaction volume). Once the ITA was completely dissolved and after 30 min of stirring at 120 rpm, the pH was 2. Then, 1 drop of blue food colourant (trodat ® Colour 7011, used only for film visualizations) was added and the solution was mixed for 10 min. The addition of colourant did not change the pH. Increasing the agitation of the solution to 200 rpm, 300 mg of HA ($\sim 1.5 - 1.8 \cdot 10^6$ Da, Sigma-Aldrich) was then added slowly. The solution was stirred until a homogeneous gel-like material formed, which took around 30-40 min. After this step, the pH increased to 3.2. Next, in a separate container, 2993 mg of PEGDE (average M_n 2,000, Sigma-Aldrich) was dissolved in the remaining distilled water (3 ml). This last step needed to be done under agitation, either by using a vortex mixer or using a magnetic stir bar with the maximum agitation possible from the stirring plate. After the PEGDE was completely dissolved (after around 20 min of agitation), it needed to be added slowly to the HA-ITA solution. Again, the agitation of the stirring plate was set to its maximum. When all the PEGDE solution was incorporated, the HA-PEGDE-ITA solution was held at maximum agitation (600 rpm) for 1h and the pH increased slightly to 4.1. After 1h, the agitation was reduced to the minimum (60 rpm), and the reaction was left to proceed for another 24 h. Even though the pH of the solution at this point was still acidic, subsequent washing steps increased the pH to the physiological range, while removing any

unreacted compounds from the HA-PEGDE-ITA material. Washing was done after film fabrication as described further in Chapter 3.

2.2.2 Results

The protocol using ITA [89] did not need much additional optimization beyond what was performed previously for TA. The main difference was that before I was working with a ratio of 2:1 HA to PEGDE, and in the study done by Calles et al. the molar ratio was 1:2. In the case of ITA, the molar ratio to HA was 1:1. I also tried to modify this ratio to determine if the material properties changed, but I did not observe any dramatic differences in mechanical properties as a function of molar ratio of HA to ITA. For this reason, the molar ratios were kept as described in the Calles protocol. The results of adding ITA to the HA-PEGDE solution are shown in Figure 11. The initial evaluation was based on homogeneity, change of shape after immersion in water, and if in general the shape that was produced at the end of the reaction was retained. As can be observed from Figure 11, the HA-PEGDE-ITA film was completely transparent and homogeneous, and the shape was restored even after manual bending. Besides this, the mechanical criteria, i.e., if the material could be handled with tweezers, was assessed, and the results showed that the film did not break or fall apart when handled by tweezers as would be necessary for surgical placement. Blue food colourant (as seen in Figure 11B) allowed visualization of the material (again important for surgical placement) with no noticeable effect on handling properties or homogeneity. To achieve a homogeneous colour, the best point to add the colour was after dissolving ITA in water.

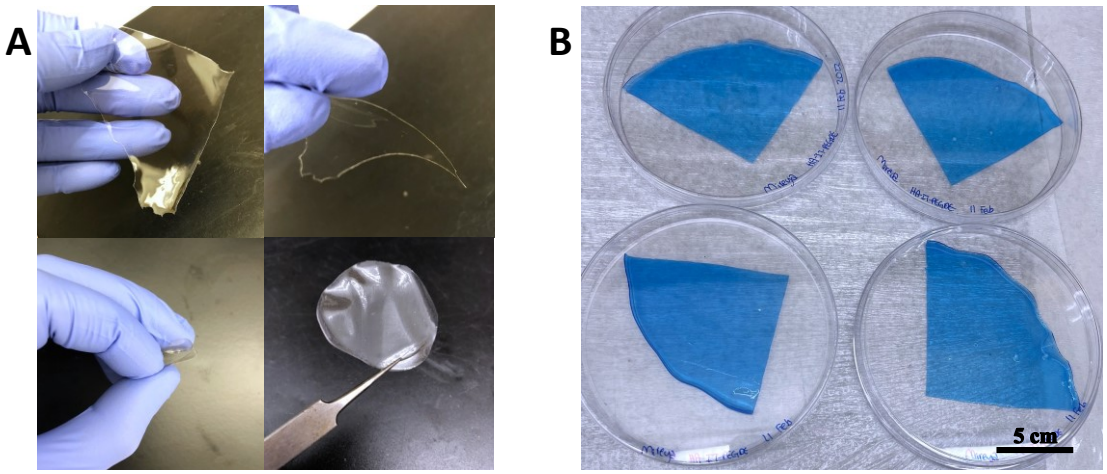

Figure 11: HA crosslinked with PEGDE and ITA. A) Spin processed and solution cast films dried after washing to remove unreacted compounds. Films are transparent, flexible, and possible to handle with tweezers. B) HA-PEGDE-ITA films with addition of blue colour.

2.3 Discussion

2.3.1 HA Crosslinked with PEGDE and TA

The first crosslinking reaction was done with PEGDE and TA as described by the protocol of Lee et al [84]. This was chosen based on the reported improvement of cell attachment and proliferation without any cytotoxicity as well as the simple and less costly procedure.

Some limitations were observed for the established protocol from Lee et al., such as weakness and brittleness of the material, meaning that it broke easily when handling (Figure 8A). Additionally, the hydrogel absorbed too much water, increasing its weight by at least 40 times compared with the completely dried form, which was not suitable for TMP repair because it made the hydrogel lose its shape. The last issue was how difficult it was to get the reactants mixed, since Lee et al. used a HA solution of 20% w/w. To overcome these limitations, first, I increased the degree of crosslinking in an effort to improve the mechanical properties of the material and reduce the swelling since the material would

have fewer hydrogen bond donors/acceptors available to bind water when covalently crosslinked [91]. This was done by increasing the ratio of crosslinking agent to HA. The protocol of Lee et al. used a ratio of 9:1 HA to PEGDE, and I explored modifying it to 2:1 and 1:1. This was decided based on literature precedents showing that a more stable hydrogel can be obtained with those ratios (i.e., a hydrogel that swells less and takes longer to degrade) [85], [89], [92], [93]. Finally, I decided to decrease the concentration of the initial HA solution from 20% to 2% w/w to make mixing of the solution easier. Furthermore, previous TMP repair studies have shown that ~2% w/w HA helps to close the injury faster than lower concentrations of 1% w/w [94]. Since the swelling was still too high (Figure 8B), adding a hydrophobic moiety by conjugation reaction to reduce the swelling was considered for the next set of experiments (Figure 8C). Some possible moieties that were considered included octadecylamine (ODA) [95] , itaconic acid [89], 3,3'-dithiobis (propionic hydrazide (DTP) [96], octenyl succinic anhydride (OSA) [97] or 1,6.diaminohexane [98].

2.3.2 HA Crosslinked with PEGDE and ITA

The formation of ester and ether bonds in HA using PEGDE and ITA produced an HA film that was stable in water and could also be handled with tweezers without breaking it (Figure 11A). The chemical modification occurred on the hydroxyl groups (-OH) of HA. In the first instance, the carboxylic acid groups (-COOH) of ITA react with the -OH of HA by forming ester bonds in a condensation reaction between those two functional groups [90], [99]. At this point, the solution is under acidic conditions, and, even though ITA is reacting with HA, the conditions lead to the formation of ester and ether bonds with the epoxide groups of PEGDE and the -COOH and -OH of HA, respectively. The ester

bonds formed between the epoxide group of PEGDE and the hydroxyl group of HA are the first to be formed because of the acidic conditions with a pH ~3 [88]. After the reaction is let to mix for a while, the pH increases to 4.1, which promotes the formation of ether bonds between the -OH group of HA and the epoxide ring of PEGDE [100]. The ability to form two different types of bonds depending on the pH is an important advantage of PEGDE as a crosslinker. In conjunction, the selected chemistry that was first presented by Calles et al. promotes the formation of bonds (i.e., ester and ether bonds) that are stable in physiological conditions of the dermis [101], which is ideal for a biomaterial used for healing the TM.

The addition of blue colour to the film to be able to visualize the HA-PEGDE-ITA material more easily was selected so as not to be confused with signs of infection, an open wound, or the colour of the earwax (Figure 11B). Consequently, red, yellow, brown, etc. colours were not explored. The next step was to select which dye would be the best option, and a couple of options were available, such as Coomassie brilliant blue and food colouring. Food colouring was selected as it is better to have a dye that does not interfere in the chemistry of the material and is unlikely to have toxic effects on cells. The best point at which to add the colour was at the beginning of the reaction, just after dissolving the ITA in water. If added after the crosslinking, the colour was not homogeneous.

2.3.3 Choice of Chemical Modification

Several chemical modification schemes have been described for the crosslinking of HA into an hydrogel or film for biomedical applications, including Diels-Alder crosslinking [102], enzymatic crosslinking [74], thiol-modified crosslinking [103], and photo-crosslinking [104]. All available options have some desirable features, but many of

them require several steps for the chemical modification and involve the use of numerous different reagents and time-consuming processing steps. Therefore, a reaction that was simple with only a few steps and reagents was preferred. The first step was then to decide what type of bonds I wanted to form. Ester and ether bonds were selected, since, as mentioned, these are stable under physiological conditions in the skin [101], which is desirable for materials that will be used in wound healing applications. The formation of these bonds can also be relatively easily achieved based on the chemical structure of HA [99]. PEGDE was the first crosslinker I found to fulfill these requirements.

PEGDE is a homobifunctional highly water-soluble crosslinker for amine, hydroxyl, and carboxyl functional groups. It is composed of two epoxy terminal groups with a long polyethylene glycol (PEG) chain between them [105]. It has been shown to produce HA films with higher stability than other commonly used crosslinkers, e.g., glutaraldehyde, divinyl sulfone and BDDE. Additionally, PEGDE presents less cytotoxicity than the previously mentioned crosslinkers [87], an important feature for any material that is intended to be used for medical applications. It also has been demonstrated that films or hydrogels crosslinked with PEGDE present better mechanical performance than those crosslinked with glutaraldehyde, due to better elongational properties, higher plasticity and stability in water [85], [89]. The PEGDE structure with long flexible PEG chains can mitigate the effect of polymer rigidity that other crosslinkers have [92], and, as was shown in the results here, the HA material that was crosslinked with PEGDE was flexible. This behavior is not common when crosslinkers are applied to HA. For example, when using a crosslinker like glutaraldehyde, the material becomes rigid, and consequently, brittle, making it necessary to add a plasticizer in order to obtain a more

ductile material [106]. Furthermore, as explained before, PEGDE can form ether links with the -OH groups of HA in solutions that have a pH of 4 or higher, and in more acidic conditions (pH of 3 or lower) it forms ester bonds via the COOH- group of HA [88].

The second selected crosslinker was ITA, an organic acid that consists of two COO- functional groups and one α, ß-unsaturated double bond. Its composition makes it a suitableprecursor for numerous chemical transformations. Some of the reactions that ITA can promote and participate in are esterification, addition, and polymerization [107]. As was already explained, when ITA reacts with HA, ITA COOH- groups form ester bonds via the OH-groups of HA. In addition to being able to crosslink HA, ITA is inexpensive, non-toxic, biocompatible, and bio-degradable [108], and can regulate inflammation and response to infection [109]–[111]. Calles et al. previously demonstrated that HA formulations crosslinked with ITA had the lowest swelling ratio (compared to HA crosslinked only with glutaraldehyde), which suggested that ITA increased the degree of crosslinking between HA chains. This was exactly what I was looking for, because when crosslinking HA only with PEGDE, the material did not dissolve in water but still absorbed several folds its weight in water.

2.3.4 Protocol Optimization

The optimizations I carried out for the HA-PEGDE-TA chemistry were based on factors that influence the degree of crosslinking because this influences the nature of the final product. One factor is the form of the HA starting material employed, i.e., how the reaction will be carried out. This can be in a homogeneous format using HA as solution or a heterogeneous one using HA as a hydrogel/film [84]. Other important factors are the concentration of HA [93] , the molar ratio of crosslinking agent to HA [100], [112], [113],

the reaction time, temperature, and pH [114]. Since there were problems mixing the reaction due to the high concentration of HA (20% w/w), as shown in Figure 8A, it was decided to lower the concentration to 2% w/w [115]. The next change was the molar ratio of HA to PEGDE. Reading studies that also used this crosslinker, I found that the most common molar ratios used for biomedical research and applications were of 2:1 HA to PEGDE or vice versa [89], [101], which was demonstrated to increase the crosslinking because the materials became more stable and absorbed less water when they were immersed in it. These modifications improved the product of HA-PEGDE-TA (Figure 8B and C) but limitations (e.g., heterogeneous crosslinking and brown colouration similar to ear wax) were still present requiring me to consider replacing TA with ITA.

Even though the second crosslinking method I followed [89] to produce HA-PEGDE-ITA films did not need much additional optimization, the optimization I made using TA helped me to know the best methods to conduct the reaction, i.e., how to mix the reagents properly and in which order. It also helped me to decide which concentrations I wanted to work with, and at the end of this analysis, I decided to use the HA-PEGDE-ITA crosslinking approach first described by Calles et al., which fulfilled the design criteria listed in Table 1.

Chapter 3. Fabrication of an HA Film

Once an appropriate chemical crosslinking method was selected, the next step was to determine which fabrication method would be best to produce crosslinked HA films. The shape of this film was intended to mimic the native human TM. Figure 1 shows that the TM is a thin and transparent piece of tissue that looks like a film. Hence, I started to investigate which methods could be used to make a film from the crosslinked HA materials. The three options I had available to me were solution casting, spin coating, and three-dimensional (3D)-bioprinting as shown in Figure 12.

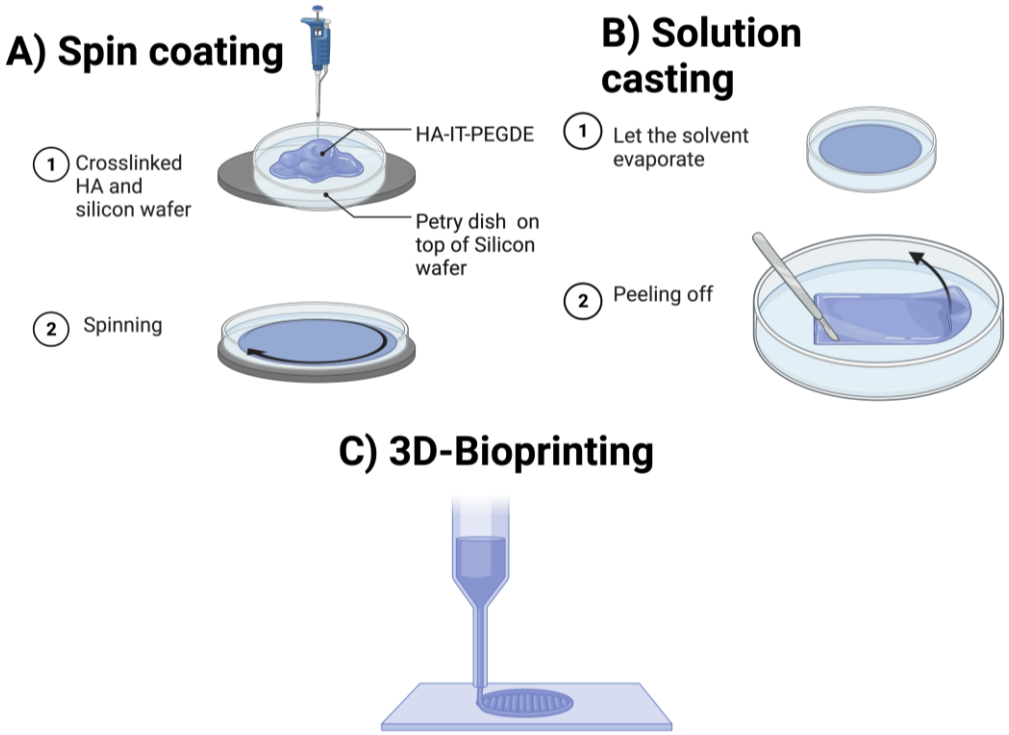

Figure 12: Schematic illustration of the possible fabrication methods to produce an HA-crosslinked film. A) Spin coating, where the required equipment is a spin processor to spin a flat substrate at a specific velocity and acceleration. B) Solution casting, the simplest of the methods because it just consists of placing a solution in a mold to then let the solvent evaporate. C) 3D-bioprinting, a method that requires a 3D bioprinter but is able to produce a specific shape that can be designed using computer programs. Created with BioRender.com

3.1 Solution Casting

Solution casting was the simplest of the three approaches and can make films in a shorter time than other methods. Solution casting is also low cost and has easily reproducible reaction conditions [116]. It consists of dissolving a polymer (e.g., crosslinked HA) in a solvent (e.g., water). The first step is to place the solution into a predefined 3D mold or on a simple carrier substrate, and then the solvent is allowed to evaporate to create a solid layer on the mold/carrier [116]. The resulting cast layer can then be peeled away to produce a standalone film. A possible limitation of this method is that the film can vary in thickness across its surface.

3.2 Spin Coating

Spin coating is based on the same principles as solution casting. The polymer to be deposited is also in solution. The substrate, usually a silicon wafer or a glass cover slip, is held by vacuum on a chuck. The solution is then placed on top of the substrate, which is rotated at an adjustable speed [117]. The solution spreads over the surface due to centrifugal forces, which also causes some of the solvent to evaporate. As a result, a thin film is formed on the substrate. Here, the thickness of the film can be determined by adjusting parameters such as rotation speed, acceleration, spinning time, the amount of the film-forming solution, solution density, and solution viscosity. The main advantage of this method is the production of uniform films of thickness in the range of nanometers to micrometers. Nevertheless, having many parameters can complicate analysis of which settings will be necessary to obtain a film of a specific thickness and films with thicknesses greater than a few hundred micrometers can be difficult to achieve. Additionally, this method is not suitable for large-scale manufacturing.

3.3 3D Bioprinting

The last option, 3D bioprinting, is a type of digital additive manufacturing technology that fabricates components layer by layer according to a specific digital 3D model. The central idea of 3D bioprinting is to realize the controllable spatial distribution of biological materials, such as HA, cells, and other active substances to build tissues or organs with highly bio-mimetic architectures and components. Here, the polymer solution containing the cells or biological material is referred to as a "bioink" [118]. This type of fabrication method can create scaffolds with individual customization and precise internal structures and surface features with short production cycles and lead times. The limitations of 3D bioprinting are the expensive equipment and the limited number of available materials that can be printed [119]. Ultimately, 3D bioprinting was ruled out for HA films because the materials far exceeded the viscosity of a typical bioink.

3.4 Materials and Methods

When the reaction of HA-PEGDE-ITA was finished, the magnetic stirring bar was removed from the beaker and the beaker with the solution still inside was transferred to a chamber. The beaker was kept inside the chamber under vacuum for around 1 h. This step was done to remove air bubbles in the HA-PEGDE-ITA solution. Afterwards, the solution was added to a Petri dish of 150 mm in diameter covered on its surface with parafilm (for release of the film in later steps). It is important that the solution is added in the centre of the dish before it starts spreading, and if the solution still has air bubbles, the Petri dish must again be placed in a chamber under vacuum. This last degassing step should not be

carried out for more than 30 min as otherwise the solution starts to dry, making it difficult to manipulate.

The Petri dish with the crosslinked solution was then placed on the chuck and the vacuum of the spin coater (a Laurell-WS-650MX-23NPPB system) was activated to keep the dish in place. Next, the solution was spin processed for 60 seconds at a velocity of 300 rpm with an acceleration of 100 rpm/s. The program was run once, and then the solution was observed for air bubbles. If it had a considerable number of bubbles, they were popped using a pipette tip, and the program was run again. In almost all cases the samples were spun twice with the described program. Once the material looked even and spread, the Petri dish was transferred to a fume hood to let the remaining solvent (distilled water) evaporate. A completely dry film was necessary to obtain a defined shape, and for this 24 h in the fume hood was required.

After the films were completely dry, they needed to be removed carefully from the parafilm to avoid cracking. Once the films were removed, a wash was done to remove unreacted compounds. The wash consisted of placing the HA-PEGDE-ITA films in a Petri dish containing distilled water. Then, the dish was transferred to a Benchmark-Orbi-Blotter™ and shaken at the minimum setting (around 10 rpm) for 30 min. Afterwards, the present distilled water was discarded, and the wash was repeated twice, before a final wash with PBS.

3.5 Results

Results for solution casting and spin coating of HA crosslinked film are shown in Figure 13. The first method that was tried was solution casting as it was the simplest and fastest method. These advantages were useful when I was optimizing and selecting which

chemical crosslinking method would be best for the film. In Figure 13A, HA-PEGDE-TA was cast in a 6-well plate with the surface of each well covered in parafilm to aid the release of the material. A uniform material was not produced by the solution casting method, mainly due to the high viscosity and stickiness of the crosslinked material. This was a property specific to TA crosslinking, as TA is known to be adhesive even after it interacts with PEGDE [120]. Moreover, when the HA-PEGDE-TA material was dried, as shown in Figure 8B, it remained uneven and adopted unpredictable shapes.

The HA-PEGDE-ITA solution was also highly viscous. However, it had a consistency that was gel-like instead of a sticky slime (which was the case for HA-PEGDE-TA). Figure 13B shows the materials in a Petri dish covered with parafilm after casting. The material was not uniform because I tried to press it with a flat heavy object (a beaker containing Drierite desiccant) to produce a thinner flat film. As can be seen, this method did not work because when I removed the beaker, some parts of the film were pulled away creating an uneven surface. The second fabrication method I tried was spin processing, shown in Figure 13C and Figure 13D. This method produced a circular and uniform film. However, after spinning was complete the solvent was not completely evaporated (Figure 13D). For this reason, the material needed to be placed in a fume hood for 24 h and then washed to obtain a flat film, as shown in Figure 11B. The wash was important because unreacted compounds remaining in the film can lead to undesired texture, as seen in Figure 13C, and potentially cause cytotoxicity. Importantly, the use of the parafilm cannot be eliminated because even though it is possible to form an even shape without it, it is almost impossible to peel the materials from a Petri dish without breaking them.

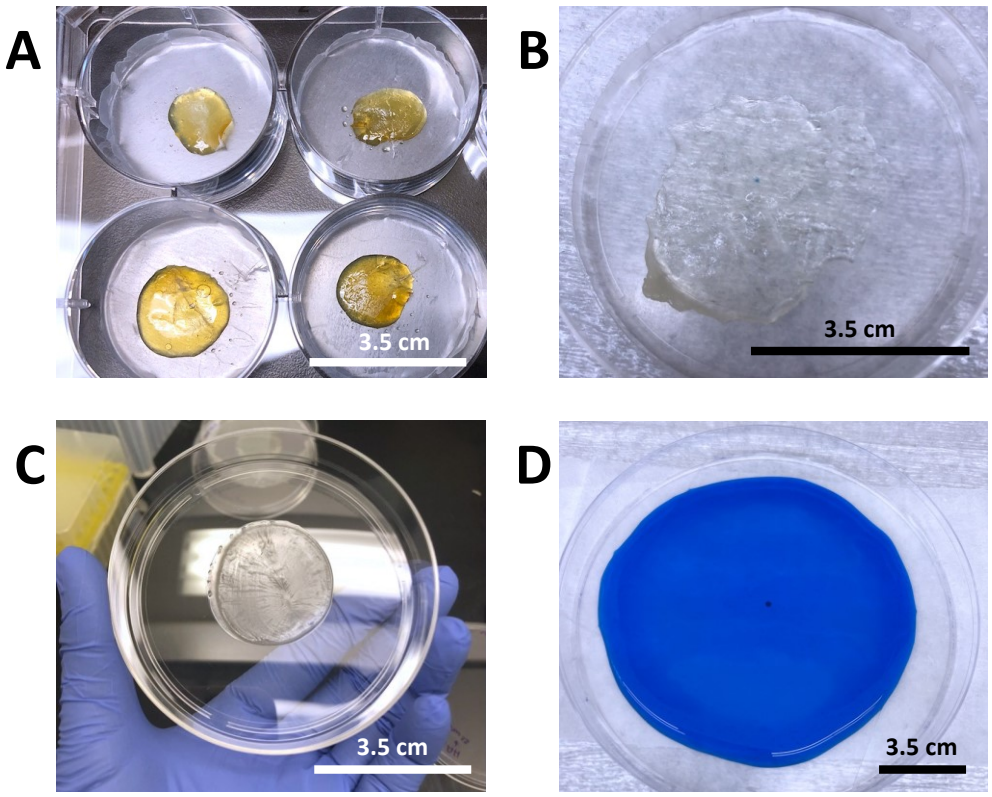

Figure 13: Solution casting and spin coating of HA crosslinked films. A) HA-PEGDE-TA hydrogels cast on a 6 well plate. B) HA-PEGDE-ITA film without addition of colour cast on a Petri dish. C) Spin processed HA-PEGDE-ITA film after drying for 24h in a fume hood (without wash). D) Hydrated and coloured HA-PEGDE-ITA film after spin processing.

3.6 Discussion

3D bioprinting is one of the most promising manufacturing technologies in the interdisciplinary field of tissue engineering. Its applications range from the production of artificial skin tissue to other types of organs and more [121]. Advantages of 3D bioprinting include the possibility of achieving high throughput manufacturing, a high level of reproducibility, and a shorter production cycle than other methods [118]. Therefore, it was an exciting option for the production of the HA-PEGDE-ITA film. Using the RX-1 3D-bioprinter from Aspect Biosystems, I tried to print crosslinked HA films. However, this

was not possible because of the high viscosity of the solution and for this reason I eliminated this fabrication method as one of the options for this project.

As noted in the previous section, solution casting was the cheapest and fastest method. This method only required the crosslinked HA solution to be placed in a mold without any extra equipment required. However, due to the high viscosity of the HA solution, it did not produce a thin and uniform film (Figure 13A and B). A thickness similar to the native human TM was the goal, which meant that I needed to form a film of around 30 to 120 μm in thickness [11].

The last method I tried was spin coating, which in theory was the ideal fabrication method because by definition it produces thin and uniform films [122]. The issue with this method was that many different parameters (e.g., amount of solution, viscosity of the solution, velocity of rotation, acceleration, and time) determine the specific thickness of the film. There are available models to predict the film thickness as a function of certain physical parameters [123], for which the viscosity of the material needs to be obtained. To avoid those measurements, I decided to determine the parameters by experimentation. As expected, with lower velocity and acceleration, I could obtain thicker films. With the parameters disclosed in the materials and methods section of this chapter, I obtained an estimated thickness of around 30 μm (Figure 13C and D). Exact thickness measurement of the HA-PEGDE-ITA film will be introduced in the next chapter. Spin processing also allowed me to obtain an HA-PEGDE-ITA film of even thickness across its surface. However, the solvent was not completely evaporated at the applied velocity [117] and the material needed to be completely dry before use.

Thus, a combination of spin coating and solution casting was chosen to produce the final HA-PEGDE-ITA film. By doing so, a uniform and thin film was obtained. Then, by letting the solvent evaporate in a fume hood, the material adopted its final shape, and all that was left to do was washing to remove any unreacted crosslinking reagents.

Chapter 4. Characterization of the HA Crosslinked Film

After the crosslinked HA had been synthesized and the films had been fabricated (Figure 14), material characterization was performed. The goal of the characterization was to determine which formulation was best with respect to the design features described in Table 1. Furthermore, I wanted to further assess chemical composition, water absorption, and degradation to be able to later evaluate if the material had potential to be applied in the repair of a TMP. In this chapter, Fourier transform infrared (FTIR) analysis was used to determine whether the chemical crosslinking worked as desired. I also wanted to determine whether crosslinking HA reduced its swelling ratio and increased its stability in a physiological relevant liquid (such as water or PBS). Therefore, I conducted a swelling analysis to obtain the swelling ratio of the material and a degradation analysis to quantify how much of the material was lost after 21 days in PBS. Additionally, thickness values for the films were measured using a profilometer.

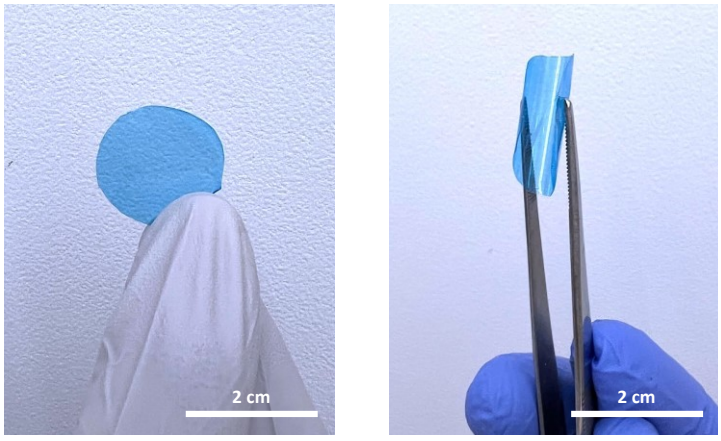

Figure 14: HA-PEGDE-ITA film fabricated by spin coating and solution casting and cut to size. Here the material is in its dried state where it is transparent and flexible.

4.1 FTIR Analysis

To determine the chemical bonds formed during the crosslinking of HA with PEGDE and ITA, FTIR spectroscopy was used. FTIR is one of the most widely used techniques in the characterization of crosslinked biomaterials [83], and is appropriate for films. Using FTIR, it was possible to detect the characteristic peaks of unmodified HA and compare the spectra with crosslinked HA to determine if the predicted bonds were produced by crosslinking HA with PEGDE. As described in detail in chapter 2, PEGDE is expected to form ester and ether bonds, and ITA is expected to form ester bonds.

4.1.1 Materials and Methods

The presence of vibrational modes of functional groups attributed to the crosslinking of HA with PEGDE and ITA were analyzed by attenuated total reflectance FTIR spectroscopy (ATR-FTIR). ATR provides an enhanced surface sensitivity compared to just using FTIR. For this, Nicolet iZ10 MX integrated FTIR spectrometer (Thermo Fisher Scientific) and the Smart iTX ATR sampling accessory (Thermo Fisher Scientific) were used. For the preparation of the unmodified HA sample, HA was dissolved in distilled water to a final concentration of 2% w/w. Once the HA was dissolved and formed a gel-like solution, it was cast in a Petri dish and placed in a convection oven at 37ºC for one day to evaporate the solvent. To prepare samples of HA-PEGDE-ITA and unmodified HA for FTIR analysis, films were cut into 5x10 mm swatches. Before cutting the HA-PEGDE-ITA films, they were washed again with distilled water to remove residual salts from the PBS. The swatches were placed on an aluminum coated ATR slide and fixed with adhesive tape. Three spectra for each sample were collected in ATR mode using a Slide-On ATR objective with a conical germanium crystal. The MCT detector was cooled with liquid

nitrogen. The spectra were collected by varying the contact pressure between the crystal and the films. Nine scans were collected for each spectrum between 800 cm^{-1} and 3800 cm^{-1} with a resolution of 2.00 cm^{-1}. Data viewing, post-processing and analysis were performed using OMNIC® software.

4.1.2 Results

Figure 15 shows the FTIR spectra obtained for unmodified HA and HA-PEGDE-ITA. Unmodified HA has a strong absorption band at 3291 cm^{-1}, suggesting -OH and -NH stretching vibrations. The band at 2889 cm^{-1} suggests -CH symmetrical and -CH_2 asymmetrical stretching. The bands at 1150 cm^{-1}, 1035 cm^{-1} and 947 cm^{-1} are typical for carbohydrates, and the bands at 1608, and 1376 can be assigned to amide I, II and III. These characteristic peaks coincide with those found in literature for HA [124]. In the FTIR spectra for HA-PEGDE-ITA, additional bands were present that were not seen in the unmodified HA. These bands were at 1744 cm^{-1}, suggesting C=O stretching that belongs to the ester compound class, and at 1252 cm^{-1}, suggesting C-O stretching that belongs to the ether compound class [125].

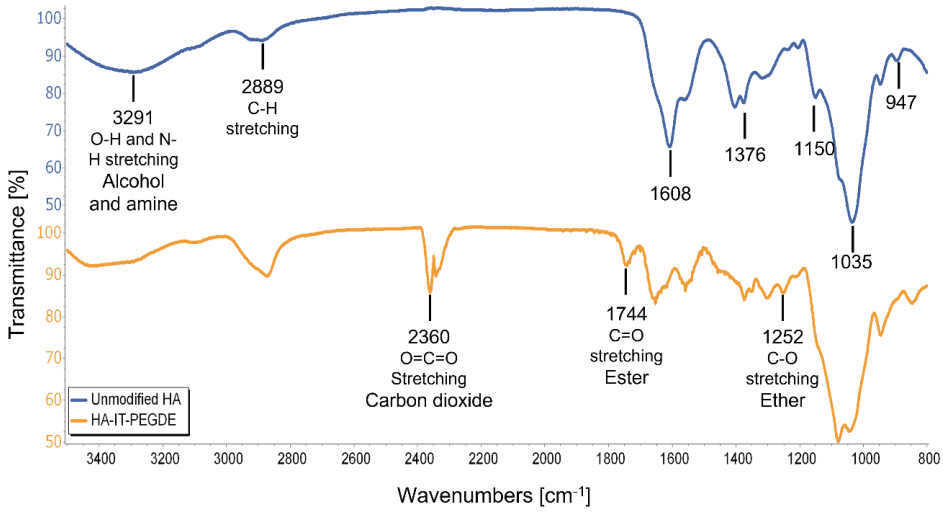

Figure 15: ATR-FTIR spectra of unmodified HA (top) and HA-PEGDE-ITA (bottom).

4.2 Thickness and Swelling Analysis

Determining the film thickness is essential to see if the spin processor parameters are appropriate for achieving the target film thickness of around 30-100 μm. Furthermore, it helps to determine if there is significant batch-to-batch variability of the HA-PEGDE-ITA films. To measure the thickness of the material, an optical profilometer was used. The advantages of using this instrument are its speed, reliability, resolution, spot size and that it does not touch the surface of the material, i.e., the material will not be damaged [126]. The principle of the optical profilometer is to scan a surface with an incident light source and measure the emissive, reflective, or refractive light to acquire information about the surface [127]. For this reason, it is also able to measure surface profiles and roughness of the HA material.

The swelling behavior of a polymer is correlated with the degree of crosslinking [128]. When a polymer is crosslinked there is a decrease in free space for water absorption [113]. Therefore, poorly crosslinked polymers will display greater swelling. Swelling can be simulated in the laboratory by soaking the material in a defined volume of fluid. For this, water is usually used as the test fluid [89]. However, for my experiments I decided to use PBS at 37ºC because I wanted to model physiological conditions. PBS is a buffer solution commonly used in biological research because its osmolarity, ionic concentration and pH are similar to those of human body fluids [129].

4.2.1 Materials and Methods

Profilometry measurements were obtained with a Profilm3D® from Filmetrics. For preparation of the HA-PEGDE-ITA sample, the film needed to be deposited onto a glass substrate. The reason for this step was to have a flat surface on the bottom of the sample

material for reference. For the substrate, it is recommended that glass is used for two main reasons. The first reason is that glass is flat, which is necessary for obtaining reliable results. The second reason is that it is a clear material that lets light pass through it. To attach the HA-PEGDE-ITA film to the glass, the film was first immersed in distilled water until it was swollen and was then transferred to the glass. Here the film was deposited onto the glass and left to dry until the liquid evaporated (~ 1 day). I measured the thickness of three different batches of HA-PEGDE-ITA that were produced using the spin processor parameters presented in the previous chapter. The data analysis and visualization of the surface of the films was performed using Profilm® software.

The swelling ratios of the films were examined using PBS at 37ºC as the swelling medium to mimic the physiological conditions of the human body. Disc samples of the HA-PEGDE-ITA films were cut using a 6 mm diameter biopsy punch. The swollen discs were removed, their diameter measured using a digital vernier caliper (D_{wet}) and weighed (W_{wet}) after excess water on the surface was removed. The films were then washed with distilled water to remove any remaining salt and dried at 40ºC for 24 h. For this an oven was used instead of the fume hood to remove the water faster. The films were then re-measured (D_{dry}) and re-weighed (W_{dry}). The swelling ratios according to the measured diameters and weights were calculated with the following equations (1) and (2) [84]:

$$Swelling\ ratio\ \left(\frac{mm}{mm}\right) = \frac{D_{wet} - D_{dry}}{D_{dry}} \quad (1)$$

$$Swelling\ ratio\ \left(\frac{mg}{mg}\right) = \frac{W_{wet} - W_{dry}}{W_{dry}} \quad (2)$$

For this analysis, three independent experiments were performed in triplicate. The swelling was analyzed for a period of 4 h, and at each hour the discs were measured for diameter

and weight (D_{wet} and W_{wet}). Statistical significance was determined using one-way ANOVA with pairwise Tukey-Kramer post-hoc analysis, $p<0.05$ using Microsoft Excel.

4.2.2 Results

The final thickness of the HA-PEGDE-ITA films is shown in Figure 16. As can be seen, a thickness of 25 µm is achieved with the parameters I selected for spin coating. Moreover, the line profile demonstrates that the film has a constant thickness around the measured area. The 3D view also provides a visual representation of the film and shows that the surface of the material is smooth with only some circle-like shapes present attributed to air bubbles that were not possible to remove when preparing the sample for analysis on the profilometer. Measuring the thickness by profilometry over three different batches gave an average thickness of 25.3 ± 0.5 µm.

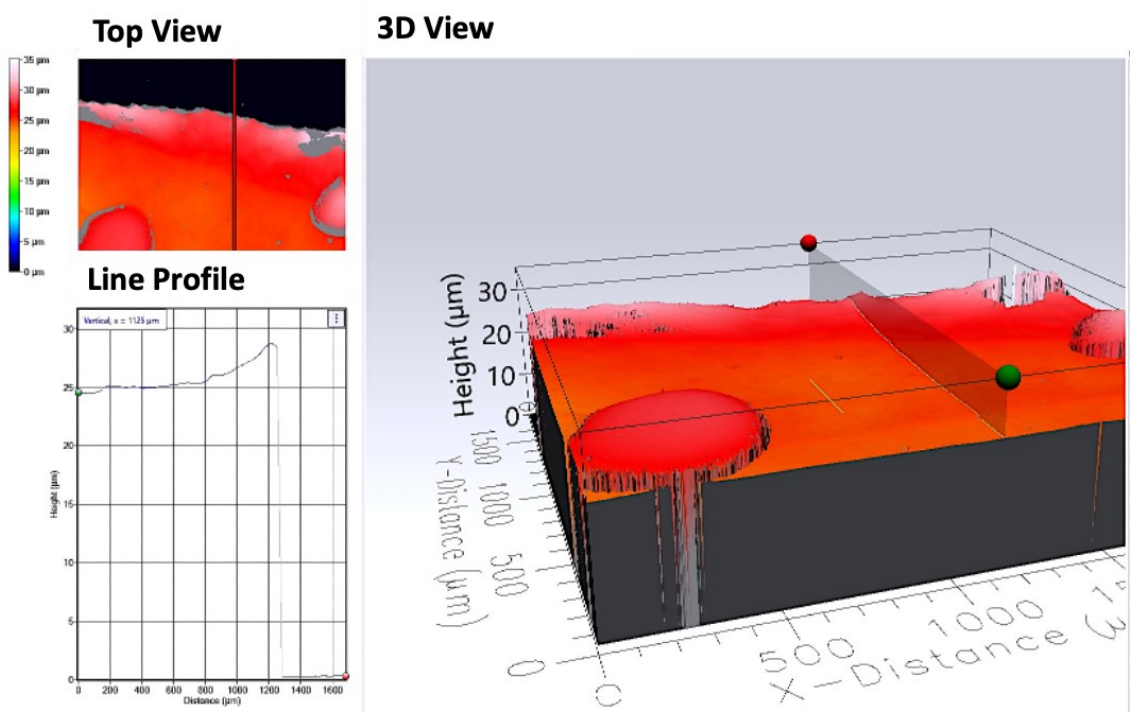

Figure 16: Thickness measurement of HA-PEGDE-ITA films using an optical profilometer. Visualizations are from the top view of the film (where it is also possible to see the roughness of the material), the line profile shows how much the thickness changes, and a 3D is shown across the sample.

Swelling analysis was first performed for HA crosslinked with PEGDE and TA. The results of this experiment are shown in Figure 17A. Here the swelling ratio was taken after 1 h of immersion of the HA-PEGDE-TA hydrogels in PBS at 37ºC. After the optimization I did to the protocol described by Lee et al., i.e., to reduce the concentration of HA and increase the degree of crosslinking (by increasing the molar ratio of crosslinker to HA), I was able to reduce the swelling ratio from 40 [84] to 11.57. Also, the results show that with increasing concentration of TA in the reaction, the swelling ratio was reduced. Figure 17B shows how much the volume of the PEGDE-crosslinked HA increases after swelling. A disc of 6 mm in diameter immersed in 1 ml of distilled water increased 5 times in diameter. Additionally, this disk had a maximum absorption of 2 ml, which made it increase 7.4 times in diameter. This demonstrated that crosslinking of HA with only PEGDE allows the material to swell and increase considerably in size in an aqueous environment.

Moving to the swelling analysis performed with HA-PEGDE-ITA films (Figure 18A), it was observed that the material still swelled, but less so compared to the HA-PEGDE-TA material. For ITA crosslinking, the average swelling ratio in terms of weight was 2.21 ± 0.12 and in terms of diameter was 0.20 ± 0.02. Moreover, the statistical analysis suggested that there was no significant difference in swelling after 4 hours. Looking at the swelling ratios of HA-PEGDE, HA-PEGDE-TA at different TA concentration, and HA-PEGDE-ITA after 1 hour of immersion in PBS at 37°C, it is evident that ITA crosslinking results in the least swelling of the conditions examined. The swelling ratio for ITA was at least 5 times smaller than the lowest observed swelling ratio for TA (Figure 18B).

A

Sample	Swelling ratio [mg/mg]
HA-PEGDE	39.78
0.05% TA	37.37
0.1% TA	35.47
0.15% TA	31.44
0.2% TA	11.57

B

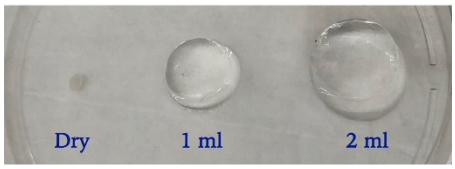

Figure 17: Swelling analysis of the crosslinked HA-PEGDE and HA-PEGDE-TA films. A) Swelling ratio values of HA-PEGDE-TA films at different TA concentrations. All measurements were taken after 1 hour of immersion in PBS at 37°C. B) Visual inspection of the swelling behavior of the crosslinked HA-PEGDE film.

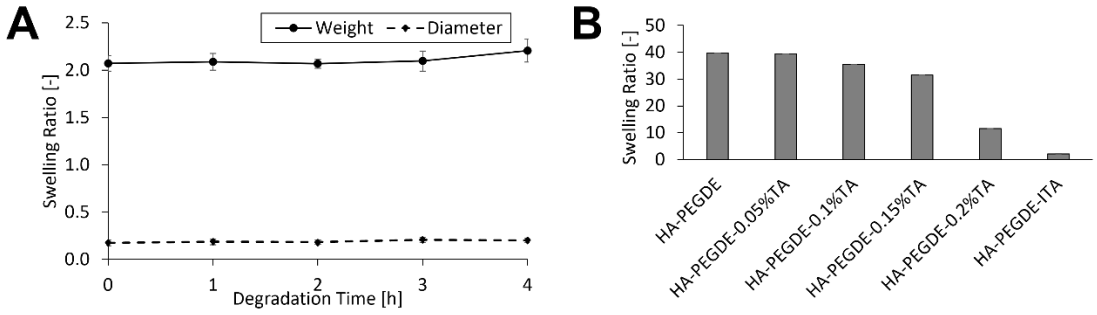

Figure 18: Swelling analysis of the crosslinked HA-PEGDE-ITA film. A) Degradation and swelling assays for crosslinked HA-PEGDE-ITA films measured in terms of weight suggesting a successful crosslinking reaction. Error bars show standard deviation between the triplicates. No significant differences were found in terms of swelling ratio and time of immersion by one-way ANOVA, $p<0.05$. B) Comparison of swelling ratios between crosslinking of HA-PEGDE, HA-PEGDE-TA at different TA concentrations, and HA-PEGDE-ITA. All swelling ratios were taken after 1 hour of immersion in PBS at 37°C.

4.3 Degradation Analysis

The final characterization method I carried out was degradation analysis. As mentioned before, HA in its natural state, i.e., unmodified HA, degrades rapidly *in vivo*. Its half-life ranges from 2 to 5 min in the bloodstream, and the half-life in the epidermis of the skin extends to 1 to 2 days [83], [130], [131]. Here, the highest degree of crosslinking

produces the most stable film [93]. To make this analysis physiologically relevant, I placed the film in an environment similar to the ear canal by immersing it in a solution of saline and antibiotic used as ear drops after a myringoplasty and/or tympanoplasty at 37ºC. Additionally, I also decided to submerge the crosslinked HA films in PBS at 37ºC. I decided to work with dry weights of the films because their measurement was more reliable than when wet. Wet weights can vary depending on how much liquid is retained on the surface.

4.3.1 Materials and Methods

The weight change of the film in the PBS at 37ºC was measured at 1, 3, 7, 14 and 21 days. The remaining weight was calculated according to:

$$Remaining\ weight\ [\%] = \frac{W_t}{W_o} x\ 100 \tag{3}$$

where, W_o is the initial weight of the dry film and W_t is the weight of the dry film after degradation time t. Films were washed with distilled water to remove salts from the PBS and dried in an oven at 40ºC for a specified time. I compared the different formulations to select the one that degraded the least by 14 days, the average time it takes for a wound to heal [50], [10].

For the experiments using antibiotic droplets, Sandoz® Cirpofloxacin/Dexamethasone, an antibacterial corticosteroid, was used. I respected the instructions of how to apply them as presented on the product sheet provided by the manufacturer, specifically the droplets should be added twice per day with 4 drops each time over 7 days. I monitored the weights at the time intervals of 1, 3, 5 and 7 days. To calculate the remaining weight, Equation (3) was used.

Statistical significance for the remaining weight of HA-PEGDE-ITA films was determined by one-way ANOVA with pairwise Tukey-Kramer post-hoc analysis ($p<0.05$ was considered significant) in Microsoft Excel.

4.3.2 Results

For HA-PEGDE-ITA in PBS at 37ºC, there was a slight but significant decline in the remaining weight starting at day 14. After 21 days, the material lost 5% of its total weight (Figure 19A). This loss of weight did not decrease the functionality as measured by the shape and handling properties with tweezers. For HA-PEGDE-ITA films in antibiotic solution, there was a minor increase in weight by day 7 (Figure 19B), likely due to the solids present in the antibiotic solution. It should be considered that for weighing the films, they were always washed after the specific time immersed in either PBS or antibiotic solution to remove residual salts. Even though this was done, it was not possible to remove all the solids/particulates from the antibiotic which explains the slight increase in weight. After a period of 7 days, it was clear that the material did not degrade in the antibiotic solution, which had a pH of 5. Thus, the material is stable in acidic conditions. Furthermore, the material did not become brittle or more fragile after immersion in the antibiotic solution as tested by handling the material with tweezers.

In Figure 20, a comparison of the degradation analysis between HA-PEGDE, HA-PEGDE-TA with the different TA concentrations (0.05%, 0.1%, 0.15% and 0.2%), and HA-PEGDE-ITA is presented. There was significant degradation for crosslinking with TA on day 4 with the remaining weight being only 15% and 30% for 0.2 and 0.15% TA,

respectively. This suggests that crosslinking with TA leads to a fast-degrading material compared to crosslinking with ITA.

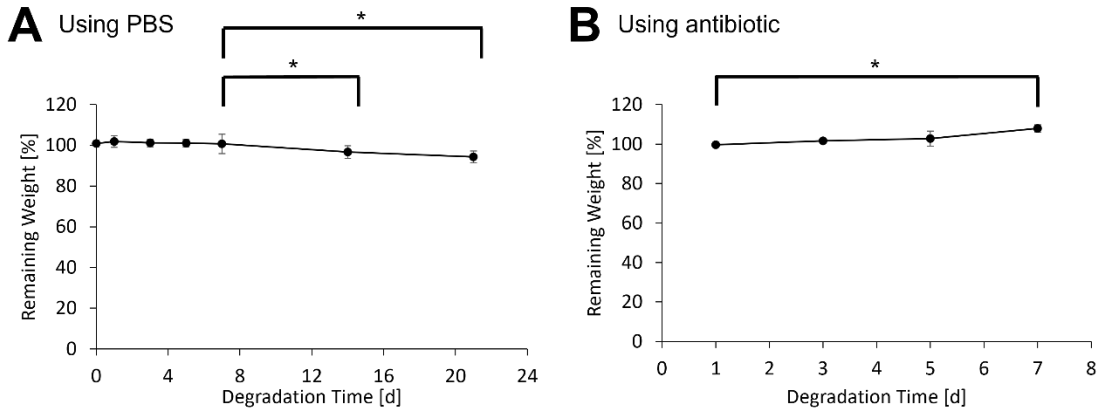

Figure 19: Degradation analysis of HA-PEGDE-ITA films. A) Remaining weight when immersed in PBS at 37ºC for a period of 21 days. B) Remaining weight when immersed in antibiotic solution at 37ºC for a period of 7 days. Error bars show standard deviation. *Indicates statistical significance as determined using one-way ANOVA and Tukey-Kramer post-hoc analysis ($p<0.05$).

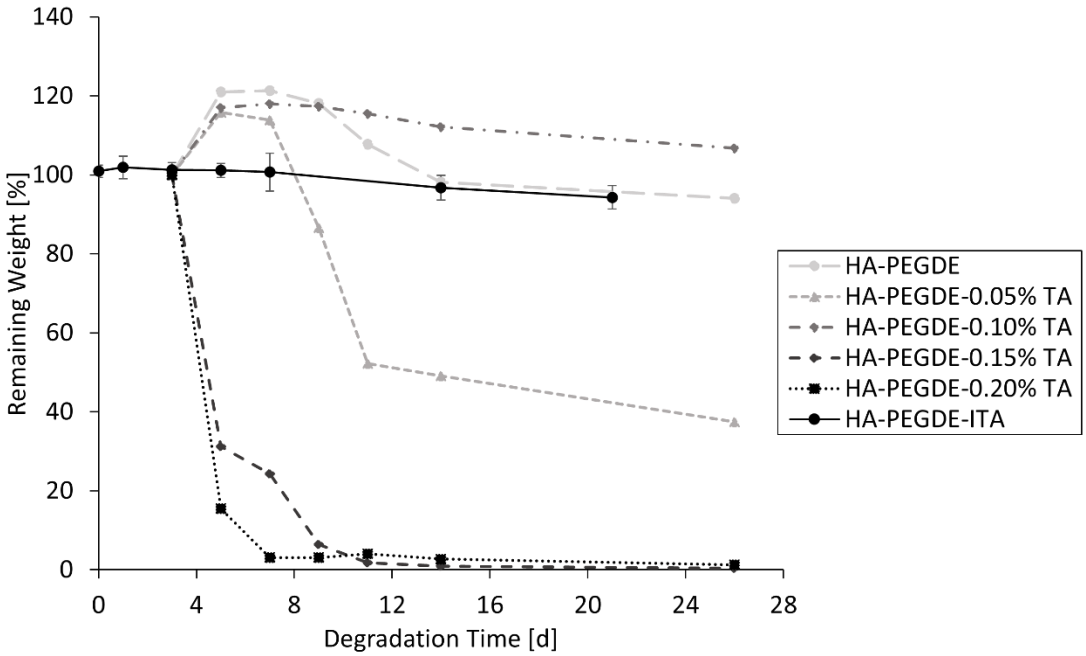

Figure 20: Comparison of remaining weights for HA-PEGDE, HA-PEGDE-TA at different TA concentrations, and HA-PEGDE-ITA films after immersion in PBS at 37°C. Error bars show standard deviation.

4.4 Discussion

Degradation and swelling analysis showed that films crosslinked with TA degraded after 4 days and presented a swelling ratio of at least 11 (Figure 17, Figure 18B and Figure 20). What could have happened is that the PEGDE and TA were not able to interact properly, and thus, the physical crosslink was not occurring as expected. Significantly, the ratio of PEGDE:TA establishes the bonding efficiency between these two compounds; at low concentrations of TA, the interaction between TA and PEGDE is strong, nonetheless, when the content of TA increases meaningfully. Thus, TA cannot effectively interact with the PEGDE chain in the hydrogels [120], and this could result in a rapid TA release and post-swelling effect. For TMP repair, films need to be stable and not swell more than 5-fold with respect to their initial weight or size as the objective of this project was to fabricate a film that acts as a scaffold for cells and not to produce a crosslinked HA material that is acting as a packing material with its big volume covering all the ear canal. To fulfill this goal, the crosslinked HA should be able to retain water and support the proliferation of cells but not increase too much in size. A great example to visualize this point is to think about contact lenses. These are made of a polymer that swells when immersed in water, but their size does not increase very much.

When using ITA as the second crosslinker for HA, the results were clearly different than with TA. Here, degradation analysis showed that the films were stable for a period of 21 days losing a weight of 5% (Figure 19). This degradation began only after day 14 and didn't influence the functionality of the film. This result is viewed favorably because, according to literature, 14 days is the average time it takes a wound to heal [50], [10]. Thus, the degradation of the crosslinked film is likely to happen after the wound has already

healed. For the case of the swelling analysis, the swelling ratio was 2.21 ± 0.12 in terms of weight and 0.20 ± 0.02 in terms of diameter (Figure 18A). These results suggest an effective crosslinking reaction that is able to produce films with a defined shape that will not increase drastically in size when immersed in water or another liquid. In conjunction, the findings reported in the results suggest that the crosslinking reaction using ITA as the second crosslinker was successful in avoiding rapid dissolution of unmodified HA films in PBS at 37ºC. Therefore, PEGDE and ITA were efficient HA crosslinkers providing a highly stable material that was still able to swell. These qualities make the HA-PEGDE-ITA films a viable material for TMP repair.

The films crosslinked with TA were not analyzed by FTIR, as their physical properties proved to be inappropriate for TMP repair. On the other hand, for the HA-PEGDE-ITA film, the expected ester and ether bonds were formed, which suggests that the crosslinking reaction was successful (Figure 15). To standardize this for future use, the degree of crosslinking could be quantified using NMR spectroscopy.

Finally, the thickness analysis showed that I was able to form even films with a thickness of 25.3 ± 0.5 μm (Figure 16), with measurements over different batches. Thus, the chosen parameters for spin coating were appropriate to produce HA-PEGDE-ITA films for TMP repair. What should be noted is that the measurement of the thickness of the films was carried out when they were in a dry state. After immersion in an aqueous solution, the thickness should increase to some extent due to swelling. The exact increase was not obtained because when the sample (i.e., HA-PEGDE-ITA) was wet, it was not laying completely flat on the glass substrate. However, based on the swelling analysis I conducted, the thickness of the hydrated films should be in the range of the human TM (30-100 μm).

Chapter 5. Functionalization of HA Film with ColI Fibers

As presented in chapter 1, ColI was selected to functionalize crosslinked HA films because of its biocompatibility and low immunogenicity in addition to its ability to promote hemostasis and accelerate wound healing through cell proliferation, migration, and angiogenesis [132]. ColI will be employed in fiber form since the fibrillar structure of ColI is important for cell adhesion, alignment, proliferation and migration of various cell types [133]. Moreover, there is growing evidence that the topography of the collagen substrate also influences cell polarity, shape, and differentiation [134].

5.1 Production and Attachment of ColI Fibers

The production of ColI fibers is difficult since it suffers from low throughput along with manufacturing and scaling challenges. The leading choice for fabrication of fibers in tissue engineering applications is electrospinning [135]. In this method, high voltage is applied to the liquid solution (i.e., polymer solution) and a collector, which lets the solution pass through a nozzle to form a jet, which enables elongation into a fiber that is deposited on the collector [136].

One of the major benefits of electrospinning is that it takes place at room temperature, providing an increased range of bio-active molecules that can be incorporated. In particular, electrospinning of collagen has attracted attention because it is possible to produce nanofiber structures that resemble native collagen fibrils. Furthermore, electrospinning offers the possibility to customize the porosity, structure, and orientation of the ColI fiber network [137]. Nevertheless, this manufacturing process has some important limitations, such as the requirement of highly specialized electrospinning equipment, frequent spinneret nozzle clogging, use of high voltages and use of hazardous

solvents. Finally, this process also exposes collagen to high shear forces, that can limit its ability to self-assemble into a stable conformation [138]. Therefore, the electrospun ColI fibers must be crosslinked before use as a biomaterial to prevent collagen dissolution in aqueous environments [137]. These limitations have been reported to affect the integrity and bioactivity of the collagen fibers scaffolds [139]. The contact drawing method developed by the Frampton Lab provides a feasible alternative for ColI fiber production since this method allows the formation of hundreds to thousands of biomaterial fibers at room temperature in seconds without the need for any specialized equipment [82].

5.1.1 Contact Drawing

For the contact drawing method, a polymer able to produce fibers and a bioactive molecule, in this case ColI, is needed to make a viscous solution. This solution is then deployed to a substrate tool, and contact between a pin array and the solution established. Afterwards, the pin tool and the solution substrate are pulled apart to elongate the fibers. Lastly, the dry fibers are suspended over a hollow collector box [140]. This procedure should be repeated until the necessary number of fibers are obtained. As a result, the contact drawing system only comprises a hollow collector, a pin array tool for nucleating the fibers, and a substrate tool for retaining the polymer solution. Polymer entanglement acts as the driving factor behind the fiber formation in this process [141]. Thus, the polymer that is chosen must be at a suitable high concentration to ensure chain entanglement. Polymer entanglement causes the creation of numerous liquid bridges when the contacting element (i.e., pin array) is quickly removed from the solution. These liquid bridges are subsequently pulled into fibers [141]. The selected polymer for this project was polyethylene oxide (PEO), because it allows fibers to form from a solution of PEO-ColI containing as low as

0.5%wt PEO. This enables the production of dry PEO-ColI fibers with mass fractions of more than 90% collagen [133]. Importantly, the PEO can later be removed through hydration of the fibers, leaving behind a fiber comprised of ColI.

There are several advantages of using the contact drawing method instead of electrospinning. First, the former is a process free from clogging issues because it does not require a nozzle to extrude the polymer, which also means that viscosity is not as much of a problem. Second, no voltage needs to be applied to the polymer solution during the fabrication process; hence, issues with denaturation of biological molecules are avoided. Third, the method does not require complex equipment and can safely incorporate biomolecules [82], [133], [137]. Since elongation of the fibers requires only a simple linear translational motion and the number of fibers generated with each elongation cycle is related to the number of pins on the pin array tool, the contact drawing approach is suitable for automation and scalability.

5.1.2 Track Spinning

The contact drawing method can be automated using track spinning devices. The term track spinning was given by Jao and Beachley [142], who described it as the automation of a simple mechanical process that produces linearly aligned fiber networks with integrated postdraw processing and control over fiber placement in the secondary assembly. In essence, this method produces fibers by the same principles of contact drawing but in an automated fashion. The track spinning device is made up of two angled rotating tracks that touch at the top, each powered by a stepper motor, and a polymer solution distributed on one of the tracks. Fibers are continuously spun by direct contact of the polymer solution-coated tracks followed by mechanical drawing as the distance

between the tracks increases (Figure 21). To control the production of fibers (i.e., final fiber length and fiber draw rate), there are three different parameters of the machine that can be adjusted: 1) the angle of the tracks, 2) the vertical collection distant from the apex of the tracks, and 3) the track speed [142].

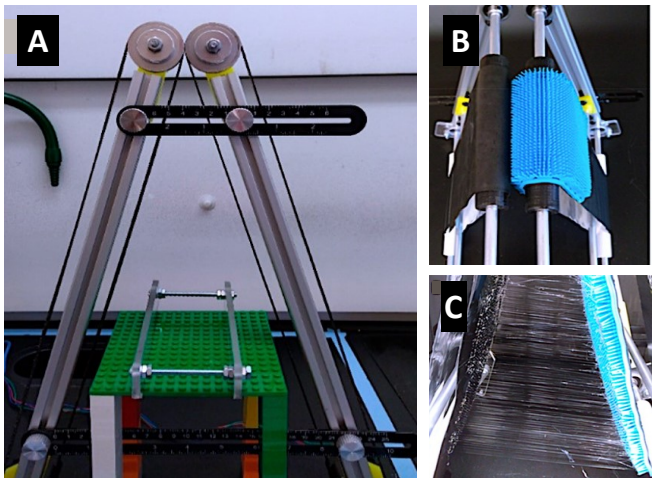

Figure 21: Track spinning device. A) Image of the spinning device with collection rack and adjustable stage placed between the two rotating tracks. B) Track spinning device with pin array tool attached to one of the tracks. C) Spinning system drawing and stretching an array of aligned fibers. Reprinted with permission from American Chemical Society, obtained from [142]. Copyright © 2019; permission conveyed through RightsLink by Copyright Clearance Center, Inc.

5.1.3 Materials and Methods

The track spinning device was used to produce the ColI fibers for attachment to the HA-PEGDE-ITA film and was accessed at 3D BioFibR™ Inc. The parameters that were selected to produce the ColI fibers (including crosslinking with UV-C) were previously optimized by the company. The only optimization I made concerned the attachment of the ColI fibers to the films. It was decided to pull the fibers in two directions, horizontally and vertically, to promote cell attachment and migration in more than one direction. Moreover, four different fiber densities were produced to later analyze if the fibers increased the strength of the material, in addition to analyzing how the cells behaved with different

amounts of fibers on the crosslinked HA film, i.e., to determine if having more ColI fibers leads to the attachment, proliferation and migration of more cells. The fiber density scales with the number of pulls across each film and each pull corresponded to one cycle of the track spinning device and one layer of fibers. The ColI fiber densities corresponded to 0 pulls (which was a control just having the HA-PEGDE-ITA film), 25 pulls, 50 pulls and 100 pulls.

For the preparation of the PEO-ColI solution, the protocol was as follows. PEO (8MDa, Sigma-Aldrich) was dissolved to a concentration of 1:1 weight ratio in type I bovine collagen (6 mg/ml in 0.02M acetic acid, Collagen Solutions) by stirring with a metal spatula for around 1 min, followed by light shaking at 4ºC. Every 24 h, the solution was mixed again with the metal spatula until a homogeneous solution was formed (normally after 72 h of shaking at 4 ºC). Thereafter, the solution was allowed to remain at 4 ºC for 24 h to eliminate any air bubbles introduced during stirring and shaking. The PEO-ColI solution was then warmed to room temperature for 15 min before being utilized for fiber contact drawing.

Once the solution was ready, the next step was to produce the ColI fibers with the track spinning device and to assess the attachment to the HA-PEGDE-ITA film. First, HA films were immersed in distilled water. Once swollen, excess water was removed using a Kimwipe. Then, swollen HA films were placed on a platform covered with parafilm that was located on the adjustable stage between the two tracks, and 1 ml of the PEO-ColI solution was spread over the track without the pins using a wooden craft stick. Next, the program optimized by 3D BioFibR™ Inc. consisting of a 90º rotation every pull using a motor beneath the platform was run for the desired number of pulls. This rotation produced

the two alignments of ColI fibers (horizontal and vertical). ColI fibers were pulled directly on top of crosslinked HA films. This process was performed at room temperature and relative humidity ≤ 40% (measured by a digital hygrometer). When the pulls were finished, the produced scaffolds (i.e., HA-PEGDE-ITA films with ColI fibers) were UV-C treated (UVP Crosslinker; Geneq inc.) for ~30 sec to a fixed energy value of 200 mJ/cm^2 to crosslink the collagen fibers and prevent their degradation. Then, the scaffolds were left for ~24 h at room temperature to let the fibers completely dry.

5.2 Characterization of the HA-ColI Scaffolds

As previously mentioned, the goal of the ColI fiber attachment was to improve cell adhesion on the crosslinked HA film. Before these cell studies could be conducted, however, the new produced scaffolds needed to be further characterized to ensure that the ColI fibers were attached to the film surface. Additionally, mechanical testing needed to be conducted to measure the tensile properties of the crosslinked HA material with and without the ColI fibers. Collagenase analysis and tensile tests were conducted for this purpose.

5.2.1 Collagenase Analysis

HA-ColI scaffolds with a total of 50 fiber pulls in one direction were cut using a 6 mm diameter biopsy punch and were placed in a 24 well plate. Only this condition was chosen to clearly visualize the fibers during the collagenase analysis as the main objective was to determine if the present fibers were collagen. For this analysis, it was not relevant to use different fiber densities. The samples were incubated with collagenase IV (200 U/mL prepared in Hanks Balanced Salt Solution (HBSS), Thermo Fisher Scientific) to confirm that the features apparent in brightfield images attributed to ColI fibers were indeed

attached collagen fibers rather than imprints left behind from contact of fibers that later lifted off or dissolved. First, the samples were rehydrated in PBS for 30 min and then brightfield images were collected using a Nikon Eclipse Ti microscope. The wash removed the PEO from the fibers. Later, the samples were treated with collagenase IV for 30 min at 37ºC. After incubation with collagenase, another set of brightfield images were collected to determine if any ColI fibers remained on the HA-PEGDE-ITA film. Samples exposed to HBSS without collagenase served as controls. This experiment was done in triplicate.

5.2.2 Mechanical Testing

Mechanical tests were conducted under dry conditions to further assess handling properties during cutting to the required size and under wet conditions as would be present during application and following surgery to repair a TMP for materials formed from 100 fiber pulls. HA-PEGDE-ITA films were also tested without fibers to characterize their baseline tensile properties. ColI fiber densities corresponding to 25, 50 and 100 pulls were analyzed under wet conditions to determine the effect of fiber density on tensile properties.

For mechanical testing, samples were examined using a Mark-10 F105-IM (TEquipment) mechanical testing system. Samples from each condition were prepared by cutting rectangular strips of 0.5 cm x 4 cm, with care taken to avoid introducing any imperfections that could lead to breakpoint artifacts and premature material failure. Samples with imperfections were discarded. To mount a strip of material for the tensile test while keeping the distance between the grippers of the machine at a fixed length, the strip was first affixed to a C-shaped cardboard cut-out by adhering 1 cm of each end of the strip to the cardboard using tape, leaving 2 cm of the strip suspended between the top and bottom of the cardboard form (Figure 24A). Next, one end of the cardboard cut-out containing the

strip was placed into the top grip of the Mark-10, and the procedure was repeated for the bottom gripper. All samples were tested until failure at 30 mm/min at room temperature and ~50% relative humidity in a location with minimal vibration. IntelliMESUR software was used to run the testing protocol and record force-displacement data. The thickness of the strips was measured using the optical profilometer, as described in the previous chapter. The average thickness of the crosslinked films was 25 µm, which was used to calculate the cross-sectional areas for computing the stress σ with F denoting the force and A denoting the cross-sectional area of the film (Equation (4) [143]).

$$\sigma = F/A \tag{4}$$

The cross-sectional area was calculated using Equation (5) [143] with w_{film} denoting the width and t_{film} denoting the thickness of the film.

$$A = w_{film} \cdot t_{film} \tag{5}$$

For calculating the strain ε, Equation (6) [143] was used. Here, ΔL denotes the change in length during the test and L_0 the initial length of the film.

$$\varepsilon = \Delta L/L_0 \tag{6}$$

From the tensile stress-strain curves, the elastic modulus, tensile strength, and ultimate strain were determined. The elastic modulus E was determined using Hooke's Law from the stress-strain curve by calculating the ratio of stress to strain [143], i.e., the slope of the linear region at the beginning of the curve (Equation (7)).

$$E = \sigma/\varepsilon \tag{7}$$

To compare different film conditions with and without ColI fibers in their dry and wet states, one batch of HA-PEGDE-ITA was tested in triplicate, while to compare different fiber densities, three different batches of HA-PEGDE-ITA were tested in

triplicate for each batch. Thus, a total number of nine replicates was used for each fiber condition. Statistical significance was determined using two-way ANOVA for the different film conditions in their dry and wet states and with and without ColI fibers (100 pulls), and using one-way ANOVA for the different ColI fiber densities, both with pairwise Tukey-Kramer post-hoc analysis using Microsoft Excel with $p<0.05$ considered statistically significant.

5.2.3 Results

The track spinning process generated ColI fibers that were attached to the HA-PEGDE-ITA film as shown in Figure 22A. These fibers did not lift from the surface of the HA film, even when transported or subject to air currents (Figure 22B). Fiber alignment was in two directions, horizontally and vertically, and it was maintained through the series of wash steps used to prepare the scaffolds for the experiments. Automation of the contact drawing process proved to be reproducible for production of HA-ColI scaffolds.

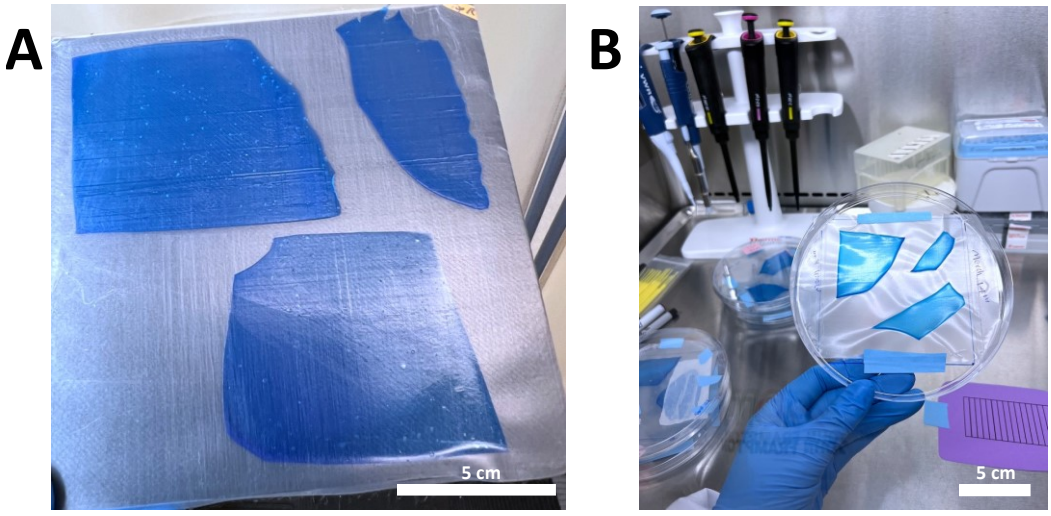

Figure 22: HA-ColI scaffolds. A) HA-PEGDE-ITA film after pulling ColI fibers by track spinning. As can be observed, the ColI fibers were pulled in two directions and were successfully attached to the film. B) Post processing of the scaffold. The scaffold was cut in different shapes based on experimental needs. All steps to deposit ColI fibers were performed in a biosafety cabinet to maintain aseptic conditions.

For the collagenase analysis, brightfield images demonstrated that treatment with collagenase IV resulted in rapid degradation of the ColI fibers (Figure 23). These findings demonstrate that the features on the surface of the HA film were attributed to ColI fibers rather than to imprints left behind by fibers that later lifted off the surface or dissolved.

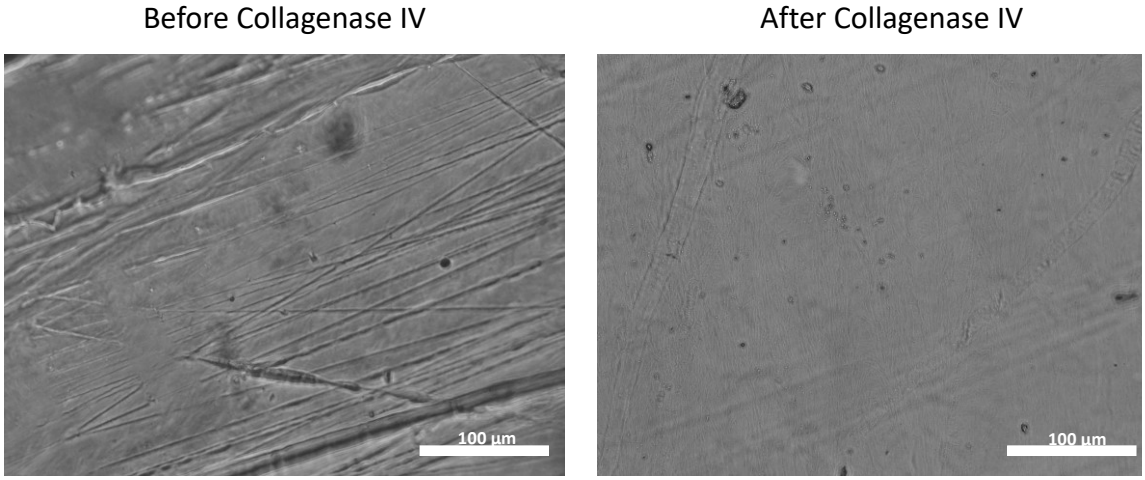

Figure 23: Collagenase analysis. Representative phase contrast images of ColI fibers on an HA-PEGDE-ITA film. The image on the left is a scaffold after hydration. Thus, the PEO was already removed from the ColI fibers. The image on the right was taken after collagenase IV digestion. Images demonstrate the presence of fibers made of ColI.

Tensile stress-strain curves are presented in Figure 24B. The dry HA-PEGDE-ITA films and dry HA-ColI scaffolds (with 100 pulls) presented elastic behavior and possessed tensile strengths of more than 42 MPa with an ultimate strain of around 10.37 ± 3.47 %. On the other hand, the wet materials displayed plastic behavior, with a strain of ~22.03 ± 0.89 % but a lower tensile strength of 9.6 ± 0.57 MPa.

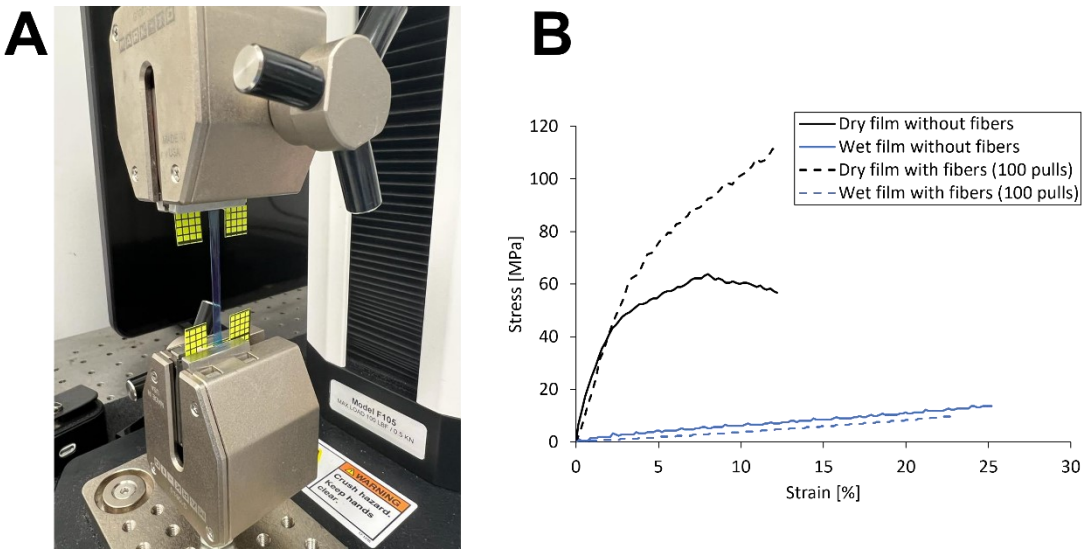

Figure 24: Mechanical testing of HA-ColI scaffolds. A) Set-up for the tensile test. For this experiment, the scaffold was cut in 0.5 cm x 4 cm rectangular strips. One cm of each end was held by the grippers of the mechanical testing machine. Scaffold were then pulled until failure. B) Representative stress strain curves until failure for the different conditions; wet and dry and with and without ColI fibers (100pulls).

The tensile properties of the films are presented in Figure 25. There were no significant differences between films with fibers and those without fibers in terms of the elastic modulus. Nevertheless, there was a significant difference in elastic modulus between the dry and wet states with the wet state having lost its stiffness. Thus, no further evaluation of the elastic modulus was conducted for the wet state. In terms of tensile strength, there was a significant difference between films with ColI fibers and those without ColI fibers in both the dry and wet states. By adding ColI fibers, the tensile strength increased from 56.76 ± 2.21 MPa to 126.31 ± 12.36 MPa for the dry state and from 3.60 ± 0.33 MPa to 9.60 ± 0.57 MPa for the wet state. Finally, in terms of ultimate strain, there was a significant increase between films with ColI fibers and those without ColI fibers in the wet state, with an increase from 16.71 ± 1.66 % to 22.03 ± 0.89 %.

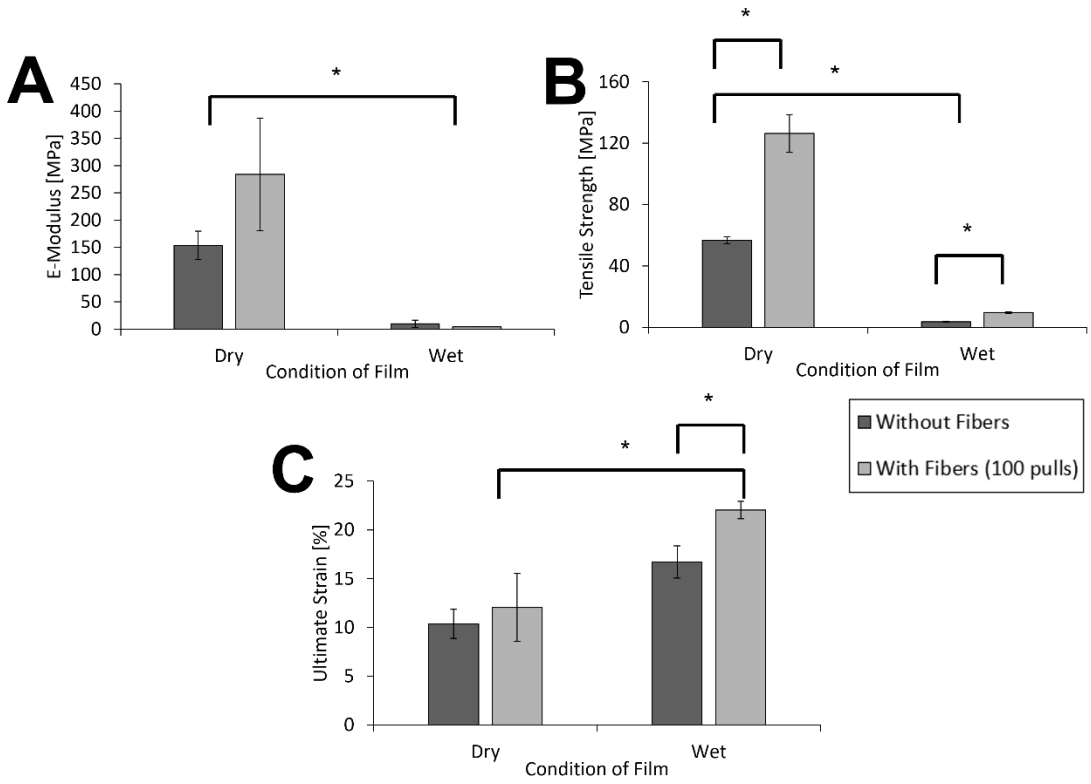

Figure 25: Comparison of the characteristic mechanical properties for the different film conditions in the wet and dry states and with and without ColI fibers (100 pulls). A) Elastic modulus, B) tensile strength, and C) ultimate strain as evaluated from stress-strain curves. Error bars show standard deviation. *Indicates statistical significance as determined by two-way ANOVA and pairwise Tukey-Kramer post-hoc analysis ($p<0.05$). Here, one batch of HA-PEGDE-ITA was used in triplicate for each condition.

An additional analysis was performed to evaluate the tensile strength and ultimate strain for different ColI fiber densities but only for samples in the wet state (Figure 26). There was a significant increase in the tensile strength (6.84 ± 2.02 MPa) for films with 100 layers of fibers relative to films without ColI fibers and films with only 25 layers of fibers (3.78 ± 1.56 MPa and 4.58 ± 1.16 MPa, respectively). The ultimate strain was significantly higher for films with 100 layers of fibers relative to films without fibers (23.88 ± 2.91 % and 18.11 ± 6.07 %, respectively).

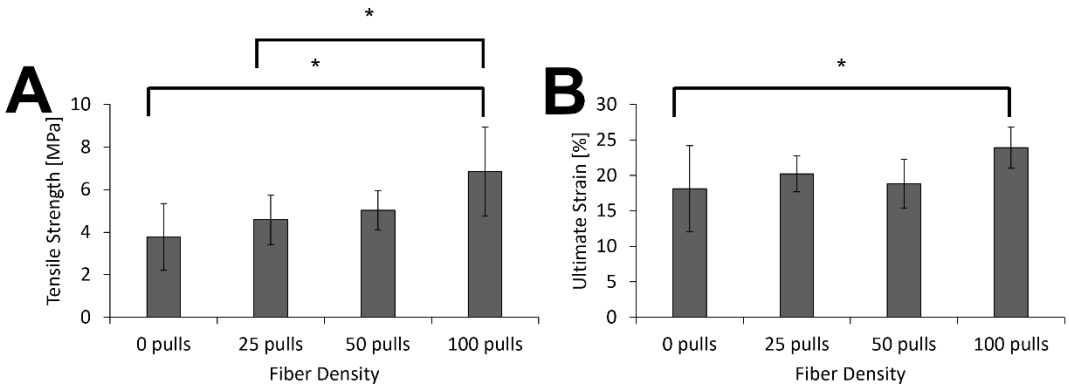

Figure 26: Comparison of the mechanical properties of films with different fiber densities. A) Tensile strength and B) ultimate strain as evaluated from the stress-strain curves. Error bars show standard deviation. *Indicates statistical significance as determined by one-way ANOVA and pairwise Tukey-Kramer post-hoc analysis ($p<0.05$). Here, three different batches of HA-PEGDE-ITA were used in triplicate for each batch. Thus, a total number of nine replicates was conducted for each condition.

5.3 Discussion

ColI fibers were attached to the crosslinked HA films to functionalize them for cell growth (as will be assessed in Chapter 6. *In vitro* Evaluation). The results showed that the optimization of the attachment worked as the fibers did not lift from the surface of the HA film (Figure 22). Attachment of the ColI fibers to the film was likely mediated by the PEGDE crosslinker [144], and swelling/water content likely also played a role in ColI fiber adhesion [128]. It should be noted, however, that it was important to remove excess water from the surface of the film to prevent the PEO-ColI fibers from partially solubilizing and fusing with each other as they were deposited. It is also important to note that the 3D BioFibR™ Inc. protocol calls for stabilization of the PEO-ColI fibers through additional UV-C crosslinking, which also serves to sterilize the material for cell culture. UV-C refers to ultraviolet light with wavelengths between 100-280 nm and is principally known for sterilizing air, water, and surfaces [145]. UV-C can crosslink collagen by making covalent bonds between the collagen fibrils, and it has been demonstrated that UV-C crosslinking

of collagen does not affect its biological functions (cell attachment, migration, and proliferation) [146]. Taking all the information and results into account, it was demonstrated that using track spinning to produce ColI fibers, followed by the optimized protocol for the attachment, as well as crosslinking the PEO-ColI fibers with UV-C are suitable methods to produce stable and reproducible HA-ColI scaffolds.

A collagenase assay was performed to show that the surface-bound ColI fibers were indeed collagen, and not an artifact of the track spinning process (Figure 23). In this assay, collagenase IV, a protease that is known to cleave the peptide bonds present between neutral amino acids (X) and glycine in the Pro-X-Gly-Pro sequence of Col1 [147], was used. To activate enzyme activity HBSS was used, a solution that provides the required inorganic salts (Ca^{2+} and Mg^{2+}) for collagenase [148]. Moreover, collagenase IV is able to cleave collagen in both monomeric and in the triple-helical form [149]. Collagenase IV has a critical role in numerous physiological processes, such as ECM degradation and remodeling, and wound healing [150]. The rapid degradation of the ColI fibers after incubation with collagenase helps to demonstrate the collagen bioavailability and suggests that cells will have the capacity to remodel the ColI fibers.

To be used in regenerating the TM, a tissue substitute needs to have proper mechanical strength to be handled during surgery. Thus, the tensile properties of the HA-ColI scaffolds were evaluated. The three main properties that were analyzed were tensile strength, ultimate strain, and elastic modulus. The tensile strength is the maximum engineering stress the material can withstand before breaking. The ultimate strain is the strain at which the material breaks and it describes the ductility of the film. Finally, the elastic modulus describes the slope of the stress-strain curve in the elastic regime,

representing the stiffness of the material [143]. The films had higher tensile strength and elastic modulus in the dry state than in the wet state as determined by the slopes of the stress-strain curves (Figure 24 and Figure 25). The curves show that the wet samples have lost its stiffness even with 100 layers of ColI fibers present, which is why the elastic modulus will no further be evaluated for this condition. Furthermore, films in the wet state had higher ultimate strain and, thus, higher ductility than in the dry state. In general, all the crosslinked films displayed plastic behavior. In other words, the films have the ability to plastically deform without fracturing when placed under a tensile stress that exceeds the yield strength. Ductile behavior not only ensures the materials can be handled by a surgeon, but also makes it more suitable and able to conform to living tissues [106]. It should be mentioned that HA alone has a gel-like behavior meaning that in mechanical testing it would not show proper plasticity due to a continuous decrease in stress instead of an increase. Therefore, crosslinking of HA was required.

Several studies have characterized the elastic modulus of the human TM, and the results range from 2 MPa to 70 MPa [151]–[154]. This large range may be due in part to the variation in thickness of the TM, but there are likely other major differences in the samples from which these values were measured (e.g., age and gender of the cadaver providing the TM). The elastic modulus of the crosslinked HA films ranged from 4.18 ± 0.30 MPa (lowest value wet state) to 284.20 ± 103.25 MPa (highest value dry state), which falls within the range of the native human TM. In Figure 25, it is evident that the presence of ColI fibers led to an increase in the elastic modulus in the dry state, the tensile strength in both the dry and wet states, and the ultimate strain in the wet state. However, in the dry state, it should be noted that PEO was still present in the ColI fibers as the wash to

remove them from the fibers had not been conducted yet. Thus, they likely contributed to the mechanical properties of the material.

For analyzing the influence of ColI fiber density (Figure 26), only wet conditions were tested. The values for tensile strength and ultimate strain approximated those observed for human TM (ultimate Strain 20.00 ± 7.00 % [153] and tensile strength 7.70 ± 2.50 MPa [153]). Thus, in the wet state, ColI fibers do not improve the mechanical properties by very much, but they do contribute to some of the mechanical performance of the material within the ranges expected for a material for TM regeneration. In addition, I noticed that the fibers helped to prevent curling of the films and also helped to maintain their swollen state for longer, potentially because the ColI fibers also absorbed water and provided additional structure to the film.

In summary, crosslinking HA imparted mechanical properties similar to a human TM. Additionally, the material was suitable for surgical handling. Even though the mechanical properties were mainly defined by the HA-PEGDE-ITA film, the adhesion of ColI fibers have the potential to provide additional functionality to the film, i.e., cell attachment and migration, as will be presented in the next chapter. Furthermore, it should be mentioned that the thickness for stress calculation was based on the thickness measurements of the film. The attached fibers will increase the thickness of the material and, thus, might influence the mechanical properties. Therefore, a thickness measurement of the HA-ColI scaffold should be carried out to determine the influence. A preliminary measurement by 3D BioFibR™ Inc. suggests that, with the number of pulls conducted here, the thickness won't increase by more than 6µm.

Chapter 6. *In vitro* Evaluation

As re-epithelialization is an important feature of TM healing after TMP, the next step was to assess cell viability, cell morphology, and cell migration. The initial cell viability analysis was conducted to determine if the HA-PEGDE-ITA film was cytocompatible (i.e., not toxic to cells) using fibroblasts and keratinocytes. Secondly, a cell morphology analysis was done using phalloidin to stain the cytoskeleton for visualization of the attachment and alignment of keratinocytes on the ColI fibers on the HA-ColI scaffold. Finally, cell migration analysis was conducted to see if keratinocytes were able to migrate along the ColI fibers without the addition of chemokines (signaling proteins secreted by cells that induce cell movement [155]). I decided to use these two types of cells (fibroblasts and keratinocytes) because as stated in the first chapter, both cell types are essential for ensuring a balanced wound-healing process [156]. Nonetheless, most of the experiments were carried out using keratinocytes because progression of the keratinocyte layer is the most important element in TMP closure [8]. Similar to when skin is injured, keratinocytes become activated and migrate across the wound, and proliferate to fill the defect [157]. Hence, it is more relevant to analyse the cell response of this type of cell with the prepared scaffold.

6.1 Cell Lines and Cell Culture

An immortalized dermal fibroblast cell line (WS1; CRL-1502, ATCC) and a keratinocyte cell line (N-TERT; 7614-1, Invitrogen®) were used in this work. I selected N-TERT keratinocytes for examining the effectiveness of my scaffold in promoting cell attachment and migration, which are desired features for a biomaterial for TMP repair. N-TERT cells possess the major characteristics of primary human keratinocytes and have

superior qualities over the most widely used keratinocyte cell lines (e.g., HEK001) with regard to epidermal differentiation and the formation of a stratified epithelium [158].

6.1.1 Materials and Methods

HA-PEGDE-ITA films and HA-ColI scaffolds with three different fiber densities (25, 50 and 100 pulls) were used to assess the response of N-TERT cells relative to films without ColI fibers, whereas as films without fibers were used to assess baseline cell attachment and cytotoxicity using WS1 cells. The HA-PEGDE-ITA films and HA-ColI scaffolds were cut into 6 mm disks using a biopsy punch and placed within cell culture well plates. Cells were cultured and maintained in a humidified incubator at 37 °C with 5% CO_2 and used before 20 passages. The WS1 cell line was cultured in Eagle's Minimum Essential Medium (Corning) supplemented with heat inactivated 10% fetal bovine serum (Avantor® USA) and 1% antibiotic-antimycotic solution (Corning). The N-TERT cell line was cultured in Keratinocyte-Serum Free Medium (Gibco™- BRL 1725-018) supplemented with 25 μg/ml bovine pituitary extract (BPE; Gibco™), 0.4 nM $CaCl_2$, and 0.4 ng/ml epidermal growth factor (EGF; Gibco™) [159]. Before cell culture, the HA-ColI scaffolds were first incubated in 1x Dulbecco's phosphate buffered saline (D-PBS, VWR, USA) for 1 h to remove the PEO from the ColI fibers. The D-PBS was then removed.

For sterilization of the HA-ColI scaffolds, heat treatments were avoided to prevent degradation of the material, and immersion in 70% ethanol was avoided to shorten the preparation time (if ethanol was used, extra washes were needed to remove all the possible ethanol retained in the HA-PEGDE-ITA film). Therefore, UV-C treatment was used again, but this time it was important for sterilization in addition to crosslinking of the ColI fibers [145]. The HA-ColI scaffolds were irradiated in the UV-C Crosslinker (Geneq inc.)

for ~30 sec to a fixed energy of 200 mJ/cm^2. Once the scaffolds were sterilized, they were immersed overnight in cell culture media and placed in the incubator at 37ºC for one day before the cells were seeded. Tissue culture plastic (TCP) and HA-PEGDE-ITA films without fibers were used as controls and were prepared in the same manner.

The N-TERT cells were sub-cultured per Invitrogen® instructions. Briefly, the cells were washed with D-PBS, then trypsin-EDTA (0.05% Trypsin/0.53 nM EDTA; Corning) was added to the cell culture dish. The cell culture dish was placed in the incubator for ~5 mins to activate the trypsin. The cell culture dishes were then gently tapped to detach any remaining adherent cells. Approximately 2.0 - 3.0 ml of Dulbecco's modified eagle's medium (DMEM) supplemented with 10% fetal bovine serum (FBS) and 1% antibiotic solution was added to the cell suspension to deactivate the trypsin. The cell suspension was centrifuged at 4 °C for 7 min at 13 rcf and the supernatant was removed. The cell suspension was re-suspended in fresh cell culture medium and either replated to continue to grow the cells or used for experiments. When used in experiments, the cells were seeded on top of the HA-ColI scaffolds.

6.2 Cell Viability: Live/dead analysis

6.2.1 Materials and Methods

Calcein AM (C-AM 2 μM; Biotium, USA) and propidium (PI, 3 μM; Sigma-Aldrich) dyes were used to label live and dead cells, respectively. C-AM itself is not a fluorescent molecule, but the calcein generated from C-AM by esterase activity in viable cells emits a strong green fluorescence signal at 530 nm upon excitation with blue light [160]. Hence, C-AM exclusively stains viable cells. On the other hand, PI is a red-fluorescent dye which is not able to pass through a viable cell membrane. PI labeling only

occurs for cells with compromised plasma membranes and when PI reaches the nucleus where it intercalates with the DNA [161]. After 1 and 3 days of cell culture, the cell culture medium was removed and replaced with fresh cell culture medium containing C-AM and PI. The cells were then returned to the incubator for 20 min before epifluorescence images were captured using the Nikon Eclipse Ti microscope.

6.2.2 Results

Cell viability was evaluated at day 1 and day 3 for WS1 cells cultured on tissue culture plastic (TCP) control substrates and HA-PEGDE-ITA films (Figure 27). For WS1 cells, the cell viability was comparable between cells cultured on TCP and cells cultured on the crosslinked HA film by the live/dead analysis. As shown in Figure 27, cells were more than 90% viable in both conditions based on a qualitative assessment due to the few numbers of cells that were stained with PI.

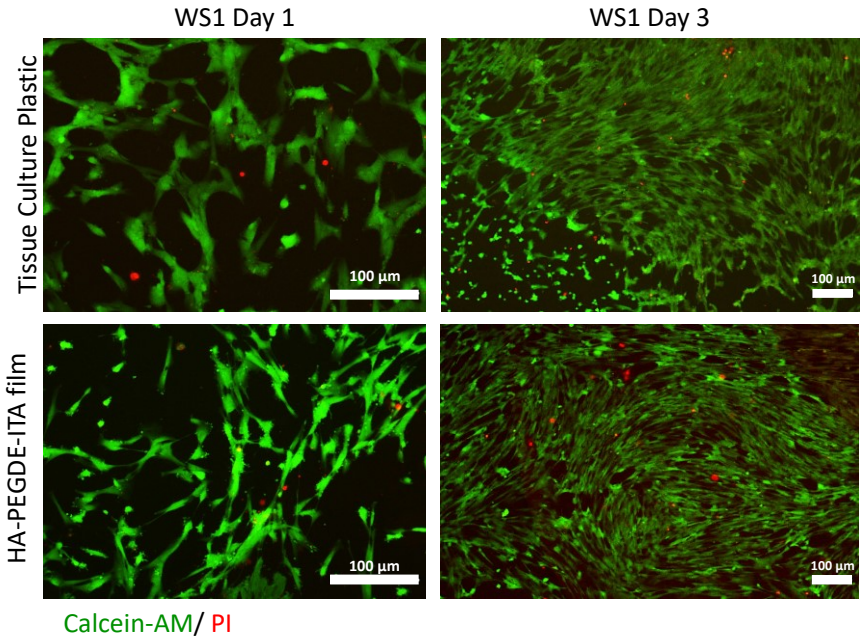

Figure 27: Viability of fibroblasts (WS1). Fluorescence micrographs showing live (green) and dead (red) WS1 cells at day 1 and day 3 of culture on TCP and on HA-PEGDE-ITA films

Cell viability analysis was also performed using N-TERT cells for the HA-ColI scaffolds with different fiber densities (25, 50 and 100 pulls), HA-PEGDE-ITA films, and TCP. The last two substrates were controls to compare if the viability was changing with the adhesion of fibers. For this experiment, evaluation was done only at day 3 since the previous experiment showed that fibroblasts were alive at day 1. Figure 28 shows that again more than 90% of the cells were viable for all conditions based on a qualitative assessment due to the few numbers of cells that were stained with PI. As expected, the films containing the ColI fibers supported cell attachment and a homogeneous distribution of cells. Additionally, there are fewer dead cells present (red fluorescence) in HA-ColI scaffolds with fiber densities of 25 and 100 pulls. These results suggest that HA-ColI scaffolds do not present cytotoxicity and that apparently there is a lower percentage of dead cells in those compared to the controls, which could be due to the improved cell attachment.

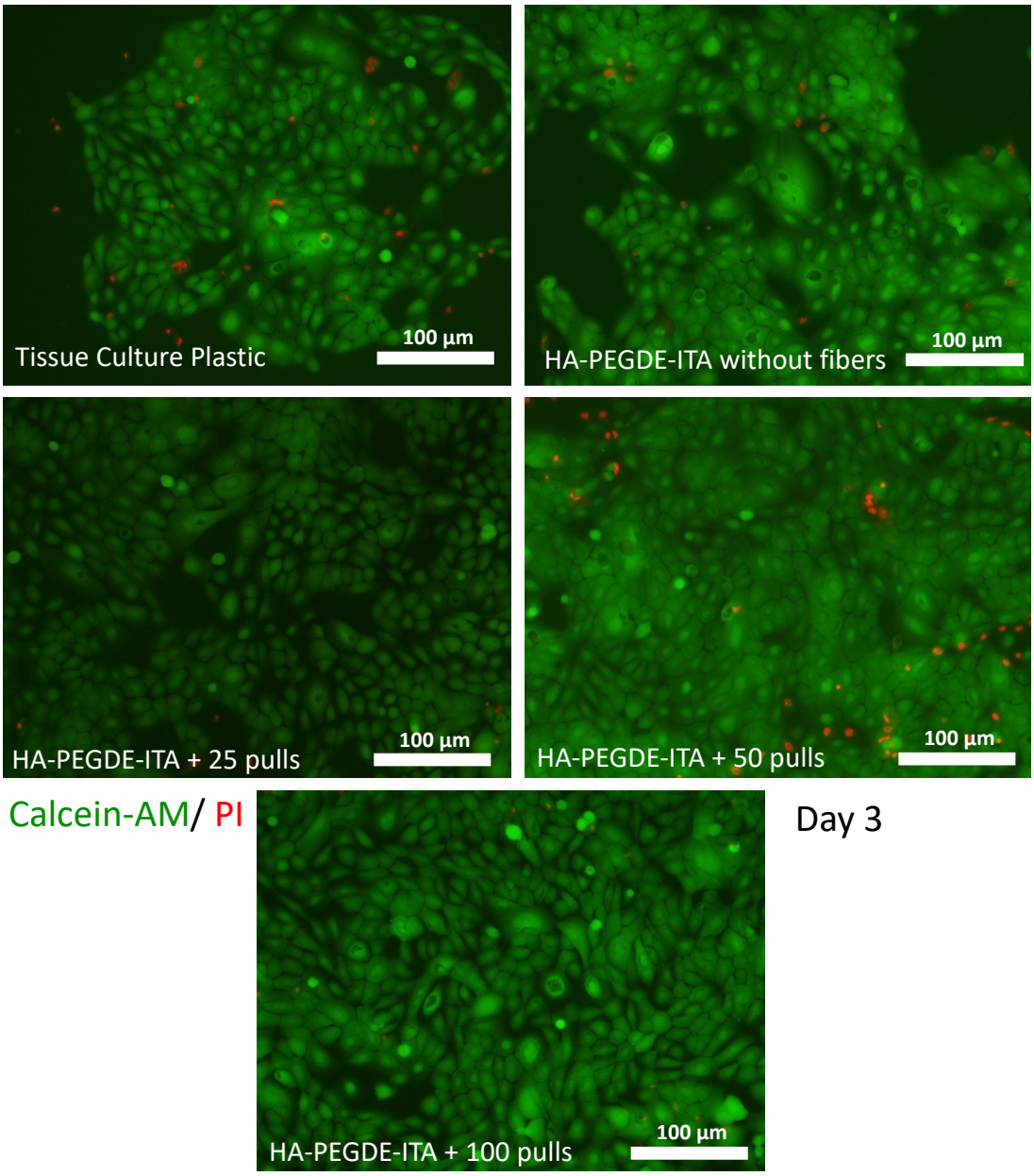

Figure 28: Viability of keratinocytes (N-TERT). Fluorescence micrographs showing live (green) and dead (red) N-TERT cells at day 3 of culture on TCP and on HA-PEGDE-ITA films as controls, and on HA-ColI scaffolds with different fiber densities (25, 50 and 100 pulls).

6.3 Cell Morphology: Phalloidin Analysis

6.3.1 Materials and Methods

Attachment, alignment, and elongation of the cells was monitored by brightfield and epifluorescence microscopy using a Nikon Eclipse Ti microscope. N-TERT cells were seeded at a density of 3×10^4 cells/well in a 48 well-plate. For detailed analysis of cell cytoskeleton organization in N-TERT cells, they were fixed with 4% paraformaldehyde (PFA; Sigma-Aldrich) for 15 min, washed with D-PBS, and permeabilized using 0.25% Triton™ X- 100 (Sigma-Aldrich) for 10 min. Cells were then washed with D-PBS and Atto 488-phalloidin (0.02 nM in PBS; Sigma-Aldrich) was added and incubated in the dark at 4 °C overnight. The phalloidin stain was then removed and samples were washed with D-PBS. Phalloidin is a highly selective bicyclic peptide used for staining F-actin (i.e., actin filaments) in tissues and cell cultures. It binds to all variants of F-actin in many different species of plants and animals [162]. To detect signal from the Atto 488 fluorophore, 480-515 nm excitation was used.

After the addition of phalloidin, Hoechst 33342 (2 μM in D-PBS; Sigma-Aldrich), a cell-permeable stain that binds to DNA and is used for staining nuclei [163], was added for 15 min as a counterstain. Finally, samples were washed with D-PBS and images were acquired by epifluorescence microscopy. The images were processed using Fiji-ImageJ software to merge the channels of the different stains into one image for visualization.

6.3.2 Results

Cells were randomly distributed when cultured on TCP and HA-PEGDE-ITA films and exhibited a cobblestone morphology with randomly oriented actin filaments. On the other hand, N-TERT cells cultured on HA-ColI scaffolds readily aligned along the surface-

anchored ColI fibers, exhibiting an elongated and aligned morphology that followed the principal direction of the fibers. In addition, aligned actin filaments were observed parallel to the axis of cell elongation. The alignment was maintained over the course of 3 days in culture (Figure 29), which was the duration of the experiment.

The control (TCP) and HA-PEGDE-ITA substrates had less cell attachment than scaffolds with higher fiber density (50 and 100 pulls), which by day 3 were completely covered with cells. However, it was still possible to observe that the cells preferred to attach to the ColI fibers (in Figure 29 with a fiber density of 50 pulls a little square is visible that was not covered with cells and was a spot where no ColI fibers were present). Moreover, the scaffold with 25 pulls provided a clear view of how the cells elongated along the fibers, and how the cells preferred to attach to the ColI fibers rather than to the HA-PEGDE-ITA film. The alignment of N-TERT cells on the HA-ColI scaffolds was also clearly shown in brightfield images, in which both fibers and cells were visible.

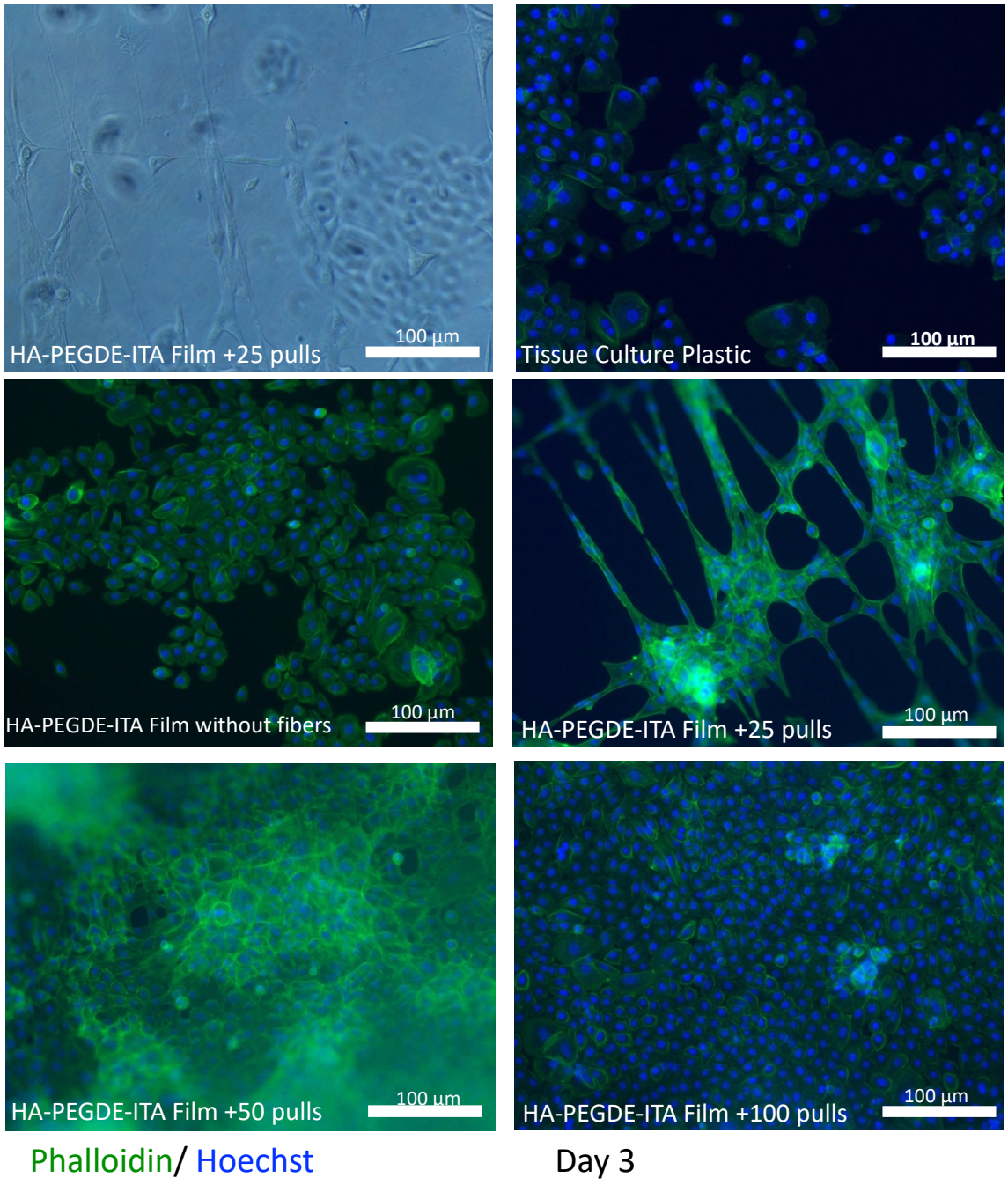

Figure 29: Cell attachment and morphology. Bright field image of HA-ColI scaffolds and fluorescence micrographs of N-TERT cells growing on the various film conditions; TCP, HA-PEGDE-ITA film, and HA-ColI scaffolds with different fiber densities (25, 50 and 100 layers/pulls of ColI). Cytoskeleton (phalloidin) and nuclei (Hoechst) staining reveled that N-TERT cells were aligned in the direction of the fibers after day 3 when seeded on HA-ColI scaffolds. Cells cultured on TCP and on HA-PEGDE-ITA films were randomly oriented and displayed cobblestone morphologies.

6.4 Time Lapse Recording of Cell Migration

6.4.1 Materials and Methods

Cell migration on HA-ColI scaffold with a fiber density of 50 pulls aligned in only one direction was monitored by brightfield microscopy using an EVOS™ FL Auto 2 Imaging system (ThermoFisher Scientific). N-TERT cells were seeded at a density of 3×10^4 cells/well in a 48 well-plate. For the migration analysis, I decided to do time-lapse live-cell imaging of the cells that were seeded on the scaffold. To maintain the cells under physiological conditions (i.e., at 37 ºC, 5% CO_2) during the recording, an EVOS™ Onstage Incubator (ThermoFisher Scientific) was used. The system was programmed to take a scan every 15 min for 24 h in a specific area of the HA-ColI scaffold. The selected area was a spot where the ColI fibers were visible as well as the seeded cells. Obtained images were then converted into video files using Fiji-ImageJ software.

6.4.2 Results

Figure 30 shows images for the migration analysis of N-TERT cells on the HA-ColI scaffold. Over 24 h, the cells migrated along the ColI fibers without the addition of chemokines. As the cells attached to the fibers, their morphology changed from a cobblestone morphology to an elongated (migratory) morphology. Cell migration did not occur in a specific direction, however, as the cell starting positions were random with respect to the surface of the material. Nonetheless, these data demonstrate that ColI fibers support the migration of keratinocytes.

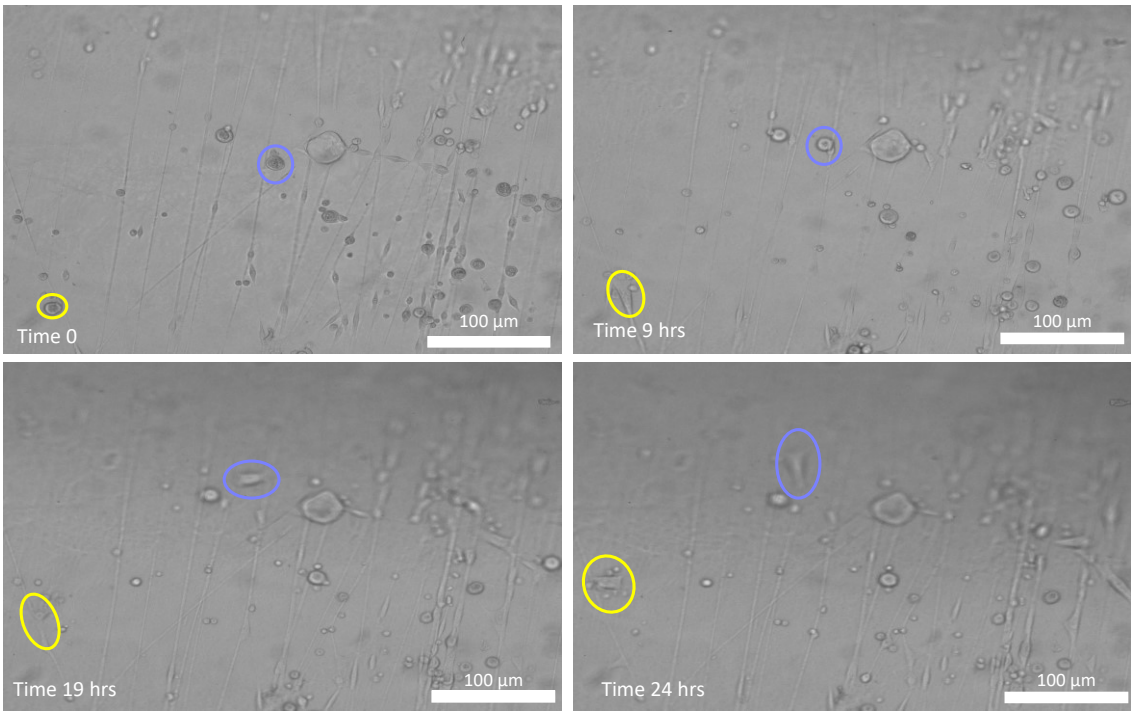

Figure 30: Cell migration analysis. Bright field images taken with the EVOS™ Imaging System every 15 min for 24 h. The N-TERT cells seeded on top of the HA-ColI scaffold attached to the ColI fibers and migrated along them. Yellow and purple circles indicate the migration of two specific cells over 24 h.

6.5 Discussion

Chemical crosslinking of HA using PEGDE and ITA as crosslinkers did not lead to cytotoxicity, which is consistent previous published studies [164]. For reference, BDDE-crosslinked HA has been reported to induce alterations in cell morphology and lead to decreased cell viability of mouse fibroblasts at concentrations of 0.5 mg/ml [165]. For this reason, cell viability of the fibroblast (WS1) was analyzed first to obtain preliminary data about the cytocompatibility of the HA-PEGDE-ITA films (Figure 27). The results of the experiments showed that the crosslinked HA film was not toxic to cells, which is in agreement with previous studies that used similar chemical crosslinking strategies for HA [89]. Next, I analyzed the viability of N-TERT cells to determine if there were any toxic effects on keratinocytes, and also to visualize if the addition of ColI fibers had any

effect on the viability of the cells (Figure 28). The HA-ColI scaffold was non-toxic to keratinocytes. Furthermore, there was an increase in cell attachment in the conditions with ColI fibers, which was expected because ColI was added to improve the bioactivity of the HA film [70]. Additionally, there were fewer dead cells visible on the films with ColI fibers, which was likely the result of improved cell attachment as keratinocytes are adherent cells that require stable attachment to maintain their viability and to proliferate [166] .

Cell morphology analysis was carried out by staining the actin filaments (Figure 29). Actin is the major cytoskeletal protein of most cells, and it polymerizes to form actin filaments (also called microfilaments), which are thin and flexible fibers within the cell. These filaments are especially abundant beneath the plasma membrane of cells, where they form a network that gives mechanical support, determines cell shape, and allows movement of the cell surface, thereby enabling cells to migrate [167]. Moreover, actin filaments also interact with the ECM via focal adhesions, mediating cell adhesion [168]. N-TERT cells seeded on the HA-ColI scaffolds exhibited an elongated and aligned morphology following the pattern of the ColI fibers. In conjunction with my observations, it has been demonstrated that the structural properties of the fibers can modulate cell migration, morphology and cytoskeleton organization [169]–[171]. For the case of cell attachment, having the ColI fibers improved the adhesion of cells on the HA-PEGDE-ITA films. Furthermore, increasing fiber density to up to 100 pulls led to a further improvement in cell attachment. Both improvements are due to the interaction of ColI with cell surface receptors (e.g., integrins) [70].

Moving forward with the *in vitro* analysis, cell migration analysis was done to further analyze the movement of the N-TERT cells on the HA-ColI scaffolds. Cell migration is an intricate, not yet fully understood process that is directed by the interaction of several signal transduction pathways initiated by diverse ligands (*e.g.*, ECM components, chemokines, growth factors) and receptors (*e.g.*, receptor tyrosine kinases, mannose receptor family, chemokine receptors, integrins), an interplay that eventually causes the reorganization of the actin cytoskeleton concomitant with reassembly of focal adhesion complexes and integrin-mediated signaling [172]. The migration of a single cell or a group of cells is observed as a cyclic process, which involves the polarization of cells in response to migratory signals, the extension of filopodial or lamellipodial protrusions, the formation of adhesions between the cell and the ECM, and movement of the cells over the adhesions through traction forces [173]. For the stated application of TMP repair, it was important that the material was able to promote cell migration to close the perforation and allow the TM to heal [8]. The results from the live-cell recording (Figure 30) demonstrated that seeded cells first attached to the ColI fibers on the films and then migrated along the fibers. With this experiment it was possible to visualize the cyclic process of migration (i.e., polarization of cells, extension of filopodial protrusions, etc.). This outcome shows that the HA-ColI scaffolds have great potential to be used for TMP repair.

Chapter 7. Conclusions and Future Directions

In this thesis, a novel scaffold comprising a crosslinked HA film with attached ColI fibers was developed for TMP repair. It was shown that crosslinking HA with PEGDE and ITA produces a film that undergoes an acceptable amount of swelling and that slows its degradation time when immersed in PBS or antibiotic droplets at 37ºC. Combining spin coating and solution casting produced a film of a defined thickness in the range of the native TM. Moreover, the crosslinked HA film functionalized with ColI fibers provided topographical and biochemical cues to cells. Track spinning was used to automate the contact drawing approach for production of the ColI fibers. It was shown that the tensile properties of the HA-ColI scaffold with 100 fiber layers approximated those of the native human tympanic membrane and was adequate for surgical handling in its wet state. The *in vitro* validation further demonstrated that dermal fibroblast and keratinocytes attached on the scaffold with no apparent cytotoxicity. Additionally, it was observed that fibers in the scaffold promoted cell attachment and migration of human keratinocytes. In summary, the objectives described at the beginning of this thesis were achieved.

There are, however, some minor limitations with the HA-Col1 fiber scaffold that need to be addressed. During the production of the crosslinked HA films, it was observed that they can sometimes contain air bubbles. Those air bubbles act as imperfections in the film that can form weak points when the material is subject to mechanical loading. Thus, additional steps to remove the air bubbles should be considered during the fabrication process. A possible way to address this issue could be to increase the time the solution remains in the degassing chamber with the vacuum connected. Furthermore, crosslinking was only evaluated based on the FTIR spectra obtained for unmodified HA and HA-

PEGDE-ITA and the visible stretching representing the bonds. The degree of crosslinking could be quantified using NMR spectroscopy. Additionally, stress calculation within the mechanical testing was based on the average thickness of the HA-PEGDE-ITA film. Profilometry should be conducted again for the HA-ColI scaffold to obtain the thickness increase by the fibers and include them into the calculations. However, the results are not expected to be affected by much since preliminary measurements by 3D BioFibR™ Inc. suggest that, with the number of pulls conducted within this thesis, the thickness won't increase by more than 6 µm. Lastly, the cell studies within this thesis were carried out for up to three days as the main goal was to demonstrate attachment and migration of cells. To be able to safely move onto further studies using *in vivo* models, a longer *in vitro* study of up to fourteen days is needed since this is the average time it would normally take for a wound to heal [50].

Additionally, future work could focus on the alignment of the ColI fibers on the crosslinked HA film. Here, an idea could be to align the fibers in a radial structure, which would mimic the anatomy of the human TM where web-like radial and concentric architecture can be seen (as shown in Figure 1). Following this structure, a connection of all fibers to the center could be ensured, which could further guide and improve cell migration and proliferation. Also, hemocompatibility analysis needs to be carried out. This study helps to examine how the scaffold reacts when it is in contact with blood. Some examples of analysis could be hemolysis and blood coagulation time. Once this is accomplished, moving to *in vivo* analysis using animal models (e.g. chinchilla) can be done. Furthermore, acoustic performance could be analyzed, which is relevant since the TM is involved in sound conduction (as was presented in chapter 1.2). A possible analysis

for this could be to examine sound transmission loss of the scaffold at various frequencies [174]. Lastly, the material has the potential to not only be used for TMP repair, but also for other tissue regeneration applications, e.g., in nervous tissue.

To conclude this thesis, a first demonstration of the HA-ColI scaffold in a human TM with a perforation has been conducted using a cadaver. Here, a perforation was made in the TM of a human cadaver and the HA-ColI scaffold was successfully attached to the perforation by cutting the necessary size and placing it with tweezers into the ear canal (pressing the scaffold against the TM in a delicate way). Optical coherence tomography (OCT) as well as light microscopy images have been taken, as shown in Figure 31.

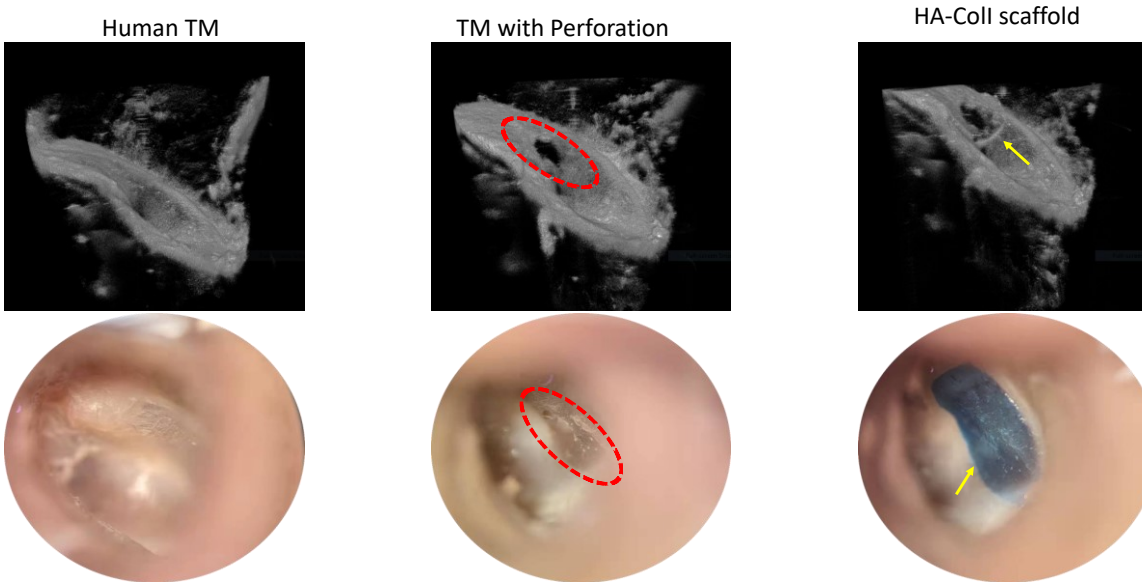

Figure 31: Demonstration of the HA-ColI scaffold in a human cadaver TMP model. Top: OCT images, bottom: Light microscopy images. The red lined circle indicates the location of the TMP and the yellow arrow points to the placement of the HA-ColI scaffold. The perforation in this cadaver was created using surgical tools.

The OCT images demonstrate that the HA-ColI scaffold is transparent enough for examination of the middle ear. This outcome is relevant since members of Dr. Robert Adamson's lab, who are working on TM imaging, pointed out that the commonly used tissue to repair TMP (cartilage) does not make it possible to examine the middle ear

because the material is opaque. On the other hand, the light microscopy images show that due to the blue colour of the film, the surgeon is still able to clearly distinguish between the ear and the scaffold, which is helpful to be sure that the scaffold is placed in the correct spot. Furthermore, this first surgical handling has demonstrated that the material was not complicated to work with in the reduced space of the ear canal. Overall, this demonstration highlights the key functions of the material for TMP repair and suggests that further development and testing are warranted.

References

[1] W. A. Haseltine, “Healing Ruptured Eardrums With A New 3-D Printed Graft,” *Forbes*, pp. 6–9, 2021.

[2] O. A. Sogebi, E. A. Oyewole, and T. O. Mabifah, “Traumatic tympanic membrane perforations: characteristics and factors affecting outcome,” *Ghana Med. J.*, vol. 52, no. 1, pp. 34–40, 2018, doi: 10.4314/gmj.v52i1.7.

[3] L. Monasta *et al.*, “Burden of disease caused by otitis media: Systematic review and global estimates,” *PLoS One*, vol. 7, no. 4, Apr. 2012, doi: 10.1371/JOURNAL.PONE.0036226.

[4] R. P. Venekamp, M. J. Burton, T. M. van Dongen, G. J. van der Heijden, A. van Zon, and A. G. Schilder, “Antibiotics for otitis media with effusion in children,” *Cochrane Database Syst. Rev.*, vol. 2016, no. 6, 2016, doi: 10.1002/14651858.CD009163.pub3.

[5] F. T. Orji and C. C. Agu, “Determinants of spontaneous healing in traumatic perforations of the tympanic membrane,” *Clin. Otolaryngol.*, vol. 33, no. 5, pp. 420–426, 2008, doi: 10.1111/j.1749-4486.2008.01764.x.

[6] J. B. FARRIOR, “THE ANTERIOR TYMPANOMEATAL ANGLE IN TYMPANOPLASTY,” *Laryngoscope*, vol. 93, no. 8, p. 992???997, Aug. 1983, doi: 10.1288/00005537-198308000-00004.

[7] C. D. Bluestone *et al.*, “Definitions, terminology, and classification of otitis media,” *Ann. Otol. Rhinol. Laryngol.*, vol. 111, no. 3 SUPPL., pp. 8–18, 2002, doi: 10.1177/00034894021110s304.

[8] B. M. Teh, Y. Shen, P. L. Friedland, M. D. Atlas, and R. J. Marano, “A review on the use of hyaluronic acid in tympanic membrane wound healing,” *Expert Opin. Biol. Ther.*, vol. 12, no. 1, pp. 23–36, 2012, doi: 10.1517/14712598.2012.634792.

[9] M. Mozaffari, D. Jiang, and A. S. Tucker, “Developmental aspects of the tympanic membrane: Shedding light on function and disease,” *Genesis*, vol. 58, no. 3–4, pp. 1–10, 2020, doi: 10.1002/dvg.23348.

[10] B. M. Teh, R. J. Marano, Y. Shen, P. L. Friedland, R. J. Dilley, and M. D. Atlas, “Tissue engineering of the tympanic membrane,” *Tissue Eng. - Part B Rev.*, vol. 19, no. 2, pp. 116–132, 2013, doi: 10.1089/ten.teb.2012.0389.

[11] S. Van Der Jeught, J. J. J. Dirckx, J. R. M. Aerts, A. Bradu, A. G. Podoleanu, and J. A. N. Buytaert, “Full-field thickness distribution of human tympanic membrane obtained with optical coherence tomography,” *JARO - J. Assoc. Res. Otolaryngol.*, vol. 14, no. 4, pp. 483–494, 2013, doi: 10.1007/s10162-013-0394-z.

[12] O. Beger *et al.*, “Comparison of fetal and adult tympanic membrane sizes: a cadaveric study,” *Surg. Radiol. Anat.*, vol. 43, no. 2, pp. 161–167, 2021, doi: 10.1007/s00276-020-02593-6.

[13] A. Kacker, D. Pierce-Smith, and M. Fraser, “Anatomy and Physiology of the Ear,” *Health Encyclopedia - University of Rochester Medical Center*. 2021, [Online]. Available: https://www.urmc.rochester.edu/encyclopedia/content.aspx?ContentTypeID=90&ContentID=P02025.

[14] B. Wang *et al.*, “Acoustic transmitted electrospun fibrous membranes for tympanic membrane regeneration,” *Chem. Eng. J.*, vol. 419, no. March, p. 129536, 2021, doi: 10.1016/j.cej.2021.129536.

[15] A. Akyigit, O. Sakallıoglu, and T. Karlidag, “Endoscopic tympanoplasty,” *J. Otol.*, vol. 12, no. 2, pp. 62–67, 2017, doi: 10.1016/j.joto.2017.04.004.

[16] Z. G. Schwam and M. K. Cosetti, “Endoscopic Myringoplasty and Type I Tympanoplasty,” *Otolaryngol. Clin. North Am.*, vol. 54, no. 1, pp. 75–88, 2021, doi: 10.1016/j.otc.2020.09.010.

[17] J. F. Anzola and J. F. Nogueira, “Endoscopic Techniques in Tympanoplasty,” *Otolaryngol. Clin. North Am.*, vol. 49, no. 5, pp. 1253–1264, 2016, doi: 10.1016/j.otc.2016.05.016.

[18] A. J. Fishman and J. Mierzwinski, “Myringoplasty/Tympanoplasty, Zone-Based Approach and Total Tympanic Membrane Reconstruction (TTMR) BT - Encyclopedia of Otolaryngology, Head and Neck Surgery,” S. E. Kountakis, Ed. Berlin, Heidelberg: Springer Berlin Heidelberg, 2013, pp. 1717–1728.

[19] R. K. Jackler and C. Gralapp, “Lateral Graft Tympanoplasty,” *Otologic Surgery Atlas*, Jun. 2022. https://www.csurgeries.com/video/lateral-graft-tympanoplasty/ (accessed Jun. 19, 2022).

[20] M. R. de Freitas and T. C. de Oliveira, “The role of different types of grafts in tympanoplasty,” *Braz. J. Otorhinolaryngol.*, vol. 80, no. 4, pp. 275–276, 2014, doi: 10.1016/j.bjorl.2014.05.018.

[21] A. Bayram, N. Bayar Muluk, C. Cingi, and S. A. Bafaqeeh, “Success rates for various graft materials in tympanoplasty – A review,” *J. Otol.*, vol. 15, no. 3, pp. 107–111, 2020, doi: 10.1016/j.joto.2020.01.001.

[22] B. Levin, R. Rajkhowa, S. L. Redmond, and M. D. Atlas, “Grafts in myringoplasty: Utilizing a silk fibroin scaffold as a novel device,” *Expert Rev. Med. Devices*, vol. 6, no. 6, pp. 653–664, 2009, doi: 10.1586/erd.09.47.

[23] A. M. Youssef, “Use of acellular human dermal allograft in tympanoplasty,” *Laryngoscope*, vol. 109, no. 11, pp. 1832–1833, 1999, doi: 10.1097/00005537-199911000-00020.

[24] K. L. Aya and R. Stern, “Hyaluronan in wound healing : Rediscovering a major player,” *Wound Repair Regen.*, vol. 22, no. 5, pp. 579–593, 2014, doi: 10.1111/wrr.12214.

[25] S. Garantziotis and R. C. Savani, “Hyaluronan biology : A complex balancing act of structure , function , location and context,” *Matrix Biol.*, vol. 78–79, pp. 1–10, 2019, doi: 10.1016/j.matbio.2019.02.002.

[26] A. Fallacara, E. Baldini, and S. Vertuani, “Hyaluronic Acid in the Third Millennium,” *Polymers (Basel).*, vol. 10, no. 7, pp. 1–36, 2018, doi: 10.3390/polym10070701.

[27] B. P. Toole, “Hyaluronan in morphogenesis,” *Cell Dev. Biol.*, vol. 12, no. 2, pp. 79–87, 2001, doi: 10.1006/scdb.2000.0244.

[28] S. Tang, K. Chi, H. Xu, Q. Yong, J. Yang, and J. M. Catchmark, “A covalently cross-linked hyaluronic acid/bacterial cellulose composite hydrogel for potential biological applications,” *Carbohydr. Polym.*, vol. 252, p. 117123, Jan. 2021, doi: 10.1016/j.carbpol.2020.117123.

[29] D. Vigetti, E. Karousou, M. Viola, S. Deleonibus, G. De Luca, and A. Passi, “Biochimica et Biophysica Acta Hyaluronan : Biosynthesis and signaling ☆,” *BBA - Gen. Subj.*, vol. 1840, no. 8, pp. 2452–2459, 2014, doi: 10.1016/j.bbagen.2014.02.001.

[30] L. Vistejnova *et al.*, “Cytokine Low molecular weight hyaluronan mediated CD44 dependent induction of IL-6 and chemokines in human dermal fibroblasts potentiates innate immune response,” *Cytokine*, vol. 70, no. 2, pp. 97–103, 2014, doi: 10.1016/j.cyto.2014.07.006.

[31] E. A. Turley, P. W. Noble, and L. Y. W. Bourguignon, “Signaling properties of hyaluronan receptors.,” *J. Biol. Chem.*, vol. 277, no. 7, pp. 4589–92, Feb. 2002, doi: 10.1074/jbc.R100038200.

[32] M. M. G. Fouda *et al.*, “Wound healing of different molecular weight of hyaluronan ; in-vivo study,” *Int. J. Biol. Macromol.*, vol. 89, pp. 582–591, 2016, doi: 10.1016/j.ijbiomac.2016.05.021.

[33] N. Zhao, X. Wang, L. Qin, Z. Guo, and D. Li, “Effect of molecular weight and concentration of hyaluronan on cell proliferation and osteogenic differentiation in vitro,” *Biochem. Biophys. Res. Commun.*, vol. 465, no. 3, pp. 569–574, 2015, doi: 10.1016/j.bbrc.2015.08.061.

[34] R. C. Gupta, R. Lall, A. Srivastava, and A. Sinha, “Hyaluronic acid: Molecular mechanisms and therapeutic trajectory,” *Front. Vet. Sci.*, vol. 6, no. JUN, pp. 1–24, 2019, doi: 10.3389/fvets.2019.00192.

[35] T. L. Nascimento, H. Hillaireau, J. Vergnaud, and E. Fattal, “Lipid-based nanosystems for CD44 targeting in cancer treatment : recent significant advances , ongoing challenges and unmet needs,” *Nanomedicine*, vol. 11, no. 14, pp. 1865–1887, 2016.

[36] H. Ponta, L. Sherman, and P. A. Herrlich, “CD44: From adhesion molecules to signalling regulators,” *Nat. Rev. Mol. Cell Biol.*, vol. 4, no. 1, pp. 33–45, 2003, doi: 10.1038/nrm1004.

[37] A. G. Tavianatou, I. Caon, M. Franchi, Z. Piperigkou, D. Galesso, and N. K. Karamanos, “Hyaluronan: molecular size-dependent signaling and biological functions in inflammation and cancer,” *FEBS J.*, vol. 286, no. 15, pp. 2883–2908, 2019, doi: 10.1111/febs.14777.

[38] C. Yang *et al.*, “The high and low molecular weight forms of hyaluronan have distinct effects on CD44 clustering,” *J. Biol. Chem.*, vol. 287, no. 51, pp. 43094–43107, 2012, doi: 10.1074/jbc.M112.349209.

[39] K. Fuchs, A. Hippe, A. Schmaus, B. Homey, J. P. Sleeman, and V. Orian-Rousseau, “Opposing effects of high-and low-molecular weight hyaluronan on CXCL12-induced CXCR4 signaling depend on CD44,” *Cell Death Dis.*, vol. 4, no. 10, 2013, doi: 10.1038/cddis.2013.364.

[40] J. Lesley, V. C. Hascall, M. Tammi, and R. Hyman, “Hyaluronan binding by cell surface CD44,” *J. Biol. Chem.*, vol. 275, no. 35, pp. 26967–26975, 2000, doi: 10.1074/jbc.M002527200.

[41] L. Markasz, R. C. Savani, A. Jonzon, and R. Sindelar, “CD44 and RHAMM expression patterns in the human developing lung,” *Pediatr. Res.*, no. October 2019, pp. 1–9, 2020, doi: 10.1038/s41390-020-0873-y.

[42] A. M. Carvalho, D. Soares, P. M. R. Paulo, and R. L. Reis, “Co-localization and crosstalk between CD44 and RHAMM depend on hyaluronan presentation,” *Acta Biomater.*, no. xxxx, 2020, doi: 10.1016/j.actbio.2020.10.024.

[43] H. Suga *et al.*, “TLR4, rather than TLR2, regulates wound healing through TGF-β and CCL5 expression,” *J. Dermatol. Sci.*, vol. 73, no. 2, pp. 117–124, 2014, doi: 10.1016/j.jdermsci.2013.10.009.

[44] D. Jiang, D. Jiang, J. Liang, Y. Li, and P. W. Noble, “The role of Toll-like receptors in non-infectious lung injury,” *Cell Res.*, vol. 16, pp. 693–701, 2006, doi: 10.1038/sj.cr.7310085.

[45] E. N. Harris and E. Baker, “Role of the Hyaluronan Receptor , Stabilin-2 / HARE , in Health and Disease,” *Int. J. Mol. Sci.*, vol. 21, pp. 1–15, 2020.

[46] R. Prevo, S. Banerji, D. J. P. Ferguson, S. Clasper, and D. G. Jackson, “Mouse LYVE-1 Is an Endocytic Receptor for Hyaluronan in Lymphatic Endothelium,” *J. Biol. Chem.*, vol. 276, no. 22, pp. 19420–19430, 2001, doi: 10.1074/jbc.M011004200.

[47] M. Dovedytis, Z. J. Liu, and S. Bartlett, “Hyaluronic acid and its biomedical applications: A review,” *Eng. Regen.*, vol. 1, no. October, pp. 102–113, 2020, doi: 10.1016/j.engreg.2020.10.001.

[48] C. B. Highley, G. D. Prestwich, and J. A. Burdick, “Recent advances in hyaluronic acid hydrogels for biomedical applications,” *Curr. Opin. Biotechnol.*, vol. 40, pp. 35–40, Aug. 2016, doi: 10.1016/j.copbio.2016.02.008.

[49] S. K. Hahn, J. K. Park, T. Tomimatsu, and T. Shimoboji, “Synthesis and degradation test of hyaluronic acid hydrogels,” *Int. J. Biol. Macromol.*, vol. 40, no. 4, pp. 374–380, Mar. 2007, doi: 10.1016/j.ijbiomac.2006.09.019.

[50] G. C. Gurtner, S. Werner, Y. Barrandon, and M. T. Longaker, “Wound repair and regeneration,” *Nature*, vol. 453, no. 7193, pp. 314–321, 2008, doi: 10.1038/nature07039.

[51] P. H. Weigel, S. J. Frost, R. D. LeBoeuf, and C. T. McGary, “The specific interaction between fibrin(ogen) and hyaluronan: possible consequences in haemostasis, inflammation and wound healing.,” *Ciba Found. Symp.*, vol. 143, pp. 248–264, 1989, doi: 10.1002/9780470513774.ch15.

[52] W. Y. J. CHEN and G. ABATANGELO, “Functions of hyaluronan in wound repair,” *Wound Repair Regen.*, vol. 7, no. 2, pp. 79–89, Mar. 1999, doi: 10.1046/j.1524-475X.1999.00079.x.

[53] P. Rooney, M. Wang, P. Kumar, and S. Kumar, “Angiogenic oligosaccharides of hyaluronan enhance the production of collagens by endothelial cells,” *J. Cell Sci.*, vol. 105, no. 1, pp. 213–218, 1993, doi: 10.1242/jcs.105.1.213.

[54] M. Slevin *et al.*, “Hyaluronan-mediated angiogenesis in vascular disease : Uncovering RHAMM and CD44 receptor signaling pathways,” *Matrix Biol.*, vol. 26, pp. 58–68, 2007, doi: 10.1016/j.matbio.2006.08.261.

[55] J. A. P. Gomes, R. Amankwah, A. Powell-Richards, and H. S. Dua, “Sodium hyaluronate (hyaluronic acid) promotes migration of human corneal epithelial cells in vitro,” *Br. J. Ophthalmol.*, vol. 88, no. 6, pp. 821–825, 2004, doi: 10.1136/bjo.2003.027573.

[56] B. K. Sun, Z. Siprashvili, and P. A. Khavari, “Advances in skin grafting and treatment of cutaneous wounds,” *Science (80-.).*, vol. 346, no. 6212, pp. 941–945, 2014, doi: 10.1126/science.1253836.

[57] H. B. Gladstone, R. K. Jackler, and K. Varav, “Tympanic Membrane Wound Healing: An Overview,” *Otolaryngol. Clin. North Am.*, vol. 28, no. 5, pp. 913–932, Oct. 1995, doi: 10.1016/S0030-6665(20)30467-9.

[58] Z. C. Lou and Z. H. Lou, “A moist edge environment AIDS the regeneration of traumatic tympanic membrane perforations,” *J. Laryngol. Otol.*, vol. 131, no. 7, pp. 564–571, 2017, doi: 10.1017/S0022215117001001.

[59] L. E. Stenfors, “Repair of tympanic membrane perforations using hyaluronic acid: An alternative to myringoplasty,” *J. Laryngol. Otol.*, vol. 103, no. 1, pp. 39–40, 1989, doi: 10.1017/S0022215100107984.

[60] P. L. S. Maria, S. L. Redmond, M. D. Atlas, and R. Ghassemifar, “Histology of the healing tympanic membrane following perforation in rats,” *Laryngoscope*, vol. 120, no. 10, pp. 2061–2070, 2010, doi: 10.1002/lary.20998.

[61] L. E. Stenfors, B. Carlsöouml;, B. Salé;n, and B. Winblad, “Repair of experimental tympanic membrane perforations,” *Acta Otolaryngol.*, vol. 90, no. 1–6, pp. 332–341, 1980, doi: 10.3109/00016488009131734.

[62] S. Hellström and C. Laurent, “Hyaluronan and healing of tympanic membrane perforations. An experimental study,” *Acta Otolaryngol.*, vol. 104, no. S442, pp. 54–61, 1987, doi: 10.3109/00016488709102840.

[63] L. E. Stenfors, “Treatment of tympanic membrane perforations with hyaluronan in an open pilot study of unselected patients,” *Acta Otolaryngol.*, vol. 104, no. S442, pp. 81–87, 1987, doi: 10.3109/00016488709102845.

[64] K. Kaur, H. Singh, and M. Singh, “Repair of tympanic membrane perforation by topical application of 1% sodium hyaluronate,” *Indian J. Otolaryngol. Head Neck Surg.*, vol. 58, no. 3, pp. 241–244, 2006, doi: 10.1007/BF03050829.

[65] K. N. O’Connor, M. Tam, N. H. Blevins, and S. Puria, “Tympanic membrane collagen fibers: A key to high-frequency sound conduction,” *Laryngoscope*, vol. 118, no. 3, pp. 483–490, 2008, doi: 10.1097/MLG.0b013e31815b0d9f.

[66] M. Kato and R. K. Jackler, “Repair of chronic tympanic membrane perforations with fibroblast growth factor,” *Otolaryngol. - Head Neck Surg.*, vol. 115, no. 6, pp. 538–547, 1996, doi: 10.1016/S0194-5998(96)70008-6.

[67] N. S. Fedarko, *Osteoblast/Osteoclast Development and Function in Osteogenesis Imperfecta*. Elsevier Inc., 2013.

[68] E. Makareeva and S. Leikin, *Collagen Structure, Folding and Function*. Elsevier Inc., 2013.

[69] M. Makuszewska *et al.*, “Expression of collagens type I and V in healing rat’s tympanic membrane,” *Int. J. Pediatr. Otorhinolaryngol.*, vol. 118, no. December 2018, pp. 79–83, 2019, doi: 10.1016/j.ijporl.2018.12.020.

[70] I. Boraschi-Diaz, J. Wang, J. S. Mort, and S. V. Komarova, “Collagen type i as a ligand for receptor-mediated signaling,” *Front. Phys.*, vol. 5, no. MAY, pp. 1–11, 2017, doi: 10.3389/fphy.2017.00012.

[71] J. Heino, “The collagen family members as cell adhesion proteins,” *BioEssays*, vol. 29, no. 10, pp. 1001–1010, 2007, doi: 10.1002/bies.20636.

[72] C. Somaiah *et al.*, “Collagen promotes higher adhesion, survival and proliferation of mesenchymal stem cells,” *PLoS One*, vol. 10, no. 12, pp. 1–15, 2015, doi: 10.1371/journal.pone.0145068.

[73] C. H. Jang, S. H. Ahn, J. W. Lee, B. H. Lee, H. Lee, and G. H. Kim, “Mesenchymal stem cell-laden hybrid scaffold for regenerating subacute tympanic membrane perforation,” *Mater. Sci. Eng. C*, vol. 72, pp. 456–463, 2017, doi: 10.1016/j.msec.2016.11.094.

[74] H. Ying *et al.*, “In situ formed collagen-hyaluronic acid hydrogel as biomimetic dressing for promoting spontaneous wound healing,” *Mater. Sci. Eng. C*, vol. 101, pp. 487–498, 2019, doi: https://doi.org/10.1016/j.msec.2019.03.093.

[75] S. Suri and C. E. Schmidt, “Photopatterned collagen–hyaluronic acid interpenetrating polymer network hydrogels,” *Acta Biomater.*, vol. 5, no. 7, pp. 2385–2397, Sep. 2009, doi: 10.1016/j.actbio.2009.05.004.

[76] Y. He *et al.*, “Assessment of biological properties of recombinant collagen-hyaluronic acid composite scaffolds,” *Int. J. Biol. Macromol.*, vol. 149, pp. 1275–1284, Apr. 2020, doi: 10.1016/j.ijbiomac.2020.02.023.

[77] T. Walimbe, S. Calve, A. Panitch, and M. P. Sivasankar, “Incorporation of types I and III collagen in tunable hyaluronan hydrogels for vocal fold tissue engineering,” *Acta Biomater.*, vol. 87, pp. 97–107, 2019, doi: https://doi.org/10.1016/j.actbio.2019.01.058.

[78] B. C. Dash, K. Duan, H. Xing, T. R. Kyriakides, and H. C. Hsia, “An in situ collagen-HA hydrogel system promotes survival and preserves the proangiogenic secretion of hiPSC-derived vascular smooth muscle cells,” *Biotechnol. Bioeng.*, vol. 117, no. 12, pp. 3912–3923, Dec. 2020, doi: 10.1002/bit.27530.

[79] S. Rother *et al.*, “Hyaluronan/Collagen Hydrogels with Sulfated Hyaluronan for Improved Repair of Vascularized Tissue Tune the Binding of Proteins and Promote Endothelial Cell Growth,” *Macromol. Biosci.*, vol. 17, no. 11, p. 1700154, Nov. 2017, doi: 10.1002/mabi.201700154.

[80] C. Abi Zeid Daou, N. Ghaoui, and M. Bassim, “Hyaluronic acid in the treatment of other miscellaneous conditions of the ear,” *Am. J. Otolaryngol. - Head Neck Med. Surg.*, vol. 42, no. 1, p. 102630, 2021, doi: 10.1016/j.amjoto.2020.102630.

[81] C. Abi Zeid Daou and M. Bassim, “Hyaluronic acid in otology: Its uses, advantages and drawbacks - A review,” *Am. J. Otolaryngol. - Head Neck Med. Surg.*, vol. 41, no. 2, p. 102375, 2020, doi: 10.1016/j.amjoto.2019.102375.

[82] J. P. Frampton *et al.*, “Elongation of fibers from highly viscous dextran solutions enables fabrication of rapidly dissolving drug carrying fabrics,” *Adv. Healthc. Mater.*, vol. 4, no. 2, pp. 313–319, 2015, doi: 10.1002/adhm.201400287.

[83] C. E. Schanté, G. Zuber, C. Herlin, and T. F. Vandamme, “Chemical modifications of hyaluronic acid for the synthesis of derivatives for a broad range of biomedical applications,” *Carbohydr. Polym.*, vol. 85, no. 3, pp. 469–489, Jun. 2011, doi: 10.1016/j.carbpol.2011.03.019.

[84] H.-Y. Lee, C.-H. Hwang, H.-E. Kim, and S.-H. Jeong, "Enhancement of bio-stability and mechanical properties of hyaluronic acid hydrogels by tannic acid treatment," *Carbohydr. Polym.*, vol. 186, pp. 290–298, Apr. 2018, doi: 10.1016/j.carbpol.2018.01.056.

[85] M. N. Collins and C. Birkinshaw, "Comparison of the effectiveness of four different crosslinking agents with hyaluronic acid hydrogel films for tissue-culture applications," *J. Appl. Polym. Sci.*, vol. 104, no. 5, pp. 3183–3191, Jun. 2007, doi: 10.1002/app.25993.

[86] I. Perelshtein, E. Ruderman, A. Francesko, M. M. Fernandes, T. Tzanov, and A. Gedanken, "Tannic acid NPs - Synthesis and immobilization onto a solid surface in a one-step process and their antibacterial and anti-inflammatory properties," *Ultrason. Sonochem.*, vol. 21, no. 6, pp. 1916–1920, 2014, doi: 10.1016/j.ultsonch.2013.11.022.

[87] C. H. Jeong *et al.*, "In vitro toxicity assessment of crosslinking agents used in hyaluronic acid dermal filler," *Toxicol. Vitr.*, vol. 70, no. June 2020, p. 105034, 2021, doi: 10.1016/j.tiv.2020.105034.

[88] X. Zhao, "US 8,080,461 B2," 2011.

[89] J. A. Calles, L. I. Tártara, A. Lopez-García, Y. Diebold, S. D. Palma, and E. M. Vallés, "Novel bioadhesive hyaluronan–itaconic acid crosslinked films for ocular therapy," *Int. J. Pharm.*, vol. 455, no. 1–2, pp. 48–56, Oct. 2013, doi: 10.1016/j.ijpharm.2013.07.063.

[90] S. Brännström, M. Finnveden, M. Johansson, M. Martinelle, and E. Malmström, "Itaconate based polyesters: Selectivity and performance of esterification catalysts," *Eur. Polym. J.*, vol. 103, no. November 2017, pp. 370–377, Jun. 2018, doi: 10.1016/j.eurpolymj.2018.04.017.

[91] B. D. Ratner, "Role of Water in Biomaterials," in *Biomaterials Science: An Introduction to Materials: Third Edition*, Third Edit., no. 1989, B. D. Ratner, Ed. Elsevier, 2013, pp. 55–59.

[92] J. A. Calles, A. López-García, E. M. Vallés, S. D. Palma, and Y. Diebold, "Preliminary characterization of dexamethasone-loaded cross-linked hyaluronic acid films for topical ocular therapy," *Int. J. Pharm.*, vol. 509, no. 1–2, pp. 237–243, Jul. 2016, doi: 10.1016/j.ijpharm.2016.05.054.

[93] T. Segura, B. C. Anderson, P. H. Chung, R. E. Webber, K. R. Shull, and L. D. Shea, "Crosslinked hyaluronic acid hydrogels: a strategy to functionalize and pattern," *Biomaterials*, vol. 26, no. 4, pp. 359–371, Feb. 2005, doi: 10.1016/j.biomaterials.2004.02.067.

[94] C. Laurent, S. Hellstrom, and E. Fellenius, "Hyaluronan improves the healing of experimental tympanic membrane perforations," *Arch.Otolaryngol.Head.Neck.Surg.*, vol. 114, pp. 1435–1441, 1988.

[95] T. K. Hill *et al.*, “Indocyanine green-loaded nanoparticles for image-guided tumor surgery,” *Bioconjug. Chem.*, vol. 26, no. 2, pp. 294–303, 2015, doi: 10.1021/bc5005679.

[96] X. Z. Shu, Y. Liu, Y. Luo, M. C. Roberts, and G. D. Prestwich, “Disulfide cross-linked hyaluronan hydrogels,” *Biomacromolecules*, vol. 3, no. 6, pp. 1304–1311, 2002, doi: 10.1021/bm025603c.

[97] C. Eenschooten *et al.*, “Novel self-associative and multiphasic nanostructured soft carriers based on amphiphilic hyaluronic acid derivatives,” *Carbohydr. Polym.*, vol. 87, no. 1, pp. 444–451, 2012, doi: 10.1016/j.carbpol.2011.08.004.

[98] B. P. and A. D., “New strategy for chemical modification of hyaluronic acid: Preparation of functionalized derivatives and their use in the formation of novel biocompatible hydrogels,” *J. Biomed. Mater. Res.*, vol. 47, no. 2, pp. 152–169, 1999, [Online]. Available: http://www.embase.com/search/results?subaction=viewrecord&from=export&id=L29409734%5Cnhttp://dx.doi.org/10.1002/(SICI)1097-4636(199911)47:2%3C152::AID-JBM5%3E3.0.CO%5Cn2-I%5Cnhttp://sfx.library.uu.nl/utrecht?sid=EMBASE&issn=00219304&id=doi:10.1002/(SICI)1.

[99] S. Khunmanee, Y. Jeong, and H. Park, “Crosslinking method of hyaluronic-based hydrogel for biomedical applications,” *J. Tissue Eng.*, vol. 8, 2017, doi: 10.1177/2041731417726464.

[100] N. Zerbinati *et al.*, “Chemical and mechanical characterization of hyaluronic acid hydrogel cross-linked with polyethylen glycol and its use in dermatology,” *Dermatol. Ther.*, vol. 33, no. 4, pp. 1–9, Jul. 2020, doi: 10.1111/dth.13747.

[101] D. Monticelli *et al.*, “Chemical characterization of hydrogels crosslinked with polyethylene glycol for soft tissue augmentation,” *Open Access Maced. J. Med. Sci.*, vol. 7, no. 7, pp. 1077–1081, 2019, doi: 10.3889/oamjms.2019.279.

[102] A. Sionkowska, M. Michalska-Sionkowska, and M. Walczak, “Preparation and characterization of collagen/hyaluronic acid/chitosan film crosslinked with dialdehyde starch,” *Int. J. Biol. Macromol.*, vol. 149, no. PG-290-295, pp. 290–295, Apr. 2020, doi: 10.1016/j.ijbiomac.2020.01.262.

[103] X. Z. Shu, Y. Liu, Y. Luo, M. C. Roberts, and G. D. Prestwich, “Disulfide cross-linked hyaluronan hydrogels,” *Biomacromolecules*, vol. 3, no. 6, pp. 1304–1311, 2002, doi: 10.1021/bm025603c.

[104] B. B. Mendes, A. C. Daly, R. L. Reis, R. M. A. Domingues, M. E. Gomes, and J. A. Burdick, “Injectable hyaluronic acid and platelet lysate-derived granular hydrogels for biomedical applications,” *Acta Biomater.*, vol. 119, pp. 101–113, 2021, doi: https://doi.org/10.1016/j.actbio.2020.10.040.

[105] M. A. Grimaudo, S. Nicoli, P. Santi, A. Concheiro, and C. Alvarez-Lorenzo, "Cyclosporine-loaded cross-linked inserts of sodium hyaluronan and hydroxypropyl-β-cyclodextrin for ocular administration," *Carbohydr. Polym.*, vol. 201, no. June, pp. 308–316, 2018, doi: 10.1016/j.carbpol.2018.08.073.

[106] J. A. Calles, J. A. Ressia, J. M. Llabot, E. M. Vallés, and S. D. Palma, "Hyaluronan–itaconic acid–glutaraldehyde films for biomedical applications: Preliminary studies," *Sci. Pharm.*, vol. 84, no. 1, pp. 61–72, 2016, doi: 10.3797/scipharm.1504-17.

[107] T. Robert and S. Friebel, "Itaconic acid – a versatile building block for renewable polyesters with enhanced functionality," *Green Chem.*, vol. 18, no. 10, pp. 2922–2934, 2016, doi: 10.1039/C6GC00605A.

[108] M. S. Birajdar, H. Joo, W. G. Koh, and H. Park, "Natural bio-based monomers for biomedical applications: a review," *Biomater. Res.*, vol. 25, no. 1, pp. 1–14, 2021, doi: 10.1186/s40824-021-00208-8.

[109] M. Sugimoto *et al.*, "Non-targeted metabolite profiling in activated macrophage secretion," *Metabolomics*, vol. 8, no. 4, pp. 624–633, 2012, doi: 10.1007/s11306-011-0353-9.

[110] J. H. Shin *et al.*, "1H NMR-based metabolomic profiling in mice infected with Mycobacterium tuberculosis," *J. Proteome Res.*, vol. 10, no. 5, pp. 2238–2247, 2011, doi: 10.1021/pr101054m.

[111] C. L. Strelko *et al.*, "Itaconic acid is a mammalian metabolite induced during macrophage activation," *J. Am. Chem. Soc.*, vol. 133, no. 41, pp. 16386–16389, 2011, doi: 10.1021/ja2070889.

[112] Y. Wei, D. Sun, H. Yi, H. Zhao, and J. Wang, "Preparation and characterization of PEGDE crosslinked silk fibroin film," *J. Wuhan Univ. Technol. Mater. Sci. Ed.*, vol. 29, no. 5, pp. 1083–1089, 2014, doi: 10.1007/s11595-014-1047-8.

[113] J. Baek *et al.*, "Facile strategy involving low-temperature chemical cross-linking to enhance the physical and biological properties of hyaluronic acid hydrogel," *Carbohydr. Polym.*, vol. 202, no. September, pp. 545–553, 2018, doi: 10.1016/j.carbpol.2018.09.014.

[114] K. Tomihata and Y. Ikada, "Crosslinking of hyaluronic acid with water-soluble carbodiimide," *J. Biomed. Mater. Res.*, vol. 37, no. 2, pp. 243–251, 1997, doi: 10.1002/(SICI)1097-4636(199711)37:2<243::AID-JBM14>3.0.CO;2-F.

[115] V. Martina *et al.*, "Viscoelastic properties and thermodynamic balance improvement of a hyaluronic acid hydrogel enriched with proline and glycyne," *J. Biol. Regul. Homeost. Agents*, vol. 33, no. 6, pp. 1955–1959, 2019, doi: 10.23812/19-252-L.

[116] F. Wahid, T. Khan, Z. Hussain, and H. Ullah, *Nanocomposite scaffolds for tissue engineering; properties, preparation and applications*. Elsevier Inc., 2018.

[117] X. Chen, Y. Hu, Z. Xie, and H. Wang, "Materials and Design of Photocatalytic Membranes," in *Current Trends and Future Developments on (Bio-) Membranes*, Elsevier, 2018, pp. 71–96.

[118] C. Gao *et al.*, "3D Bioprinting for Fabricating Artificial Skin Tissue," *Colloids Surfaces B Biointerfaces*, p. 112041, Aug. 2021, doi: 10.1016/j.colsurfb.2021.112041.

[119] P. K. Chandra, S. Soker, and A. Atala, *Tissue engineering: current status and future perspectives*. INC, 2020.

[120] K. Kim *et al.*, "TAPE: A medical adhesive inspired by a ubiquitous compound in plants," *Adv. Funct. Mater.*, vol. 25, no. 16, pp. 2402–2410, 2015, doi: 10.1002/adfm.201500034.

[121] Muskan, D. Gupta, and N. P. Negi, "3D bioprinting: Printing the future and recent advances," *Bioprinting*, vol. 27, no. May, p. e00211, 2022, doi: 10.1016/j.bprint.2022.e00211.

[122] S. Sokolov, A. Balynin, D. Bakhtin, and I. Borisov, "Influence of Spin Coating Parameters on Gas Transport Properties of Thin-Film Composite Membranes," *Materials (Basel).*, vol. 14, no. 17, p. 5093, Sep. 2021, doi: 10.3390/ma14175093.

[123] A. G. Emslie, F. T. Bonner, and L. G. Peck, "Flow of a viscous liquid on a rotating disk," *J. Appl. Phys.*, vol. 29, no. 5, pp. 858–862, 1958, doi: 10.1063/1.1723300.

[124] H. Chen, J. Qin, and Y. Hu, "Efficient Degradation of High-Molecular-Weight Hyaluronic Acid by a Combination of Ultrasound, Hydrogen Peroxide, and Copper Ion," *Molecules*, vol. 24, no. 3, p. 617, Feb. 2019, doi: 10.3390/molecules24030617.

[125] SigmaAldrich, "IR Spectrum Table & Chart," *Sigma Aldrich*, 2021. https://www.sigmaaldrich.com/technical-documents/articles/biology/ir-spectrum-table.html.

[126] V.-M. Airaksinen, *Silicon wafer and thin-film measurements*. INC, 2020.

[127] N. Sanjeeva Murthy, "Techniques for analyzing biomaterial surface structure, morphology and topography," *Surf. Modif. Biomater. Methods Anal. Appl.*, pp. 232–255, 2011, doi: 10.1533/9780857090768.2.232.

[128] J. A. Calles *et al.*, "Cross-linked hyaluronan films loaded with acetazolamide-cyclodextrin-triethanolamine complexes for glaucoma treatment," *Ther. Deliv.*, vol. 9, no. 3, pp. 205–219, 2018, doi: 10.4155/tde-2017-0087.

[129] Y. Park, S. H. Kim, S. Matalon, N.-H. L. Wang, and E. I. Franses, "Effect of phosphate salts concentrations, supporting electrolytes, and calcium phosphate salt precipitation on the pH of phosphate buffer solutions," *Fluid Phase Equilib.*, vol. 278, no. 1–2, pp. 76–84, Apr. 2009, doi: 10.1016/j.fluid.2009.01.005.

[130] A. Maleki, A. L. Kjøniksen, and B. Nyström, "Characterization of the chemical degradation of hyaluronic acid during chemical gelation in the presence of different cross-linker agents," *Carbohydr. Res.*, vol. 342, no. 18, pp. 2776–2792, 2007, doi: 10.1016/j.carres.2007.08.021.

[131] B. Tavsanli and O. Okay, "Preparation and fracture process of high strength hyaluronic acid hydrogels cross-linked by ethylene glycol diglycidyl ether," *React. Funct. Polym.*, vol. 109, pp. 42–51, 2016, doi: 10.1016/j.reactfunctpolym.2016.10.001.

[132] S. S. Mathew-Steiner, S. Roy, and C. K. Sen, "Collagen in wound healing," *Bioengineering*, vol. 8, no. 5, 2021, doi: 10.3390/bioengineering8050063.

[133] S. K. Verma *et al.*, "Multi-pin contact drawing enables production of anisotropic collagen fiber substrates for alignment of fibroblasts and monocytes," *Colloids Surfaces B Biointerfaces*, vol. 215, no. March, p. 112525, Jul. 2022, doi: 10.1016/j.colsurfb.2022.112525.

[134] D. H. Kim, P. P. Provenzano, C. L. Smith, and A. Levchenko, "Matrix nanotopography as a regulator of cell function," *J. Cell Biol.*, vol. 197, no. 3, pp. 351–360, 2012, doi: 10.1083/jcb.201108062.

[135] M. Rahmati *et al.*, "Electrospinning for tissue engineering applications," *Prog. Mater. Sci.*, vol. 117, no. October 2016, p. 100721, 2021, doi: 10.1016/j.pmatsci.2020.100721.

[136] V. Bambole and J. V. Yakhmi, *Tissue engineering: Use of electrospinning technique for recreating physiological functions*. Elsevier Inc., 2016.

[137] G. Y. Liu, R. Agarwal, K. R. Ko, M. Ruthven, H. T. Sarhan, and J. P. Frampton, "Templated Assembly of Collagen Fibers Directs Cell Growth in 2D and 3D," *Sci. Rep.*, vol. 7, no. 1, pp. 1–9, 2017, doi: 10.1038/s41598-017-10182-8.

[138] J. Bürck *et al.*, "Resemblance of electrospun collagen nanofibers to their native structure," *Langmuir*, vol. 29, no. 5, pp. 1562–1572, 2013, doi: 10.1021/la3033258.

[139] S. Akhshabi, E. Biazar, V. Singh, S. Heidari Keshel, and G. Nagaraja, "The effect of glutaraldehyde cross-linker on structural and biocompatibility properties of collagen-chondroitin sulfate electrospun mat," *Mater. Technol.*, vol. 33, no. 4, pp. 253–261, Mar. 2018, doi: 10.1080/10667857.2017.1410998.

[140] S. J. Baldwin *et al.*, "Non-Woven Textiles Formed from Contact Drawn Poly(ethylene oxide) Fibers Provide Tunable Filtration and Virucidal Properties via Entrapment of Silver Nanoparticles," *ACS Appl. Polym. Mater.*, 2021, doi: 10.1021/acsapm.1c00697.

[141] G. Chowdhry, Y. M. Chang, J. P. Frampton, and L. Kreplak, "Polymer entanglement drives formation of fibers from stable liquid bridges of highly viscous dextran solutions," *Soft Matter*, vol. 17, no. 7, pp. 1873–1880, 2021, doi: 10.1039/d0sm01550d.

[142] D. Jao and V. Z. Beachley, “Continuous Dual-Track Fabrication of Polymer Micro-/Nanofibers Based on Direct Drawing,” *ACS Macro Lett.*, vol. 8, no. 5, pp. 588–595, 2019, doi: 10.1021/acsmacrolett.9b00167.

[143] R. Sakaguchi, J. Ferracane, and J. Powers, “Fundamentals of Materials Science,” in *Craig’s Restorative Dental Materials*, 14th Editi., Elsevier, 2016, pp. 29–68.

[144] H. Yang *et al.*, “Multifunctional wound dressing for rapid hemostasis, bacterial infection monitoring and photodynamic antibacterial therapy,” *Acta Biomater.*, no. xxxx, Aug. 2021, doi: 10.1016/j.actbio.2021.08.037.

[145] M. Lualdi *et al.*, “Ultraviolet C lamps for disinfection of surfaces potentially contaminated with SARS-CoV-2 in critical hospital settings: examples of their use and some practical advice,” *BMC Infect. Dis.*, vol. 21, no. 1, pp. 1–13, 2021, doi: 10.1186/s12879-021-06310-5.

[146] N. Davidenko *et al.*, “Optimisation of UV irradiation as a binding site conserving method for crosslinking collagen-based scaffolds,” *J. Mater. Sci. Mater. Med.*, vol. 27, no. 1, p. 14, Jan. 2016, doi: 10.1007/s10856-015-5627-8.

[147] J. L. Seltzer, H. Weingarten, K. T. Akers, M. L. Eschbach, G. A. Grant, and A. Z. Eisen, “Cleavage specificity of type IV collagenase (gelatinase) from human skin,” *J. Biol. Chem.*, vol. 264, no. 33, pp. 19583–19586, 1989, doi: 10.1016/s0021-9258(19)47153-6.

[148] Y. T. Konttinen *et al.*, “Matrix metalloproteinase (MMP)-9 type IV collagenase/gelatinase implicated in the pathogenesis of Sjogren’s syndrome,” *Matrix Biol.*, vol. 17, no. 5, pp. 335–347, 1998, doi: 10.1016/S0945-053X(98)90086-5.

[149] L. Chung *et al.*, “Collagenase unwinds triple-helical collagen prior to peptide bond hydrolysis,” *EMBO J.*, vol. 23, no. 15, pp. 3020–3030, 2004, doi: 10.1038/sj.emboj.7600318.

[150] A. Jabłońska-Trypuć, M. Matejczyk, and S. Rosochacki, “Matrix metalloproteinases (MMPs), the main extracellular matrix (ECM) enzymes in collagen degradation, as a target for anticancer drugs,” *J. Enzyme Inhib. Med. Chem.*, vol. 31, pp. 177–183, 2016, doi: 10.3109/14756366.2016.1161620.

[151] L. Caminos, J. Garcia-Manrique, A. Lima-Rodriguez, and A. Gonzalez-Herrera, “Analysis of the mechanical properties of the human tympanic membrane and its influence on the dynamic behaviour of the human hearing system,” *Appl. Bionics Biomech.*, vol. 2018, 2018, doi: 10.1155/2018/1736957.

[152] J. Aernouts, J. R. M. Aerts, and J. J. J. Dirckx, “Mechanical properties of human tympanic membrane in the quasi-static regime from in situ point indentation measurements,” *Hear. Res.*, vol. 290, no. 1–2, pp. 45–54, 2012, doi: 10.1016/j.heares.2012.05.001.

[153] H. Luo, C. Dai, R. Z. Gan, and H. Lu, "Measurement of young's modulus of human tympanic membrane at high strain rates," *J. Biomech. Eng.*, vol. 131, no. 6, 2009, doi: 10.1115/1.3118770.

[154] J. T. Cheng, M. Hamade, S. N. Merchant, J. J. Rosowski, E. Harrington, and C. Furlong, "Wave motion on the surface of the human tympanic membrane: Holographic measurement and modeling analysis," *J. Acoust. Soc. Am.*, vol. 133, no. 2, pp. 918–937, 2013, doi: 10.1121/1.4773263.

[155] P. Ertl, D. Sticker, V. Charwat, C. Kasper, and G. Lepperdinger, "Lab-on-a-chip technologies for stem cell analysis," *Trends Biotechnol.*, vol. 32, no. 5, pp. 245–253, May 2014, doi: 10.1016/j.tibtech.2014.03.004.

[156] A. M. Wojtowicz, S. Oliveira, M. W. Carlson, A. Zawadzka, C. F. Rousseau, and D. Baksh, "The importance of both fibroblasts and keratinocytes in a bilayered living cellular construct used in wound healing," *Wound Repair Regen.*, vol. 22, no. 2, pp. 246–255, 2014, doi: 10.1111/wrr.12154.

[157] I. Pastar *et al.*, "Epithelialization in Wound Healing: A Comprehensive Review," *Adv. Wound Care*, vol. 3, no. 7, pp. 445–464, 2014, doi: 10.1089/wound.2013.0473.

[158] J. P. H. Smits *et al.*, "Immortalized N/TERT keratinocytes as an alternative cell source in 3D human epidermal models," *Sci. Rep.*, vol. 7, no. 1, pp. 1–14, 2017, doi: 10.1038/s41598-017-12041-y.

[159] G. Sriram *et al.*, "Full-thickness human skin-on-chip with enhanced epidermal morphogenesis and barrier function," *Mater. Today*, vol. 21, no. 4, pp. 326–340, 2018, doi: 10.1016/j.mattod.2017.11.002.

[160] S. A. Weston and C. R. Parish, "New fluorescent dyes for lymphocyte migration studies: Analysis by flow cytometry and fluorescence microscopy," *J. Immunol. Methods*, vol. 133, no. 1, pp. 87–97, Oct. 1990, doi: 10.1016/0022-1759(90)90322-M.

[161] T. Suzuki, K. Fujikura, T. Higashiyama, and K. Takata, "DNA staining for fluorescence and laser confocal microscopy," *J. Histochem. Cytochem.*, vol. 45, no. 1, pp. 49–53, 1997, doi: 10.1177/002215549704500107.

[162] M. Romani and J. Auwerx, "Phalloidin Staining of Actin Filaments for Visualization of Muscle Fibers in Caenorhabditis elegans," *BIO-PROTOCOL*, vol. 11, no. 19, p. e4183, 2021, doi: 10.21769/BioProtoc.4183.

[163] N. W. Tam *et al.*, "Material properties of disulfide-crosslinked hyaluronic acid hydrogels influence prostate cancer cell growth and metabolism," *J. Mater. Chem. B*, vol. 8, no. 42, pp. 9718–9733, 2020, doi: 10.1039/D0TB01570A.

[164] S. C. Choi *et al.*, "Modulation of biomechanical properties of hyaluronic acid hydrogels by crosslinking agents," *J. Biomed. Mater. Res. - Part A*, vol. 103, no. 9, pp. 3072–3080, 2015, doi: 10.1002/jbm.a.35437.

[165] Y. Xue, H. Chen, C. Xu, D. Yu, H. Xu, and Y. Hu, “Synthesis of hyaluronic acid hydrogels by crosslinking the mixture of high-molecular-weight hyaluronic acid and low-molecular-weight hyaluronic acid with 1,4-butanediol diglycidyl ether,” *RSC Adv.*, vol. 10, no. 12, pp. 7206–7213, 2020, doi: 10.1039/c9ra09271d.

[166] J. J. Roberts and P. J. Martens, “9 - Engineering biosynthetic cell encapsulation systems,” in *Woodhead Publishing Series in Biomaterials*, L. Poole-Warren, P. Martens, and R. B. T.-B. P. for M. A. Green, Eds. Woodhead Publishing, 2016, pp. 205–239.

[167] B. Alberts *et al.*, *Molecular Biology of the Cell*, 6th ed., vol. 53, no. 9. 2015.

[168] A. I. Bachir, A. R. Horwitz, W. J. Nelson, and J. M. Bianchini, “Actin-based adhesion modules mediate cell interactions with the extracellular matrix and neighboring cells,” *Cold Spring Harb. Perspect. Biol.*, vol. 9, no. 7, 2017, doi: 10.1101/cshperspect.a023234.

[169] B. M. Baker, A. M. Handorf, L. C. Ionescu, W. J. Li, and R. L. Mauck, “New directions in nanofibrous scaffolds for soft tissue engineering and regeneration,” *Expert Rev. Med. Devices*, vol. 6, no. 5, pp. 515–532, 2009, doi: 10.1586/erd.09.39.

[170] L. A. Bosworth, N. Alam, J. K. Wong, and S. Downes, “Investigation of 2D and 3D electrospun scaffolds intended for tendon repair,” *J. Mater. Sci. Mater. Med.*, vol. 24, no. 6, pp. 1605–1614, 2013, doi: 10.1007/s10856-013-4911-8.

[171] W.-J. Li, R. L. Mauck, J. A. Cooper, X. Yuan, and R. S. Tuan, “Engineering controllable anisotropy in electrospun biodegradable nanofibrous scaffolds for musculoskeletal tissue engineering,” *J. Biomech.*, vol. 40, no. 8, pp. 1686–1693, 2007, doi: https://doi.org/10.1016/j.jbiomech.2006.09.004.

[172] N. Rommerswinkel, B. Niggemann, S. Keil, K. S. Zänker, and T. Dittmar, “Analysis of cell migration within a three-dimensional collagen matrix,” *J. Vis. Exp.*, no. 92, pp. 1–10, 2014, doi: 10.3791/51963.

[173] D. Wu and F. Lin, *Cell migration*. 2019.

[174] B. Wang *et al.*, “Acoustic transmitted electrospun fibrous membranes for tympanic membrane regeneration,” *Chem. Eng. J.*, vol. 419, no. March, p. 129536, 2021, doi: 10.1016/j.cej.2021.129536.